SEMMELWEIS EGYETEM

DOKTORI ISKOLA

Ph.D. értekezések

2984.

RÓNASZÉKI ALADÁR DÁVID

Gasztroenterológia

című program

Programvezető: Dr. Molnár Béla, egyetemi tanár

Témavezetők: Dr. Kaposi Novák Pál, egyetemi docens

NEW QUANTITATIVE ULTRASOUND BIOMARKERS FOR THE DIAGNOSIS OF CHRONIC HEPATITIS AND FATTY LIVER DISEASE

PhD thesis

Rónaszéki Aladár Dávid

Károly Rácz Doctoral School of Clinical Medicine

Gastroenterology Program

Supervisor: Pál Novák Kaposi, M.D. Ph.D.

Official reviewers: Dénes Horváthy M.D. Ph.D.
Mónika Szilard M.D. Ph.D.

Head of the Complex Examination Committee: Viktor Bérczi, M.D. D.Sc.

Members of the Complex Examination Committee: Krisztina Hagymási M.D. PhD., Ádám Tárnoki M.D. PhD.

Budapest
2023

TABLE OF CONTENTS

LIST OF ABBREVIATIONS

2D-SWE	Two-dimensional shear wave elastography
AC	Attenuation coefficient
ACLD	Advanced chronic liver disease
AFP	Alpha-fetoprotein
ALP	Alkaline phosphatase
ALT	Alanine aminotransferase
APRI	AST to platelet ratio index
ARFI	Acoustic radiation force impulse
ASQ	Acoustic structure quantification
AST	Aspartate aminotransferase
ATI	Attenuation imaging
AUC	Area under the ROC curve
BMI	Body mass index
BSC	Backscatter distribution coefficient
CAP	Controlled attenuation parameter
CEUS	Contrast enhanced ultrasound
CI	Confidence intervals
CLD	Chronic liver disease
CRE	Serum creatinine
CT	Computed tomography
CTP	Child-Turcotte-Pugh
CSD	Capsule to skin distance

DAA	Direct-acting antivirals
DC	Dendritic cell
DWI	Diffusion weighted imaging
EASL	European Association for the Study of the Liver
ECM	Extracellular matrix
eGFR	Estimated glomerular filtration rate
ELISA	Enzyme-linked immunosorbent assay
EUS-LB	Endoscopic ultrasound-guided liver biopsy
FIB-4	Fibrosis-4 index
FLI	Fatty liver index
GGT	Gamma-glutamyl transferase
HBV	Hepatitis B virus
HCC	Hepatocellular carcinoma
HCV	Hepatitis C virus
HIV	Human immunodeficiency virus
HRI	Hepatorenal index
HS	Hepatic steatosis
HSI	Hepatic steatosis index
HTT	Hepatic transit time
HU	Hounsfield units
ICC	Intraclass correlation coefficient
IFG	Impaired fasting glucose
IGT	Impaired glucose tolerance
INF	Interferon

INR	International normalization ratio
IR	Insulin resistance
IU	International units
kPa	kilopascal
LS	Liver Stiffness
LSN	Liver surface nodularity
MELD	Model for end stage liver disease
MRE	Magnetic resonance elastography
MRI	Magnetic resonance imaging
MRI-PDFF	Magnetic resonance imaging proton density fat fraction
MRS	Magnetic resonance spectroscopy
MS	Metabolic syndrome
NAFLD	Non-alcoholic fatty liver disease
NASH	Non-alcoholic steatohepatitis
NK	Natural killer
NPV	Negative predictive value
OR	Odds ratio
PDFF	Proton density-based fat content measurement
PH	Portal hypertension
PNPLA3	Patatin-like phospholipase domain-containing protein 3
PPV	Positive predictive value
pSWE	Point shear wave elastography
QUS	Quantitative ultrasound
RMI	Reliable measure index

RNA	Ribonucleic acid
ROC	Receiver operating characteristic curve
ROI	Region of interest
SVR	Sustained virological response
SWE	Shear-wave elastography
T2DM	Type 2 diabetes mellitus
TAI	Tissue attenuation imaging
TE	Transient elastography
TIMP-1	Tissue Inhibitor of Metalloproteinase 1
TM6SF2	Transmembrane 6 superfamily member 2
TNF	Tumor necrosis factor
TSI	Tissue scatter distribution imaging
UDFF	Ultrasound derived fat fraction
US	B-mode ultrasound
US-FLI	Ultrasonographic fatty liver indicator
VNT	Varices needing treatment
WHO	World Health Organisation

1. INTRODUCTION

Chronic hepatitis C virus infection is a global problem, and it affects approximately 71 million people worldwide. Hepatitis C virus (HCV) infection is a major cause of liver morbidity. Due to notable progress in the medical therapy of HCV, the World Health Organization (WHO) is targeting the elimination of HCV infection as a public health threat by 2030, reaching a 90% drop in incidence compared with 2015 (1).

As the infection progresses, the liver of these infected people is rebuilt in a symptom-free manner, often over decades, with a series of connective tissue changes, until finally, the previous healthy liver becomes fibrotic, then it becomes cirrhotic. It is a proven fact that those affected in the stage of cirrhosis have a significantly higher risk of further, in many cases, life-threatening complications, such as portal hypertension, liver failure, and hepatocellular carcinoma (HCC)(2).

Direct-acting antivirals (DAAs) have become the standard therapy for HCV hepatitis since 2014 (1,3). The therapeutic effect of DAAs is high, with an eradication rate as high as 90% of non-cirrhotic patients (1,4).

In chronic liver disease (CLD), it is essential to estimate the severity of liver fibrosis from the point of view of disease prognosis and therapeutic decision-making. For long liver biopsy was the gold standard (5). Procedures that are based on non-invasive measurement of liver stiffness (LS) are collectively called elastography. These include vibration-controlled transient elastography (TE), shear wave elastography (SWE), and magnetic resonance elastography (MRE) (6).

Nowadays hepatic steatosis (HS) is also becoming more and more important. The most significant risk factors for the disease, such as metabolic syndrome (MS), obesity, and type 2 diabetes (T2DM) have become part of the modern social lifestyle due to unhealthy eating and a sedentary lifestyle (7). Non-alcoholic fatty liver disease (NAFLD) is the most common chronic liver disease in the world, and according to some estimates, nearly 1 billion people are affected by the disease (8).

Based on the recommendation of the European Association for the Study of the Liver (EASL), the diagnosis of NAFLD can be established when other factors causing liver damage (hepatitis B, hepatitis C, drugs) are not present and the daily alcohol consumption less than 20g for women, and less than 30g for men (9).

The importance of early recognition of fatty liver is not only due to its increased incidence rate, but also the possibility of serious late consequences. NAFLD in some cases leads to non-alcoholic steatohepatitis (NASH), which may lead to fibrosis, cirrhosis and HCC, due to this fact it is becoming the leading cause of liver transplantation for both end-stage liver disease and hepatocellular carcinoma in the United States (10). Due to the frequent occurrence and the late risk, it is essential to diagnose the disease and continuously monitor its progression.

The gold standard procedure for establishing the diagnosis is ultrasound -guided liver biopsy, either percutaneously or nowadays more commonly used endoscopic manner, which is an invasive procedure with limited repeatability. Biopsy sampling is an unpleasant, expensive examination procedure that requires hospital care and carries the risk of numerous complications (bleeding, pneumothorax, infection). In addition only a small fraction of the liver parenchyma is represented in the biopsy sample, which causes significant diagnostic challenge and suboptimal reproducibility (11).

Although the widely validated magnetic resonance spectroscopy (MRS) and the non-invasive proton density-based fat content measurement (PDFF) based on magnetic resonance imaging (MRI) serve as standardized reference (12), they are only limitedly available in medical institutions. Recent guidelines suggest B-mode ultrasound (US) as the initial diagnostic procedure in patients with NAFLD, as it is non-invasive, safe and cost-effective (13).

Classical sonography signs of fatty liver are increased echogenicity compared to the renal cortex, blur of liver parenchyma, poorly visualized portal venous wall and diaphragm (14). Quantitative ultrasound (QUS) techniques determine tissue composition based on acoustic analysis, including tissue attenuation imaging (TAI) and tissue scatter distribution imaging (TSI). Magnetic resonance imaging proton density fat fraction (MRI-PDFF) and TSI showed a significant correlation (13,15).

1.1. THE CLINICS OF HCV INFECTION

HCV infection is a multifaceted, systemic disease, the hepatic and extrahepatic complications of which are well known today. HCV is one of the most prominent causes of chronic liver disease. The virus, which was previously called non-A-non-B hepatitis,

was identified in 1989 using molecular biology methods, which were considered new at the time. In the past 30 years, researchers have successfully discovered the pathomechanism of the infection and learned the structure of the virus (16).

In patients with chronic liver disease, cirrhosis and HCC, HCV antibody positivity is very high, 20-90%. The shared use of needles and syringes by intravenous drug users results in a very high prevalence of HCV among those involved. In addition to the above, homosexual men are also a high-risk group (17,18)

HCV shows great structural variability. Several genotypes of the virus are known, based on the sequencing of the genome, its 7 types and 67 subtypes can be distinguished. A 2018 study conducted in Hungary revealed that more than 95% of domestic infected people have genotype 1, 84.6% have 1b, and 5.6% have 1a (Figure 1) (19).

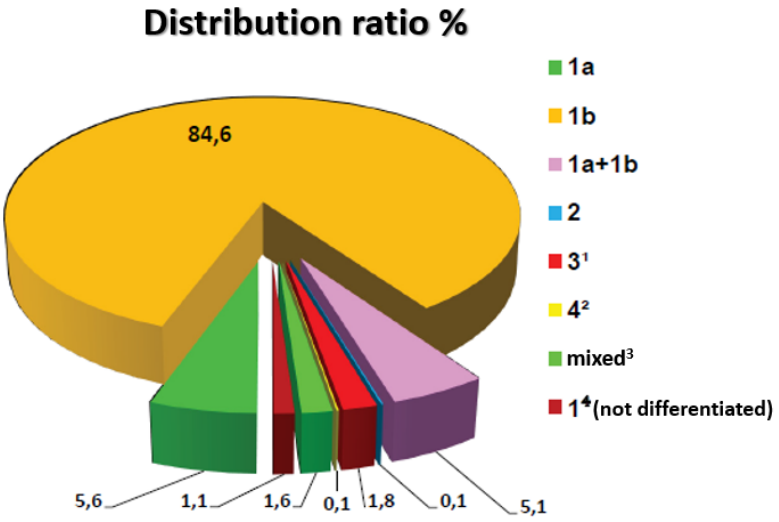

Figure 1. *Distribution of HCV genotype/subtype in Hungary between 2000 and 2017 (19)*

1.1.1. Etiology And Pathogenesis Of HCV

The HCV reaches the liver via the bloodstream, where it penetrates the liver cells and begins to replicate. HCV causes cell death in several different ways, including immune-mediated cytolysis, oxidative stress and insulin resistance (IR). Large number of natural killer (NK) cells found in the sinusoidal spaces of the liver encounter the virus. The virus activates them in the infection's early phase, then they stimulate the antiviral immune response in the liver, virus-specific T cells, Kupffer cells and dendritic cells (DC) are also mobilized. In addition, they also participate in cleaning infected liver cells, with cytolytic

mechanisms and cytokine, interferon (INF) gamma and tumor necrosis factor (TNF) alpha production. NK cells contribute to liver damage during their antiviral activity (20). HCV becomes chronic causing long-lasting damage to liver cells. Liver injury can range from minimal histological changes to extensive fibrosis. Roughly 80% of the liver is made up of the liver cells themselves, 20% of the other cells are lymphocytes, Kupffer cells, endothelial cells, NK cells and bile duct cells (21).

Hepatic stellate cells play a key role in the pathogenesis of fibrosis. These cells are located in the perisinusoidal space of Disse. They are activated and turn into myofibroblasts, which are extracellular matrix-producing cells of the liver. The inflammatory environment when the liver cells are destroyed favors the differentiation of these cells. As more and more extracellular matrix (ECM) are produced, matrix metalloproteinases, which normally maintain balance, are unable to break down the excess ECM, so it accumulates and initiates fibrosis, which disrupts normal liver function. Fibrosis can worsen into cirrhosis, in which case cirrhotic nodules surround the remaining healthy liver cells significantly affecting blood flow and liver function (21). If the effect that started the injury persists for a long time, fibrosis develops, and as the process progresses, cirrhosis, liver failure, HCC can occur, and finally the changes can lead to the patient's death (18).

1.1.2. Diagnostics Of Acute And Chronic HCV Infection

It is typical for patients infected with the HCV that they live without symptoms or complaints for many years. Just a few patients present general symptoms in the acute phase, such as lethargy, loss of appetite, weakness or digestive system complaints. These symptoms can go away in a few days. Discoloration of the skin and conjunctiva may occur in approximately 20% of the patients who show symptoms in the early stages.

As the disease progresses, more and more changes take place in the liver, disrupting its normal functioning. Despite this, many chronically infected individuals do not have any symptoms, but if they do, they usually complain of mild fatigue, joint pain, and loss of appetite. In many cases, a routine blood test ordered by a general doctor for a patient without symptoms or complaints raises the first suspicion of liver disease (22).

The diagnosis of chronic hepatitis is based on both the detection of anti-HCV antibodies and the detection of HCV virus ribonucleic acid (RNA). According to the Hungarian

professional recommendation, the first step in testing for infection is detection of anti-HCV antibodies with enzyme-linked immunosorbent assay (ELISA) test (18).

Not all acutely HCV-infected patients show anti-HCV antibody positivity. In the very early stages of infection or in immunosuppressed patients, the tests may be negative. If the possibility of acute hepatitis is raised based on the clinical picture, it is recommended to continue the investigation with molecular biological methods. This means the detection of viral RNA (3,23).

HCV-RNA test is the next step in all patients who have received a positive or doubtful result during the detection of anti-HCV antibodies. It is recommended to carry out tests that work with measurement limits of less than 15 international units/ml (IU6ml), despite the fact that patients who need treatment mostly have HCV-RNA levels above 50.000 IU/ml (3). Chronic HCV hepatitis is diagnosed when both active HCV infection and hepatitis are present. There are 3 conditions for establishing a chronic HCV infection diagnosis:

1. Presumed, or confirmed HCV infection that existed more than 6 months ago.
2. Detectable HCV-RNA.
3. Proof of liver damage based on elevated alanine aminotransferase (ALT) and/or liver biopsy and/or non-invasive testing method and/or hepatic decompensation (18).

After the diagnosis has been established, the activity and progress of the liver disease, as well as possible extrahepatic manifestations should be examined in all confirmed HCV-infected patients, partly for the purpose of determining the treatment priority, and partly for the purpose of choosing the treatment method and follow-up strategy, but this is not a condition for the treatment indication (23).

For a more accurate assessment of liver disease, complete blood count, aspartate transaminase (AST), gamma-glutamyl transferase (GGT), alkaline phosphatase (ALP), serum albumin, bilirubin, prothrombin, kidney function tests including in serum creatinine (CRE) and estimated glomerular filtration rate (eGFR) are needed. Abdominal US examination (and if focal liver disease/HCC is suspected either a computer tomography (CT) or MR examination is also needed (18).

1.1.3. Serum Markers Of Liver Fibrosis

Many serum biomarkers have been proposed to measure the amount of liver fibrosis in chronic HCV infection. These markers can be divided into two major groups: the indirect and the direct markers of fibrosis (24). The indirect markers reflect the hepatocyte dysfunction caused by the distorted liver architecture, and include transaminases such AST, ALT and platelet count. Meanwhile, direct serum markers are products of the fibrotic matrix deposition and fibrinolysis and include extracellular matrix components such as hyaluronic acid, procollagen and laminin, as well as cytokines such as tissue inhibitor of metalloproteinase 1 (TIMP-1)(5). Various combinations of direct and indirect serum markers have been tested for non-invasive staging of fibrosis (Table 1). Some of the most commonly used included the AST/ALT ratio, the AST to platelet ratio index (APRI) and the Fibrosis-4 index (FIB-4), which are relatively inexpensive and easy to obtain (25–27). In addition, several licensed combinations are used in commercially available tests including among others FibroTest® and HepaScore® (28).The advantages of serum tests are their good reproducibility, widespread availability and high applicability (5). Most serum tests do not require special instrumentation and can be calculated during routine outpatient visits. Meanwhile, none of the tests are specific for liver fibrosis and caution is needed during interpretation of the results, as the scores can be influenced by other diseases or metabolic conditions ie. Gilbert-syndrome, or active hepatitis. Also, there are individual variations in the patients` metabolism, which could alter serum levels of indirect markers lowering the reproducibility of some of the tests. Although serum tests can detect cirrhosis with slightly lower accuracy compared to elastography, they cannot be used to classify lower grades of fibrosis (5).

Table 1. *Serum tests commonly used for quantification of liver fibrosis (28). Apo-A1, Apolipoprotein A-1; α2M, α2-macroglobulin; HA, hyaluronic acid; BMI, body mass index; TIMP-1, tissue inhibitor of metalloproteinase 1; PIIINP, procollagen III N-terminal peptide.*

Test	**Serum markers**
AST to platelet ratio index	AST, platelets
AST/ALT ratio	AST, ALT
BARD score	AST/ALT ratio, BMI, diabetes
European Liver Fibrosis panel (ELF)	Age, HA, TIMP-1, PIIINP
FIB-4 index	Age, AST, ALT, platelets
FibroIndex	AST, platelets, γ-globulin
FibroTest, FibroSure	Age, sex, bilirubin, GGT, α2M, haptoglobin, apo-A1
Hepascore	Bilirubin, GGT, α2M, HA, age, sex
NAFLD fibrosis score	Age, BMI, IFG/diabetes, AST/ALT ratio, platelets, albumin
PGA index	prothrombin time, GGT, apo-A1
Proteomics and Glycomics	Various biomarker fragments

1.2. THE CLINICS OF FATTY LIVER DISEASE

1.2.1. Epidemiology Of Fatty Liver Disease

Nowadays, fatty liver is considered one of the most common chronic liver diseases in the world, affecting 25% of the adult population in Europe (29). Between 1990 and 2017, the prevalence of the disease increased from 391.2 million to 882.1 million. While the frequency of occurrence was highest in North America and the Middle East, the largest increase occurred in Western Europe (30)

Due to its frequent occurrence, the recognition of risk factors, early diagnosis and effective therapy are extremely important. NAFLD is defined as the excessive accumulation of the fat in the liver, which can be detected in at least 5% of hepatocytes and is not caused by alcohol consumption (9). Two major subtypes of NAFLD are known: non-alcoholic fatty liver, which independently means the accumulation of fat in liver cells, and NASH, where inflammatory elements are already present in the liver. Based on previous studies, steatosis progresses to steatohepatitis in 35% of cases, and patients diagnosed with steatohepatitis have approximately 10% later develop liver cirrhosis, which can even have life-threatening complications (31).

1.2.2. Risk Factors Of Hepatic Steatosis

The presence or absence of risk factors plays an important role in the time of onset of the disease, as well as in assessing the risk progression. There are controllable and uncontrollable risk factors. Genetics and viral infection cannot be influenced. Studies have shown that the transmembrane 6 superfamily member 2 (TM6SF2) gene has a role in the development of NAFLD, and the patatin-like phospholipase domain-containing protein 3 (PNPLA3) gene in the course and severity of the disease (32,33).

In terms of virus infection, HCV and Hepatitis B virus (HBV) play a prominent role in the disease process. Regarding the HCV, the direct steatogenic effect of the virus was detected, which is caused by the core protein of HCV by influencing the pathways of fat metabolism, increasing the synthesis of fatty acids, reducing their breakdowns, and reducing the secretion of lipoproteins. The steatogenic effect of the HBV is less known, rather the existing metabolic risk factors play a role in the fatty liver of chronic hepatitis B infected patients (34).

Among the risk factors that can be influenced, it is worth highlighting the excessive consumption of fat and carbohydrates, as well as high-calorie foods, because these lead to obesity. A retrospective study conducted in the USA showed 70% of obese patients have steatosis. The reason for this is the diseases associated with obesity (diabetes, polycystic ovary syndrome, etc.) are also independent risk factors in the development of NAFLD, so the risk value is amplified by obesity. In terms of additional risk factors, IR and T2DM play a significant role. It is also higher risk in case of already impaired fasting glucose (IFG) and impaired glucose tolerance (IGT) of developing steatosis.

In addition, there is a huge risk for people suffering from MS, as they have many risk factors together. These are T2DM, hypertriglyceridemia, reduced HDL levels, increased abdominal circumference and hypertension (34).

1.2.3. Pathophysiology Of NAFLD

In case of NAFLD, excessive accumulation of triglycerides occurs in the cytoplasm of hepatocytes without the existence of other secondary causes (e.g. alcohol consumption, virus hepatitis). The name refers to the spectrum of abnormal changes in the liver tissue that transform into each other, in which different stages can be distinguished. In the case of a fatty liver, the amount of accumulated triglyceride affects more than 5% of the hepatocytes, which is either present without inflammation or hepatocyte damage, or with minimal inflammation and cell damage. NASH is characterized by the infiltration of inflammatory cells, primarily neutrophil granulocytes, liver cell damage in the form of balloon cell degeneration necrosis, and fibrosis (Figure 2) (9).

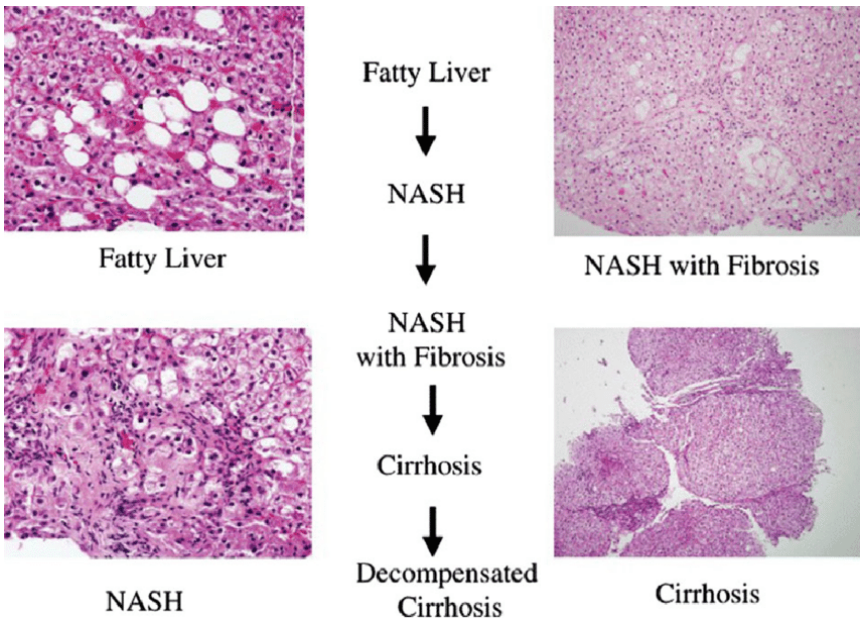

Figure 2. *Mechanism of non-alcoholic steatohepatitis. During the development of NASH, fatty transformation and balloon cell degeneration of hepatocytes, inflammation of the liver parenchyma and tissue necrosis appear. Chronic inflammation leads to the initiation of the fibrosis stage, which can progress to end-stage cirrhosis as the process progresses, eventually even causing liver failure (35).*

The process of the development of fatty liver is best described by the ‘two hit theory’. The main motive of the pathogenesis is the development of IR (34). The first blow is the accumulation of lipids, which increases the liver’s sensitivity to various damaging factors, which acts as a second blow and promotes the development of NASH. Oxidative stress, proinflammatory cytokines, and the effect of bacterial endotoxins from the gut can all be considered a second blow. The so-called ‘multi-hit hypothesis’ described in 2010 explains the development of fatty liver in genetically susceptible individuals much more precisely with the interaction of many factors, such as IR, hormones secreted by fat cells, and intestinal flora (36).

Insulin hormone produced by the beta cells of the pancreas is responsible for regulating blood sugar level. The hormone inhibits gluconeogenesis in the liver, promotes the uptake of glucose into the muscle and liver, so the molecule can go through the process of glycolysis and glycogenesis. It plays a prominent role not only in carbohydrate metabolism, but also in fat metabolism. By inhibiting hormone-sensitive lipase, insulin hormone inhibits lipolysis and contributes to the esterification of free fatty acids, thus creating triglycerides (37).

In the presence of IR, the cell's sensitivity to insulin decreases, and the body tries to compensate for this with increased insulin production, since only larger amounts of cells can utilize glucose in the presence of insulin. In this state, inhibition of hormone-sensitive lipase ceases and lipolysis begins, resulting in the release of free fatty acids from adipocytes. The free fatty acids circulating in the blood are taken up by the organs (e.g. liver), and in the absence of oxidation, are accumulated intracytoplasmic in the form of triglycerides (37).

IR plays a central role in the development of NAFLD, which can be considered the hepatic manifestation of MS. A diagnosis of MS requires the presence of three or more of the following features:

1. Waist circumference greater than 102 cm for men and greater than 88 cm for women.
2. Triglyceride level greater than or equal to 1.69 mmol/L.
3. High-density lipoprotein cholesterol level less than 1 mmol/L in men and less than 50 mg/dl in women.

4. Systolic blood pressure greater than or equal to 130 Hgmm or diastolic blood pressure greater than or equal to 85 Hgmm.
5. Fasting plasma glucose level is at least 6.1 mmol/L. Patients with MS features are at high risk of NAFLD. In addition, ethnicity also influences the prevalence of NAFLD. Hispanics and Asians, even with lower levels of obesity, are at greater risk than African Americans, who have less severe NAFLD and a lower prevalence despite having MS criteria (38).

1.2.4. Serum Biomarkers Of Fatty Liver Disease

Nowadays, non-invasive procedures are playing an increasingly important role, as they do not cause discomfort to the patient. They are cheaper, and can be performed several times in a short time, so they are suitable for monitoring (9). We distinguish two major approaches to non-invasive techniques: biological and physical. The biological approach means the quantitative determination of the biomarkers present in the serum, while the physical approach detects the loss of elasticity caused by fat accumulation or fibrosis with imaging methods. Different points and indices can be calculated from the serum biomarkers, from which we can infer the presence and degree of steatosis (Table 2). In addition, the level of circulating kreatin-18 fragments can be used to distinguish non-alcoholic steatohepatitis, which shows an elevated value in case of direct liver cell damage (39).

Table 2. *Popular serum biomarker indexes used in the diagnosis of steatosis (39).*

INDEX	**COMPONENTS**
Fatty Liver Index (FLI)	BMI, GGT, Triglyceride, Waist circumference
Hepatic Steatosis Index (HSI)	BMI, Diabetes, AST/ALT ratio
SteatoTest™	Age, Sex, BMI, ALT, GGT, Triglyceride, α2-macroglobulin, Apolipoprotein A1, Haptoglobin, Total bilirubin, Total cholesterol, Glucose

1.3. LIVER BIOPSY FOR DIAGNOSING CHRONIC LIVER DISEASE

Liver biopsy is the gold standard method for diagnosing and staging liver fibrosis. Different liver fibrosis staging systems are used depending on the cause of underlying chronic liver disease. Some of the most frequently used staging systems include the METAVIR, Ishak, Laennec and Brunt systems applied for hepatitis C and NAFLD (40). The highly popular METAVIR system classifies fibrosis into five consecutive stages based on involvement of the periportal spaces, sinusoids, and hepatic veins, presence of fibrous septae and bridging fibrosis. Stage F0 indicates normal liver and absence of fibrosis; F1 is minimal fibrosis in periportal areas; F2 is significant fibrosis with a few bridges between portal and hepatic veins; F3 is severe fibrosis with architectural distortion; and F4 is liver cirrhosis (41,42). In addition, liver biopsy is currently the only diagnostic modality, which can determine necroinflammatory activity in chronic hepatitis. The Knodell, Ishak and METAVIR systems grade piecemeal and lobular necrosis as well as portal and sinusoidal inflammation separate from liver fibrosis providing important information on activity and prognosis of the disease (43).

The gold standard method for the diagnosis and staging of fatty liver is traditionally a liver biopsy, although the most recent professional recommendations also include MRI-based fat quantification as a reference method . Liver biopsy is only recommended for the diagnosis of unclear etiology or NASH, to exclude it or to assess its progression (9).

The biopsy is a percutaneous, ultrasound-guided procedure. After the puncture, a cylinder of tissue is aspirated with the help of a cannulated needle, which is fixed in formalin. It is usually 16-20 mm long and 1.2-1.8 mm wide, and must contain at least 10-11 portal triads to make an accurate diagnosis. Accurate data can be obtained from the liver cylinder taken as a sample through histology (44). Not only can we determine the degree of fat deposition, but we can also obtain information about the zonality of fat deposition, its micro- or macrovesicular form, the extent of iron deposition, inflammation and fibrosis. The histological classification is usually based on the percentage of hepatocytes with detectable lipid accumulation: grade 0 (<5%), grade 1 (5-33%), grade 2 (33-66%), grade 3 (>66%) (45).

However, the disadvantage of the procedure is that being an invasive diagnostic method, it can lead to serious complications (bleeding, infection, pneumothorax, intestinal perforation). It examines only a small part of the liver parenchyma, so it does not provide sufficient information about the condition of the liver as a whole. In addition, it is subjective and the result is significantly influenced by the interobserver and intraobserver sampling differences (46). Recently, endoscopic ultrasound-guided liver biopsy (EUS-LB) has been gaining increasing popularity as it has several advantages over percutaneous biopsy. EUS-LB is safer, as the liver lesions are closer to the endoscopic than to a surface probe and can be visulized with higher resolution, and targeted with higher precision. EUS-LB is also performed under sedation causing less anxiety to the patient (47). On the other hand the procedure requires special instrumentation, it costs more than a percutaneous biopsy, and not all patients can tolerate endoscopy. Due to the mentioned disadvantages, the most recent professional recommendations emphasize the role of non-invasive method in the diagnosis of CLD (9,48).

1.4. THE ROLE OF IMAGING IN NON-INVASIVE DIAGNOSTICS

Imaging plays an increasing role in the diagnosis of CLD. Large numbers of patients with various etiology of CLD need continuous monitoring and repeated evaluation of liver status for identification of high-risk individuals and for guiding therapeutic decisions. The widespread use of modern medical imaging techniques has revolutionized patient care and produces large amounts of information on morphology, physical properties of various organ systems. There is an increasing demand for quantifiable biomarkers, which can be extracted from imaging studies used for objective non-invasive assessment of CLD (31). Imaging has a role in diagnosing and staging of clinically significant fibrosis and steatosis, as well as identifying complications of CLD and portal hypertension (PH)(49).

1.4.1. B-mode Ultrasound

An early diagnosis of cirrhosis is particularly important in patients with compensated CLD, because it necessitates screening for PH and HCC. Also, non-invasive detection and staging of clinically significant fibrosis (≥F2 grade) is significant as it can predict prognosis and cause modification in therapy (50). Unfortunately, the US has relatively

low sensitivity for liver fibrosis. Cirrhosis on the other hand, leads to changes in morphology of multiple abdominal organs, which can be well detected with US. The classic signs of cirrhosis include nodularity of liver surface, heterogeneity of liver echotexture, the increase in the size of left liver lobe and caudate lobe compared to the right lobe and splenomegaly (51) (Figure 3). Cirrhosis also results in a distorted liver vasculature, PH, portosystemic varicosity and even reversal of the flow in the portal vein (52). Although the altered circulation can be easily detected with Doppler US, the signs of PH can be only observed in advanced stages of liver fibrosis.

Perfusion studies, using contrast enhanced ultrasound (CEUS), can reveal changes in the microvascular circulation by detecting increase in hepatic transit time (HTT), the time it takes for microbubble contrast after entering the portal vein to reach hepatic veins, as HTT progressively shortens in advancing grades of fibrosis (53). Nevertheless, staging of liver fibrosis with CEUS is time consuming and invasive procedure. Furthermore, there is still no agreement on a CEUS protocol as different perfusion parameters have been tested by multiple research groups, who reported varying rates of accuracy (54).

Figure 3: *B-mode ultrasound signs of liver cirrhosis include surface nodularity, inhomogeneous echotexture and signs of portal hypertension such as ascites and gallbladder wall edema.*

The US has been among the first and one of the most commonly used methods in the assessment of HS. Because of its excellent availability, low cost, no risk from ionizing radiation and minimal patient burden US is also the recommended imaging modality to screen for high risk patients who have high BMI, diabetes or other metabolic risk factors. Meanwhile, US has weak points including high interobserver variability, low sensitivity for detection of mild steatosis (liver fat content <20%) and lower accuracy in patients with liver fibrosis (55). The sensitivity of US decreases if the patient is obese and the fat content of the liver is less than 30% (56). The performance of US is also highly dependent on the operator`s experience. Due to its low reproducibility, the US also has only limited utility in the follow up of patients diagnosed with HS. Still, in many cases, especially in patients with advanced stage disease, the combination of physiology parameters, serum markers and other biochemical factors together with the patient's clinical history are sufficient to establish the diagnosis of HS and NAFLD. Recently, multiple semi-quantitative and quantitative image analysis techniques have been proposed to overcome the drawbacks of US and increase its sensitivity and reproducibility.

The classic ultrasound signs of fatty liver include the increased echogenicity of the parenchyma, often referred to as a “bright liver”. Another important sign is the increase in the posterior attenuation of the US signal, which causes reduced visibility and blurring of the contours of the hepatic veins, portal vein, gallbladder wall, and the diaphragm. Often, the HS is not evenly distributed throughout the liver resulting in areas of focal sparing or focal deposition, which typically show up on US as poorly defined low or high echogenicity areas within the parenchyma and cause a common differential diagnostic problem (55).

The brightness of the liver is often compared to the right kidney cortex. The ratio of the signal intensities in the two organs at the same imaging depth is called the hepatorenal brightness index (HRI). In the liver, the designated area must be defined away from large vessels, in the kidney, this area must be in the cortex. HRI correlates well with histologically determined fat content of the liver, and can determine steatosis of more than 5% with excellent accuracy, but the cut-off values used differ from study to study (57,58).

Multiple working groups have proposed semi-quantitative evaluation of classic signs of HS, and constructed US scoring systems. The Hamaguchi score or ultrasonographic fatty

liver indicator (US-FLI) index can be calculated from systematic assessment of the B-mode US images. To calculate Hamaguchi score, the system takes four characteristics of the liver as a basis: the hepatorenal echo contrast, the brightness of the liver, the obstruction of the blood vessels, and the tissue's ability to absorb echo. Studies have confirmed that if the Hamaguchi score is more than 2 (the maximum score of Hamaguchi score can be 3), the test has a sensitivity of 91.7%, and has 100% specificity in the diagnosis of fatty liver (Figure 4) (59).

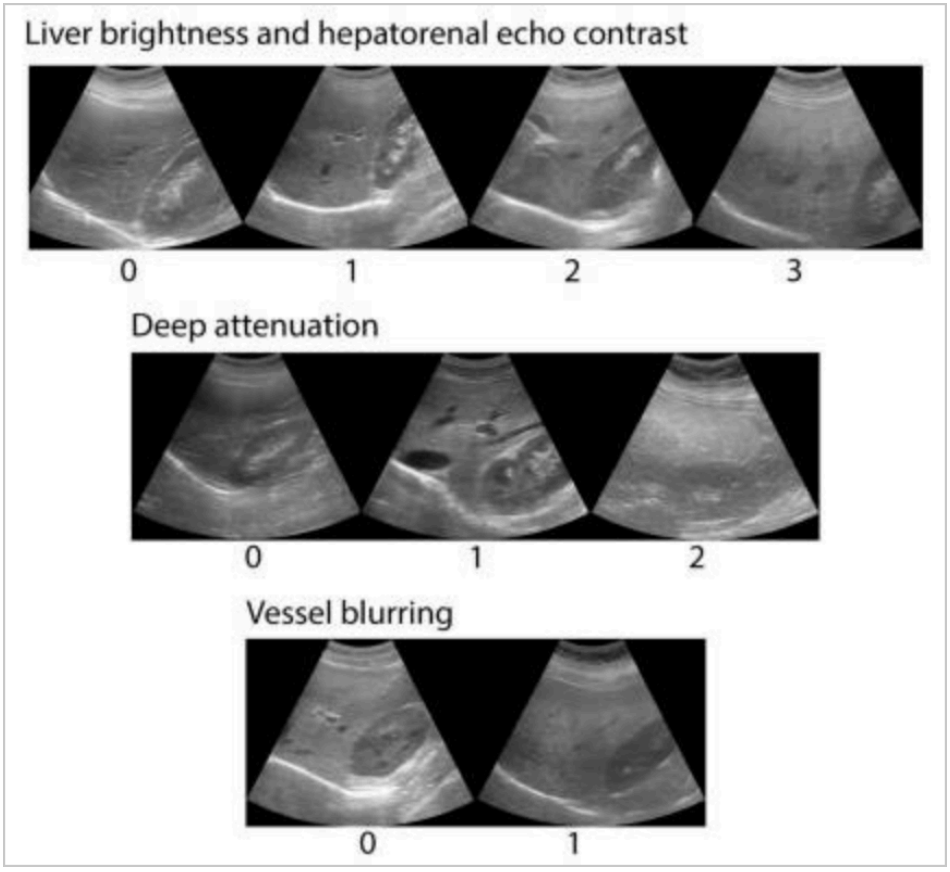

Figure 4: *Semiquantitative score system by Hamaguchi et al. The system scores liver brightness from 0 to 3, diaphragm attenuation from 0 to 2 and vessel blurring from 0 to 1 (59).*

Another scoring system is the so-called US-FLI showed good sensitivity and specificity for both in the detection of mild (sensitivity 90.1%, specificity 90%), moderate (sensitivity 86.4%, specificity 92.5%), and severe steatosis (sensitivity 88.5%, specificity 87%) (Figure 5). A US-FLI score < 4 also had a NPV of 94% and a specificity of 45.71% for NASH (60).

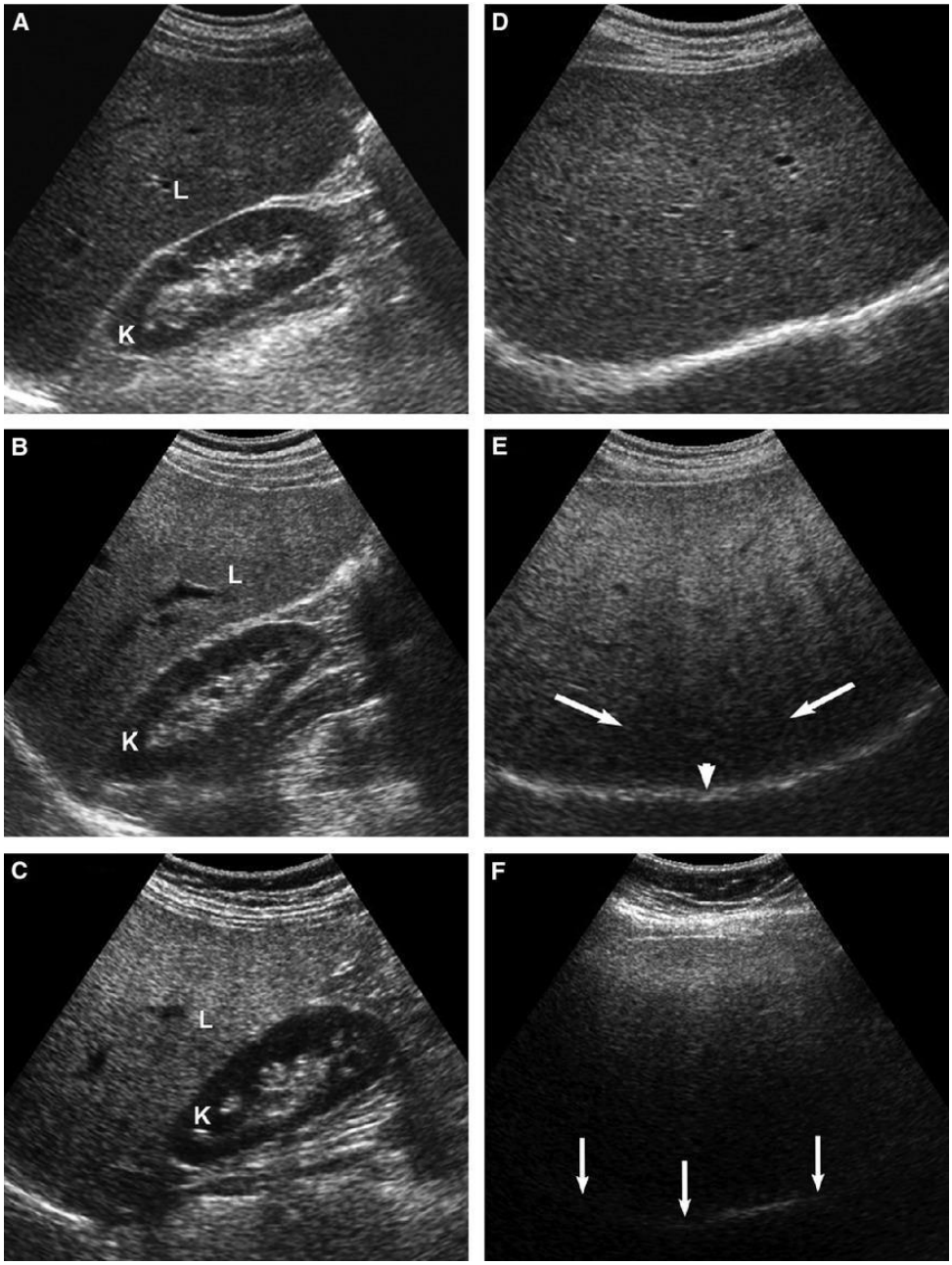

Figure 5. *US-FLI score system US morphological signs. A: Normal visualization of the contour of the hepatic vein. B: The wall of the hepatic vein is blurred. C: Normal visualization of the wall of the portal vein and the wall of the gallbladder. D: Blurring of the wall of the portal vein. E: Focal sparing phenomenon. F: Blurring of the wall of the gallbladder(60).*

1.4.2. Computer Tomography

CT is extensively used to diagnose complications of CLD such as HCC, splenomegaly, or ascites. Well-known imaging features of cirrhosis on CT and MRI include surface nodularity, heterogeneous enhancement, small size, caudate lobe enlargement, splenomegaly, decreased right to left lobe volume ratio, varices, expanded gallbladder fossa, posterior notch, and ascites (61). Unfortunately, the sensitivity of CT for liver fibrosis is low. In a multicentre study conducted by Kudo et al., the diagnostic accuracy, sensitivity and specificity of CT for hepatic cirrhosis were 67–86%, 77–84% and 53–68%, respectively (62). Recently, liver surface nodularity (LSN) and multiple radiomics parameters have been identified as new biomarkers, which could be calculated from routine portal-venous phase CT scans and used for differentiating cirrhosis from non-cirrhotic livers (63,64).

The average density of the healthy liver parenchyma on a native, non-contrast CT examination is approx. 60 Hounsfield units (HU). In clinical practice the density of the liver is measured using the region of interest (ROI), the circle-shaped designated areas on the native CT scan (Figure 6). Previous research has shown that the fat content of the liver shows a negative correlation with HU density values measured on native CT scans. According to Kodama et al., 40 HU measured on native CT corresponds to an approx. 30% histological steatosis, which suggests a moderate degree of steatosis (65). The ratio of the density of the liver and spleen measured on native CT scans can also be used to assess steatosis, but the main limitation of its use is that it is less suitable for measuring mild fatty liver. It can detect steatosis of at least 30%, early detection of inflammation, necrosis and fibrosis is not possible with this imaging method. Due to ionizing radiation, it cannot be used for examination and follow-up of children (66).

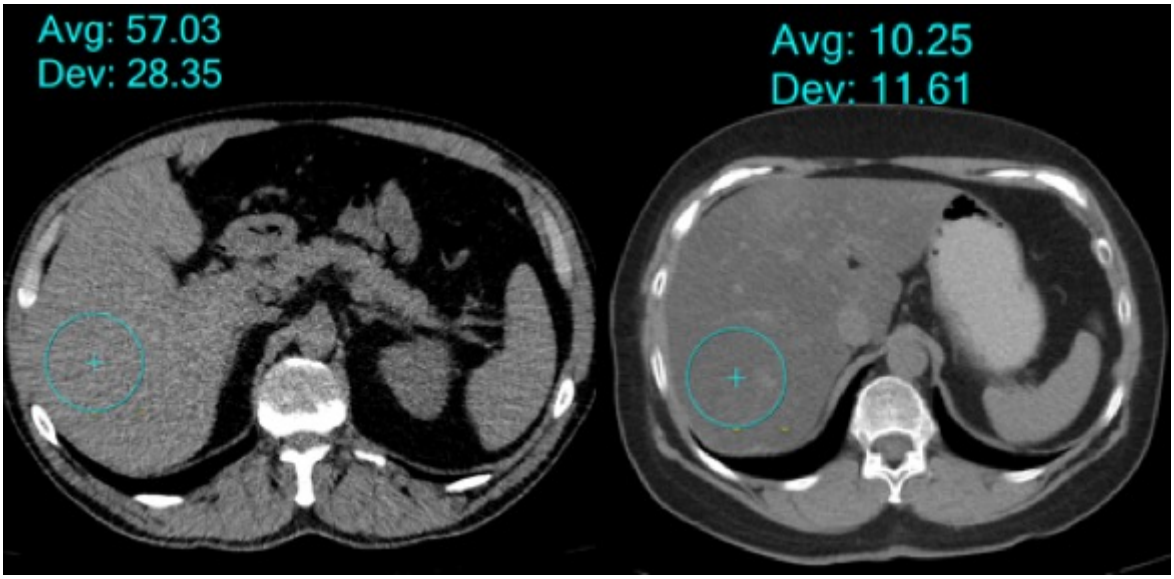

Figure 6: *Diagnosis of fatty liver using a native CT scan. The average density of the liver in case of healthy parenchyma on a native CT scan is around 60 HU (A). Native density measured below 40 HU suggests the diagnosis of fatty liver. In case of severe steatosis, the average density can even take on a negative value (B)*

1.4.3. Magnetic Resonance Imaging

Similar to CT, MRI has limited value in diagnosing liver fibrosis. The classic morphological signs of advanced CLD detected on MRI are identical to those that can be visualized with other modalities. MRI has a sensitivity of 87% and specificity of 54% in diagnosing cirrhosis based on morphology signs alone (61). Advanced MRI techniques have also been investigated for quantification of liver fibrosis. These include texture analysis, perfusion studies, diffusion weighted imaging (DWI), hepatocyte function imaging with hepatocyte specific contrast media, T1 mapping, and calculation of the extracellular fraction (40). MRE is a technique for measuring liver stiffness (LS) and its basic concept will be discussed in the next section.

There are two methods for measuring fatty liver based on magnetic resonance: magnetic resonance spectroscopy and tissue fat fraction measurement determined using proton density measurement based on MRI. Both are based on the difference in the resonance frequency of the protons in water and fat (chemical shift) (67).

For several decades, MR spectroscopy (MRS) has proven to be the most widely accepted method for MR determination of liver fat content; and many consider it to be the non-

invasive reference standard for measuring steatosis (68,69). MRS enables the direct measurement of chemical components characteristic of tissues, by displaying the signal intensity characteristic of a given chemical composition (70). MRS shows protons from water as a single peak, while protons from fat as multiple peaks. Since this method takes signal intensity into account, liver fat fraction (FF) can be easily expressed as the ratio of the signal intensity of protons from fat (F) to the signal intensity of protons from fat and water (F+W) (Figure 7):

$$FF = \frac{F}{W+F}$$

The examined area is usually a voxel with a volume of 2x2x2 cm or 3x3x3 cm, which is selected during a breath hold and does not contain larger vessels and bile ducts. MRS requires the mapping of the resonance frequency spectrum, on which we can then identify the differences (71). The main limiting factor of the method is the T1 and T2 relaxation effect, and the use of a small area sample, which does not allow examination of the liver as whole, and thus can give misleading results in case of uneven fat distribution. The T1 relaxation effect can be eliminated by using the long repetition time, the T2 relaxation effect can be eliminated by the multi-echo technique (72).

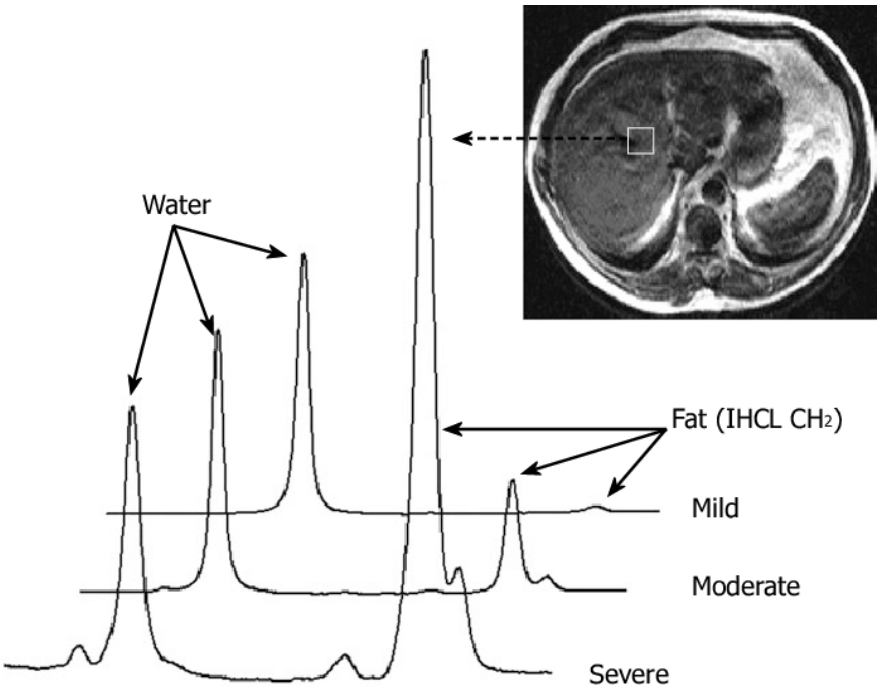

Figure 7. *Magnetic resonance spectroscopy Protons from water are represented as a single signal intensity peak, while protons from fat are represented as multiple peaks corresponding to the different side chain fat molecules. The figure shows the typical curves for mild, moderate and severe fatty liver (69).*

The resonance frequency of the protons in water and fat is different was detected during imaging. The introduction of this into the literature is attributed to W. Thomas Dixon. The value of the chemical shift is obtained here in the coding of the phase of the protons, from which water and fat are separated during post-processing (73).
If the vector of protons from water and fat points in the same direction, then we speak of a so-called 'in-phase' sequence. Then the signal intensity from the protons in the fat is added to the signal intensity from the protons in the water. In the case of so-called 'opposed phase', the vectors point in the opposite direction, so in this case the signal intensity is not added, but subtracted. The signal intensity difference between 'in phase' and 'opposed phase' can be used to determine the signal intensity of protons from fat (Figure 5) (70).

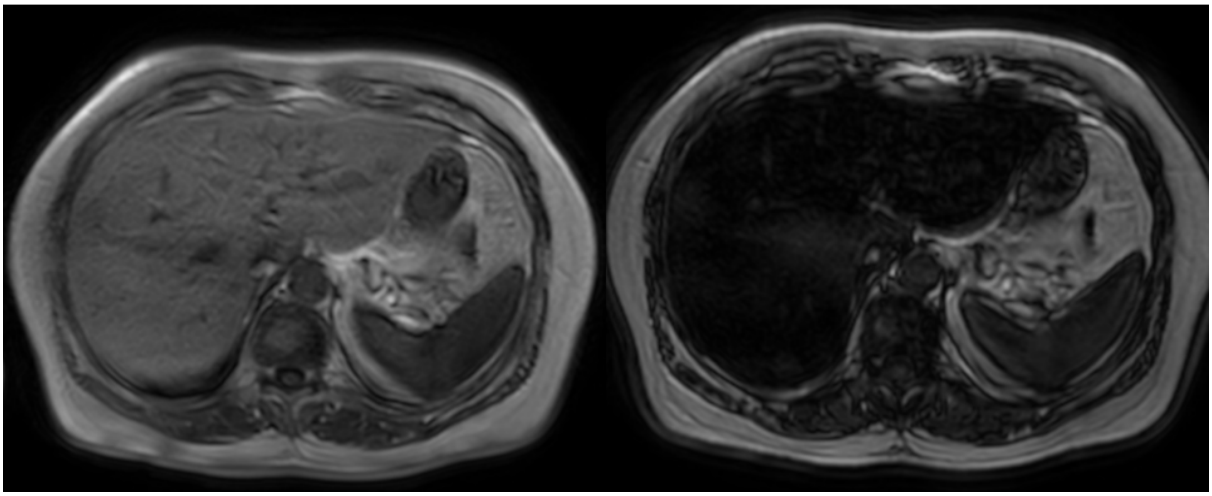

Figure 8. *In phase (left side) and opposed phase (right side) images made using the magnitude-based techniques.*

The difference between the signal intensity of the 'in phase' and 'opposed phase' gives the signal intensity of the protons from the fat, from which the MRI proton density fat

fraction (MRI-PDFF) can be calculated. MRI-PDFF, derived from chemical shift imaging, enables the exact amount of fat to be determined, so this method can also be used in case of uneven fat deposition, unlike MRS (74).

The signal of the fat fraction is distorted by a number of distributing factors, which can hinder the accurate assessment of the fat content, such as T1 distributing effect and the T2* distributing effect (74). Proton density fat fraction measurement eliminates these distributing factors by using a small tilt angle (<20 degrees) and by taking into account the signal intensity peaks from different fat components with the so-called complex curve fitting (75). The MRI-PDFF measurement is most often measured on the basis of T2-weighted multi echo gradient echo MRI images.

If all complicating factors are eliminated when measuring the fat signal fraction, then the proton density is equal to the fat fraction, which can be considered a reliable biomarker of steatosis hepatis. It is important to note that this is not the same as the in-vitro fat content measured by chemical methods, since the liver lipids are also present in a bound form (e.g. in the membranes), which cannot be measured by MRI (76). It is also not equal to the degree of steatosis determined by histology, although it shows a strong correlation with both values (77).

At its 2012 event, the representatives of 13 countries of the International Society of Magnetic Resonance in Medicine agreed that the PDFF technique was chosen as the most reliable and practical MR-based biomarker for the detection and quantification of fatty liver (74).

1.5. QUANTITATIVE ULTRASOUND FOR DIAGNOSING DIFFUSE LIVER DISEASES

Recently, several new US examination techniques have been introduced into clinical practice, which can be used to collect quantitative information on diffuse liver diseases. The QUS techniques can significantly reduce the subjectivity and improve intra- and interobserver agreement of US diagnosis (78,79). QUS markers also make it easier to compare US with other imaging techniques and serum biomarkers. Eventually, QUS methods can be tailored into disease specific examination protocols, aimed at quick,

focused, non-invasive and highly reproducible evaluation of the liver facilitating the screening, diagnostic work up and follow up of patients with diffuse liver diseases (80,81). Although some QUS techniques require specialized instrumentation, in general, modern US scanners can perform conventional morphological and functional evaluation simultaneously with QUS measurements. Therefore, there is a good chance that at least a subset of the QUS methods will be rapidly added to routine scanning protocols and could transform clinical practice.

1.5.1. Quantitative Ultrasound Biomarkers Of Liver Fibrosis

Fibrotic remodeling in advanced chronic liver disease (ACLD) leads to increased stiffness of the liver parenchyma (82). This is a well established diagnostic sign of liver fibrosis, which has been traditionally detected by palpating the liver edge below the rib cage. In recent times, various types of elastography techniques have been developed capable of non-invasive measurement of the elastic compressibility, otherwise known as elasticity of human tissues (83). The LS has become a non-invasive biomarker, and it is defined as the elastic compressibility or Young modulus of the tissue, which is measured in kilopascal (kPa). The most commonly used approach for measuring the Young modulus (*E*) is to detect the propagation speed of the elastic deformation waves, also known as shear waves in the tissue using different types of imaging modalities (84). When a static force is applied to a tissue, the longitudinal elastic deformation can be either imaged directly, this is called acoustic radiation force impulse (ARFI) elastography, or when a dynamic force is applied and shear waves arise and travel perpendicular to the axis of the force, the propagation speed (c_s) of the shear waves can be recorded, this is the common basis of the TE, SWE and MRE methods (85–87). The c_s of shear waves is in the range of 1 to 10 m/s in most of the tissues, and it can be determined by detecting the displacement of the tissue segments as a function of time. The c_s is directly proportional to tissue stiffness, and the Young modulus can be calculated from c_s using the simplified formula:

$$E = 3 * \rho * cs^2$$

where E is the Young modulus, ρ is the tissue density, and c_s is the propagation speed (84). It is important to remark that shear waves do not propagate in non-viscous fluids; therefore, vessels, cysts and other structures filled with clean fluid should be avoided during selection of the site of the measurement.

US is the most commonly used imaging modality for SWE. During SWE, the ARFI is emitted by the same US probe, which is also used for imaging; and the focused acoustic impulse causes displacement of a few micrometers in the liver tissue. Repeated ARFI pulses cause subtle resonation and generate shear waves. During SWE the c_s is recorded in m/s and also converted to kPa for easier interpretability. Point shear wave elastography (pSWE) is the technique when the E is determined as a single value for a tissue segment without mapping of regional variations (88). Conversely, two-dimensional shear wave elastography (2D-SWE) is when E is measured at multiple points in a tissue segment and regional variations are displayed on a color-coded heatmap (1). TE has been used for liver elastography for the longest time and it also detects shear wave propagation with US. An important difference compared to SWE is that TE uses a small plastic piston to generate resonation in the liver through the skin surface, and detects the shear wave propagation with a single US beam (89,90). TE can only be performed with a specialized device marketed as the FibroScan® and it does not image the liver morphology.

Currently TE is the most commonly used elastography technique in clinical practice (90). A TE scan performed by a trained technician in a short time, at the bedside or outpatient clinic. It has excellent intraobserver reproducibility in large case series, and a good detection rate of advanced fibrosis. The failure rate of TE 3.1% has been reported for TE, and in 15.8% the measurement did not meet the <30% threshold of the interquartile range median (IQR/med.) ratio deemed necessary for a reliable result (89). TE measurements can be more difficult to perform in obese patients who have a BMI > 28; also various conditions, which increase the hydrostatic pressure of the liver parenchyma including active hepatitis, extrahepatic cholestasis, or heart failure can alter fibrosis measurements (5). Postprandial status also can result in a falsely elevated LS reading; therefore, elastography measurement should be performed after at least two hours of fasting. The effect on steatosis on elastography measurements is still unclear, as conflicting results have been reported.

The SWE methods, which combine elastography with grayscale US imaging and instead of a surface resonator use a focused ARFI impulse to generate shear waves, have managed to overcome some of the drawbacks of TE (86). The size and the exact location of measurement can be controlled by the examiner during SWE; thus, the failure rate of SWE (2.9% vs. 6.4%, $p < 0.001$) is significantly lower compared to TE (5). Furthermore, SWE can be performed in patients with ascites, as ARFI pulses can travel through fluids unobstructed. A significant obstacle standing in the way of widespread use of SWE in clinical practice has been the differences in the technical specifications of the scanners resulting in variations in the diagnostic thresholds. Recently, a group of experts came up with a vendor neutral diagnostic criteria named as the "rule of four", which can be applied universally in chronic viral hepatitis and NAFLD and defines the threshold of normal LS as <5 kPa (1.3 m/sec) , and <9 kPa (1.7 m/sec) in the absence of clinical signs as strong indicator of no significant liver fibrosis, while ≥ 13 kPa (2.1 m/sec) as the threshold for diagnosing compensated ACLD (91). It also recommends follow-up and additional testing of patients with an indeterminate LS measurement between 9 kPa and 13 kPa. Highly elevated liver elasticity is also an independent risk factor of PH and shortened survival in ACLD. The patient group, in which a combination of LS ≥ 20 kPa, and model for end stage liver disease (MELD) score ≥ 10 was detected, had both much higher 2-year mortality and decompensation rates compared to patients without these risk factors (92). In addition, the Baveno VI Consensus Conference in 2015 defined the criteria of high-risk compensated ACLD patients who have to be screened with endoscopy for esophageal varices needing treatment (VNT) as LS measured with TE ≥ 20 kPa and platelet count 150×10^9 cells/L (93). Since then, multiple studies have also confirmed the usefulness of the Baveno VI criteria in ruling out VNTs using SWE (1,94). The updated Baveno VII criteria modified the diagnostic criteria to LSM by TE ≤ 15 kPa plus platelet count ≥ $150x10^9$/L, which could rule out clinically significant PH with .> 90% sensitivity and NPV (95). There is also growing evidence that both SWE and TE can be used for following patients and reassessing the risk from complications of compensated ACLD after successful antiviral treatment in chronic HCV and HBV hepatitis.

Current clinical guidelines universally agree that for initial assessment of liver fibrosis non-invasive diagnostic methods should be used including serum markers, TE and SWE in chronic viral hepatitis and NAFLD (96). Meanwhile, there is also agreement between

the guidelines that LS values measured in ACLD should be interpreted by expert clinicians who also take the etiology, clinical findings and reliability of the LS measurement into consideration. The same guidelines also include several other recommendations (80). The same quality assurance criteria should be applied to both TE and SWE when deciding on the reliability of the results: IQR/med. < 30%, serum transaminase levels < 5x of the upper limit of normal (ULN), absence of extrahepatic cholestasis, heart failure and ongoing excess alcohol consumption. The combination of elastography and serum markers should be used for initial assessment of liver fibrosis. Liver cirrhosis is the clinically most important endpoint in all etiologies of ACLD including chronic viral hepatitis, NAFLD, alcoholic liver disease (ALD) and chronic cholestasis. Elastography is superior to serum markers for the detection of liver cirrhosis. The diagnostic performance of SWE is similar to TE as both of these methods perform better for detecting cirrhosis than significant fibrosis. SWE, which has >90% negative predictive value (NPV), is more useful to rule in than to rule out liver cirrhosis (5,96,97). Both TE and SWE are more extensively tested, and more reliable to diagnose fibrosis in chronic viral hepatitis than in NAFLD. Patients diagnosed with cirrhosis based on non-invasive tests should be followed with US and screened for HCC and PH (98) .

1.5.2. Quantitative Ultrasound Biomarkers Of Hepatic Steatosis

QUS is a new, emerging field in the US diagnosis of CLD. Conventional B-mode images show only a fraction of information carried by radiofrequency data (RF) about physical properties of the liver tissues. The aim of QUS imaging is to assess the various acoustic parameters, which contribute to reflectivity and acoustic impedance, separately as they can correlate at different levels with pathophysiological processes. Multiple new QUS techniques have been proposed for fat quantification including the attenuation coefficient (AC), backscatter coefficient (BSC), speckle distribution statistics, speed of sound (SS) and LS (99). These parameters can be measured with modern US scanners guided by B-mode imaging, or with the FibroScan® instrument at the time of TE, allowing for fast, complex, non-invasive evaluation of CLD (81).

The US waves lose more energy traveling through fat than soft tissues. By losing their energy, high-frequency sound waves are filtered out at lower tissue depths than low-frequency waves causing a shift in the median frequency of the reflected signal. Two

principal methods have been developed to quantify acoustic attenuation; these are the controlled attenuation parameter (CAP) and the sonographic attenuation imaging (ATI) (79). The CAP is the most commonly used method for non-invasive quantification of HS; and the measurement is performed during TE with the FibroScan® instrument. The CAP is calculated together with LS using the same RF data, and it is expressed in dB/m units (100). CAP has been extensively validated by studies conducted on large patient cohorts, which have shown that CAP is strongly correlated with the grade of HS determined with liver biopsy and MRI-PDFF (101). Various studies have reported different diagnostic accuracies for CAP; in a meta-analysis summarizing the findings of 19 studies in 2735 patients, based on area under the receiver operating curve (AUC) values, CAP had a 0.823, 0.865, and 0.882 accuracy for ≥ S1, S2 and S3 steatosis grades indicating a good diagnostic performance (102).

B-mode US guided measurement of AC is now available from most vendors of commercial US scanners. The physical principle of AC measurement is identical to CAP; however the technical specifications are different impeding the direct comparison between AC and CAP values. Also, AC is expressed in dB/cm/Mhz units. AC has been compared with MRI-PDFF and biopsy for grading of HS, and could diagnose HS with a 0.76 - 0.98 AUC accuracy depending on reference method and steatosis severity (99). TAI also measures AC on B-mode US and it has been validated against MRI-PDFF in two studies, which have reported highly similar diagnostic accuracies 0.89 and 0.86 for ≥5% and 0.93 and 0.84 for 10% HS in different ethnic groups(13,99) .

Scattering of the reflected sound waves adds noise to B-mode US; therefore, scatter is filtered out to improve image quality. Meanwhile, the intensity of the scattered speckles depends significantly on the physical parameters of the tissue. When the probability distribution of the scattered sound intensities is displayed on a histogram the signal envelope follows a Rayleigh distribution. An increased amount of fat results in a shift of the envelope statistics to a post-Rayleigh distribution, while decrease of fat as well as the presence of fibrosis change the envelope statistics to a pre-Rayleigh distribution (103). The shift in the envelope statistics can be quantitated by calculating the Nakagami parameter. A Nakagami parameter from 0 to 1 indicates pre-Rayleigh and a parameter larger than 1 indicates a post-Rayleigh distribution of the signal intensities (78). Another method to evaluate the change in signal intensity distribution is called acoustic structure

quantification (ASQ), which measures the difference between the theoretical and real envelope distributions (104). TSI is calculated based on the Nakagami parameter and it showed a good correlation with both CAP (r = 0.68), and MRI-PDFF (r = 0.68 - 0.73). According to recent studies, TSI also showed excellent performance for the diagnosis of ≥ 5% and 10% HS with AUCs of 0.87 - 0.96 and 0.86 - 0.94, respectively (13,105). The effect of fibrosis on TSI has not been clearly determined, and contradicting data have been reported.

The BSC is a quantitative measure of the "brightness" of the liver parenchyma, which increases in HS due to larger intensity of the reflected US signal. The BSC strongly correlates with HS and can be used to diagnose HS with good accuracy (106). However, BSC measurement has only been tested in an experimental setup with custom made software.

An important future direction in HS quantification with QUS is measurement of an ultrasound-derived fat fraction (UDFF). The UDFF can be either calculated from AC and BSC parameters using multivariable regression models or directly estimated from RF data with a deep learning algorithm (107,108). Introduction of UDFF can simplify the interpretation of QUS results and improve comparability between results obtained by different types of scanners. Also, QUS may be able to differentiate between simple HS from NASH in at risk NAFLD patients (109).

2. OBJECTIVES

Examination of the ultrasound measurement of fatty liver is important during the follow-up of patients treated for chronic HCV infection or NAFLD. Fibrosis and fatty liver are common complications of multi-metabolic syndrome, chronic viral hepatitis, and other chronic liver diseases. QUS parameters may facilitate earlier, more accurate and more reproducible than B-mode ultrasound, and may substitute for liver biopsy in the diagnosis and follow-up of CLD.

Our hypothesis is that LS may improve or return to the normal range after successful antiviral therapy of HCV patients due to regression of inflammatory activity and liver fibrosis. 2D-SWE can be used to assess therapeutic response in chronic hepatitis C patients who attained sustained virologic response (SVR) after DAA treatment, and can be used to identify a subset of patients who need continued screening for PH and VNT. Therefore, our first aim is to follow-up a group of patients treated for chronic HCV infection with 2D-SWE and monitor changes in LS and correlate them with clinical status and serum markers.

We also hypothesize that QUS parameters including TAI and TSI can be applied for diagnosing HS in patients with risk factors of NAFLD, and that QUS parameters diagnostic performance is comparable to the MRI-PDFF, which is a gold-standard method of fat quantification. Therefore our second aim is to determine the diagnostic thresholds for low-grade and moderate HS and examine the interobserver reproducibility of TAI and TSI in patients with clinically suspected NAFLD or secondary HS.

3. METHODS

3.1. SHEAR WAVE ELASTOGRAPHY IN CHRONIC HCV INFECTION

Our research was approved by the Regional and Institutional Research Ethics Committee of Semmelweis University (SE-RKEB-140/2020). The patients participating in our prospective research signed a written consent form in accordance with the Helsinki Declaration established by the World Medical Association.

3.1.1. Patient Population

We included 35 patients in our research, all of whom were diagnosed with chronic HCV infection. The patients were treated and followed up by the doctors of the Department of Internal Medicine.

The final patient cohort included 19 males and 16 females. Their average age at the end of our research was 61 years. The inclusion criteria were the following: the HCV infection had to be proved with anti-HCV antibody and HCV RNA positivity, patients had to accept to get antiviral therapy and have attained SVR after the antiviral therapy, the patients also had to be above the age of 18 years. Patients were excluded, if they have extrahepatic cholestasis, congestive heart failure, HCC, BMI above 30 kg/m^2, pregnancy, breastfeeding or if the SWE measurements were unsuccessful.

Previous data on the degree of fibrosis, as well as liver function tests and serum enzyme levels were obtained from the patients' previous documentation and the Hepatitis Register, and the BMI index was also determined for the examined patients.

Our patients are treated by the 1st Department of Internal Medicine Clinic with direct antiviral preparation based on domestic professional protocols. The following drugs were used: ombitasvir/paritaprevir/ritonavir/dasabuvir (n=15); sofosbuvir/ledipasvir/ribavirin (n=10); sofosbuvir/ledipasvir (n=5); peginterferon alfa-2a/ribavirin (n=2); glecaprevir/pibrentasvir (n=1); sofosbuvir/simeprevir (n=1); peginterferon alfa-2a/ribavirin/boceprevir (n=1).

3.1.2. Shear Wave Elastography Measurements

We used A Samsung RS85 Prestige US scanner (Samsung Medison, Hongcheon, Korea) equipped with the CA1-7A convex probe. S-Shearwave™ application was applied during the SWE measurements following the recommended protocol. Only measurements with a reliable measure index (RMI) more than 0.4 were accepted. The examination was successful, if the interquartile range of the individual measurement was less than 30% of the median, and we could collect at least 5 reliable LS values (Figure 9).

Before the treatment, based on TE, or in some patients SWE values, we determined the liver fibrosis stage according to METAVIR categories. TE and SWE measurement results before treatment were collected by the Hepatitis Register System. The limit values of the METAVIR categories were determined based on previously published studies. We used the following cutoff values: F0/1<1.46 m/s; F2≥1.46 m/s; F3≥1.63m/s; F4≥1.95 m/s (88).

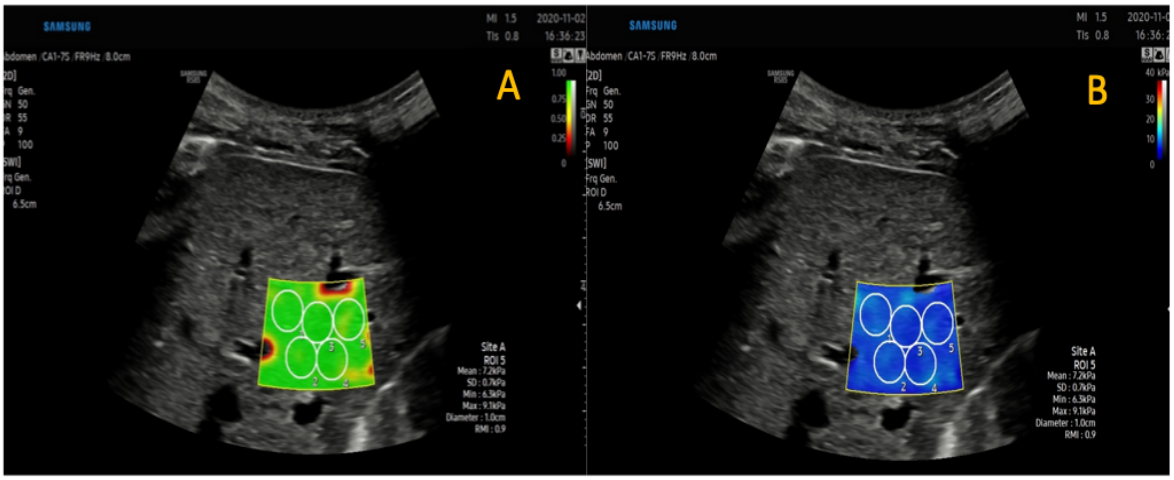

Figure 9. *Liver stiffness measurement with 2D SWE of a liver without significant fibrosis*

A: Color-coded map of RMI we used for the selection of ROI. B: SWE measurement of the liver.

3.1.3. Laboratory Tests And Clinical Data

We collected the following laboratory test results of all the patients from electronic medical records at the baseline and after the treatment: serum creatinine, sodium (Na),

AST, ALT, GGT, albumin levels, platelet count, total bilirubin, international normalization ratio (INR).

We used AmpliPrep/COBAS, TaqMan version 2 assay (Roche, Pleasanton, CA, USA) to detect the HCV RNA in the serum. After treatment SVR was undetectable at both 24 and 48 weeks. With the help of MDCalc (www.mdcalc.com), we calculated the FIB4, the MELD and the Child-Turcotte-Pugh (CTP) scores. The patients were also divided into 2 groups: low-risk and high risk groups of esophageal varices needing treatment (VNT), following the Baveno VI guidelines (Figure 10) (93).

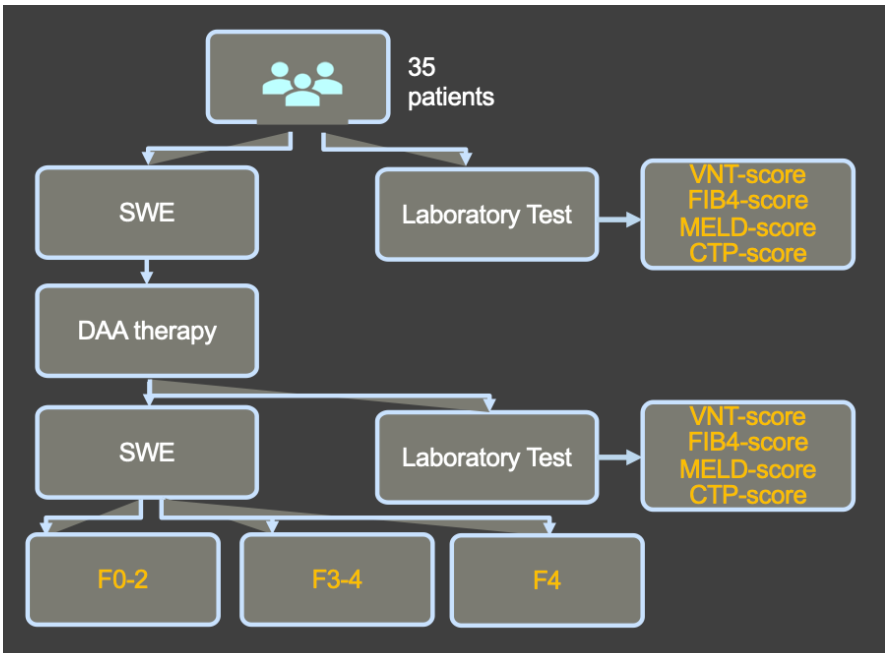

Figure 10. *Prospective study flowchart. We involved 35 patients to the study, who had the diagnosis of chronic HCV infection, and attained sustained virological response with DAA agents or interferon-based treatment. SWE was performed before the DAA therapy, and 48 weeks after successful antiviral treatment. METAVIR score of liver fibrosis was also determined both before and after the treatment for all the patients. The number of patients with VNT, the FIB4-score, the MELD-score and the CTP class were calculated from the results of the laboratory.*

3.1.4. Statistical analysis

To compare LS values and laboratory parameters before and after the DAA therapy we used the paired Student's-test. Fisher's exact test was also performed, to compare the categorical variables distributions such as cirrhosis stage. The odds ratios (OR) are reported together with the confidence intervals (CI) of 95%. We have reported the mean and the standard deviation in case of continuous variables, and the frequency and percentage in case of categorical variables. We used the R x64 v3.4.1 software package (www.r-project.org) for statistical analysis (1).

3.2. MEASUREMENT OF FATTY LIVER IN NAFLD PATIENTS

Our research was approved by the Regional and Institutional Research Ethics Committee of Semmelweis University (SE-RKEB-140/2020). The patients participating in our prospective research signed a written consent form in accordance with the Helsinki Declaration established by the World Medical Association.

3.2.1. Patient Population

In our prospective research, we included patients referred to the Medical Imaging Centre for abdominal US and/or MRI examination between July 2020 and September 2022 due to a diagnosis of fatty liver. Data on the height, weight, alcohol consumption, and other liver diseases of the patients were recorded when the patient history was taken before the examinations. Liver enzyme values were collected retrospectively from laboratory test results stored in the Medsol computer system. The exclusion criteria were the following: age under 18 years, active hepatitis, ascites, acute biliary obstruction, decompensated liver disease (CTP score>7 points), excessive alcohol consumption (for men >30g alcohol/day, for women >20g alcohol/day). Morbidly obese patients who were not suitable for examination with the MRI device were excluded. Patients who were previously diagnosed with hereditary hemochromatosis based on genetic test, and those patients whose liver showed an abnormal level of iron accumulation (>2mg/g) during the MRI examination, were also excluded from the research.

The final patient group consisted of 101 patients, of whom 49 were men and 52 were women. 62 of the patients came to the examination with a presumptive diagnosis of NAFLD based on their clinical symptoms in accordance with European professional recommendations (9). An additional 39 patients were investigated due to the suspicion of NAFLD of secondary origin. 22 of them were treated with chemotherapy agents with hepatotoxic side effects, 9 had a history of chronic HCV infection, which became virus-free as a result of successful antiviral treatment, 4 patients were being treated for chronic autoimmune hepatitis, and 4 more patients were diagnosed with Wilson's disease (Table. 3).

Table 3. *Population if the patient population according to hepatic steatosis (13).*

	All participants with suspected HS			
	All patients	**Controll (<5% MRI-PDFF)**	**NAFLD (>5% MRI-PDFF)**	**p-value**
Total (n)	101	47	54	-
Male (n)	49/101 (48.51%)	27/47 (57.45%)	22/54 (40.74%)	0.0938
Age* (yrs)	56.4 ± 12.4	58.1 ± 10.9	54.2 ± 14.0	0.3131
Female (n)	52/101 (51.49%)	20/47 (42.55%)	32/54 (59.26%)	-
Age* (yrs)	56.9 ± 12.0	53.7 ± 13.1	59.0 ± 10.9	0.1514
p-value for age between sex	0.6935	0.3309	0.2232	-
Secondary etiology:				
Chemotherapy	22/101 (21.78%)	14/47 (29.79%)	8/54 (14.81%)	
Chronic HBV/HCV infection	9/101 (8.91%)	8/47 (17.02%)	1/54 (1.85%)	
Autoimmun hepatitis	4/101 (3.96%)	2/47 (4.26%)	2/54 (3.70%)	
Wilson disease	4/101 (3.96%)	1/47 (2.13%)	3/54 (5.56%)	
	suspected NAFLD			
Total (n)	62	22	40	-
Male (n)	28/62 (45.16%)	10/22 (45.45%)	18/40 (45.00%)	0.9725
Age* (yrs)	55.3 ± 14.0	55.1 ± 13.9	55.4 ± 14.5	0.8667
Female (n)	34/62 (54.83%)	12/22 (54.55%)	22/40 (55.00%)	-
Age* (yrs)	56.5 ± 12.6	48.3 ± 12.8	60.9 ± 10.2	0.0041
p-value for age between sex	0.5522	0.4872	0.2765	-

3.2.2. Fatty Liver Measurement With Quantitative Ultrasound Examination

The ultrasound examinations of the patients were performed at the Medical Imaging Clinic using a Samsung RS85 Prestige ultrasound device (Samsung Medison, Hongcheon, Korea). The tests were performed by a radiologist with more than 10 years of experience in abdominal ultrasound diagnostics. During the examination, the patients were placed in a supine position, with their right arm raised above their head. During the examination, a CA 1-7A convex probe was used, and the right lobe of the patient's liver was examined from an intercostal view during medium inhalation using a B-mode image. The TAI and TSI measurements were performed using the quantitative imaging mode of the ultrasound equipment. During the measurements, based on the B-mode, 5-5 pieces of ROI were placed in the liver parenchyma (taking care to avoid the blood vessels), at least 1.5 cm from the liver capsule. During the TAI measurement, the tissue signal intensity obtained on the basis of the ultrasound signals reflected from the tissues is displayed as a colored heat map on the display. While the color heat map created during the TSI test shows the amount of ultrasound signals backscattered by the tissues compared to the amount of Rayleigh scattering. For each measurement, we recorded the average TAI and average TSI value of the designated area. We performed 5 measurements per patient, and the median value of the 5 measurements was used to measure liver fat. In order to demonstrate the effect of abdominal obesity on the quantitative ultrasound measurement results, the distance between the liver and the skin surface, the capsule to skin distance (CSD) was also measured in all cases with the help of B-mode ultrasound image.

In order to investigate the reproducibility of the new quantitative measurement techniques, a resident radiologist with 4 years of experience repeated the TAI and TSI measurements on the same day in the case of 52 patients. The two examiners performed the measurements independently, without knowing each other's results or knowing the patient's liver fat percentage determined by MRI-PDFF. During the ultrasound examination, in the case of 98 patients, the S-Shear Wave Imaging^{TM} mode of the equipment was used to simultaneously measure LS using 2D-SWE technique. TAI values are expressed in dB/cm/MHz units, TSI values are expressed without units, and liver softness values are expressed in kPa units.

3.2.3. Fatty Liver Measurement With Magnetic Resonance Imaging

Abdominal MRI images were taken of the examined patients with Philips Ingenia 1.5 T MRI device (Philips Healthcare, Amsterdam, the Netherlands) using a Q-Body coil. During the examination, in addition to the sequences included in the routine abdominal MRI examination, a multi-echo gradient echo sequence was also prepared from the axial slices of the liver. During the MRI-PDFF examination, the main parameters were the following: slice thickness 7 mm, distance between slices 10 mm, repetition time 120 msec, FOV: 400x350, reconstruction matrix: 128x116 pixels. In order to reduce the T1 effect, we chose a small deflection angle (flip angle: 20 degrees). The tests were carried out using a total of 12 different echo times. The smallest echo time was 1.2 msec, the echo times were increased in steps of 1.2 msec.

After the MRI examination, the MRQuantif software was used to calculate the proton density-based fat fraction of the liver (https://imagemed.univ-rennes1.fr/en/mrquantif). For each echo, we measured the signal intensity of the liver (3 ROIs), the signal intensity of the spleen (1 ROI), the signal intensity of the paraspinal muscles (2 ROIs) and the background noise (1 ROI). The MRI-PDFF values were calculated using the complex curve fitting method of Hernando et al. (75). The software uses R2* values and MRI-PDFF values published by Hamilton et al , calculated with the help of the exponential attenuation model (Figure 11) (71).

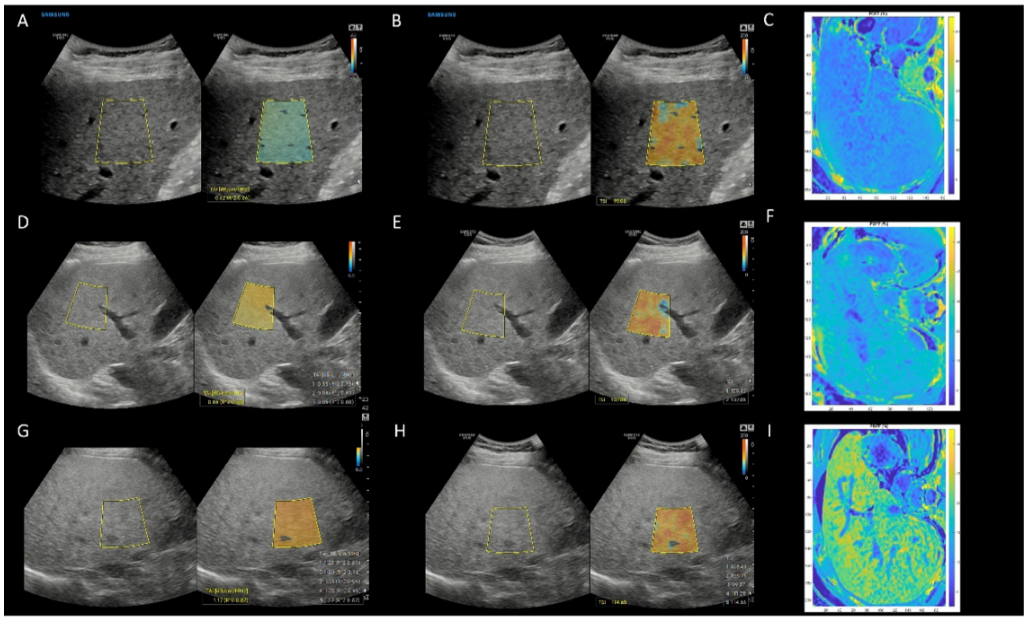

Figure 11. *QUS examination of the liver and fat measurement based on MRI-PDFF*
The patients' TAI and TSI values were determined during a QUS examination using a Samsung RS85 device (A and B). Visual reference was created from the MRI-PDFF values calculated based on the multi-echo Dixon sequence measured during the abdominal MRI examination according to the axial slices, where the liver parenchyma showing an MRI-PDFF value of less than 5% was depicted in blue (C). MRI-PDFF of 5-10% had higher TAI and TSI values compared to those without steatosis (D and E). The MRI-PDFF contour map showed green color. (F). MRI-PDFF values more than 10%, TAI and TSI showed the highest values (G and H). MRI contour map indicated steatosis of the liver parenchyma with yellow color. (I).

The MRI-PDFF values are expressed as a percentage, which indicates the percentage of fat-bound protons compared to the total (water-bound and fat-bound) protons. Finally, in order to visualize the result of the MRI-PDFF measurement and examine the heterogeneity of steatosis within the parenchyma, the MRI-PDFF values were calculated by Bydder et al developed by Matlab (The Mathworks, Natick Ma, USA) with the help of the "pdff" program (https://github.com/marcsous/pdff), we projected it back onto the original MRI recording, resulting in a color map.
Based on the MRI-based PDFF measurement results, the patients were diagnosed with steatosis using a 5% threshold in accordance with the currently valid professional recommendations. In accordance with previous research, we used an MRI-PDFF threshold of >10% to define severe steatosis (101,105)

3.2.4. Statistical Analysis

The normal distribution of continuous variables was examined with the Shapiro-Wilk test. Comparing the patient group diagnosed with steatosis (25% MRI-PDFF) and non-steatotic (<5% MRI-PDFF), categorical variables were analyzed with the chi-square test, and continuous variables with the Mann-Whitney U-test. The patients were classified into three groups based on the severity of steatosis, the difference in continuous variables between the groups was examined using the Kruskal.Wallis test and post hoc Dunn's test. Due to multiple comparisons between groups, Benjamini-Hochberg correction was performed on p-values. Spearman's correlation analysis was performed to examine the

correlation of clinical parameters. Receiver operating characteristic (ROC) curve analysis was performed to evaluate the diagnostic accuracy of the TAI and TSI ultrasound methods. The cut-off values with the best diagnostic accuracy were identified based on the so-called “closest topleft” point of the ROC curve, based on a formula:

$$\mathbf{- ((1 - sensitivity)^2 + r \times (1 - specificity)^2)}.$$

The diagnostic performance was characterized by the area under the ROC curve (AUC), sensitivity, specificity, positive predictive value (PPV), NPV and accuracy. Univariate and multivariate linear regression analysis was performed to identify con ófounding factors affecting the accuracy of TAI and TSI measurements. The reproducibility of the measurements was examined with intraclass correlation coefficient (ICC) and Spearman's correlation analysis.

Statistical analyzes were performed using RStudio using the R programming language with with the help of the following program packages: (www.r-project.org), “stats”, “dplyr”, regclass”, “pROC”, “spearmanCI”, “dunn.test”, and “irr”.

4. RESULTS

4.1. FOLLOW-UP OF LIVER STIFFNESS

4.1.1. Liver Stiffness Changes After Successful Antiviral Treatment

The average liver elastography value of the patients was LS=20.04 kPa ± 11.68 (2.59±0.89 m/s) before the treatment, which value changed to LS = 11.34 kPa ± 5.56 (1.90±0.50 m/s) after the treatment, which change proved to be significant ($p<0.001$) (Figure 12).

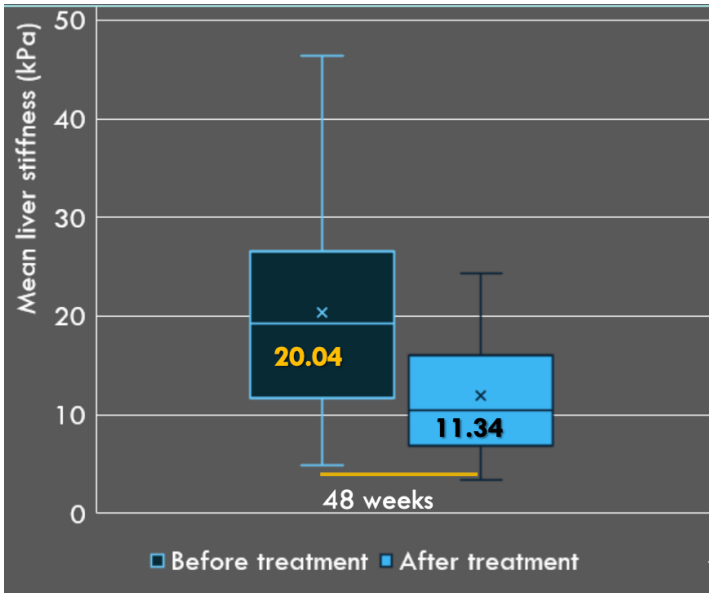

Figure 12. *Average liver hardness values measured in our patients. The shear wave elastography was repeated an average 48 weeks. Compared to the matched values before treatment the LS was significantly lower at 48 weeks after the end of the antiviral treatment .*

Patients whose LS value is above 20 kPa are at high risk of developing complications, their number in the examined patient group decreased as a result of treatment. The METAVIR score was calculated based on the SWE measurements, and it showed notable improvement ($p < 0.028$) after the antiviral therapy (F0/1=9; F2=2; F3=10; F4=14) compared to the baseline (F0/1=2; F2=1; F3=7; F4=25) (Figure 13) (Table 4).

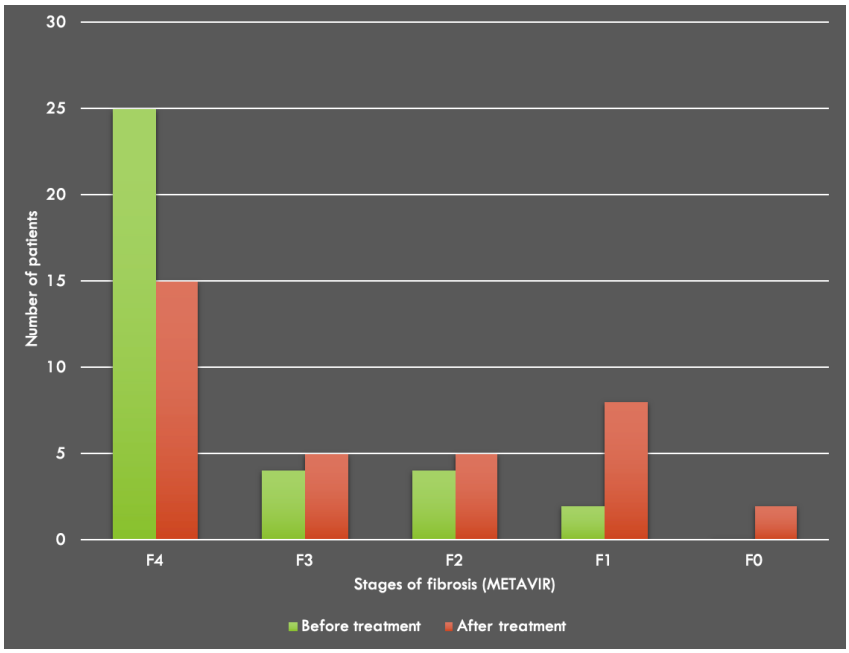

Figure 13. *Distribution of the patients according to METAVIR stages, direct antiviral treatment before (green) and after (red).*

	Baseline	**EOT48w***	**p-Value****	**Odds-Ratio**
LS	20.04 ± 11.68 kPa	11.34 ± 5.56 kPa	$p < 0.001$	NA
METAVIR***			$p < 0.028$	NA
F0/1	2 (5.7%)	9 (25.7%)	$p < 0.045$	5.71 (1.13-28.74)
F2	1 (2.8%)	2 (5.7%)	$p < 1.00$	2.06 (0.18-23.82)
F3	7 (20%)	10 (28.6%)	$p < 0.578$	1.60 (0.53-4.83)
F4	25 (71.4%)	14 (40%)	$p < 0.015$	0.27 (0.09-0.72)

Table 4. *Pre-and post-treatment liver stiffness and METAVIR scores. *48 weeks after the antiviral therapy with SVR. **The paired Student's t-test was used for comparing means between before and after treatment groups; the Fisher's exact test was used for frequencies.*

****METAVIR score was calculated from LS by using cutoff values. NA: not applicable*

The number of the cirrhotic patients was significantly lower (OR=0.27; 95% CI=0.09-0.72; $p < 0.016$) 48 weeks after the successful treatment (Figure 14). The LS improved un 31 out of 35 patients in SVR, and it increased a bit in case of 4 patients, including 2 F2 grade fibrosis patients and 2 cirrhotic patients.

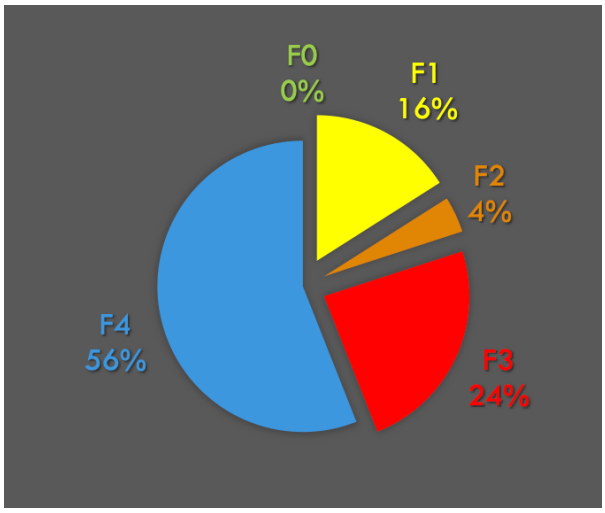

Figure 14. *Patients distribution with initial F4 fibrosis stage after DAA therapy. Based on measurement after treatment, the patients who were initially classified the highest category according to METAVIR, were placed in a 44% lower METAVIR group.*

4.1.2. Laboratory Test Results

The improvement of the monitored liver-specific enzymes and values was also as expected. The liver enzyme values decreased significally as a result of treatment. The ALT level improved after the therapy, and only in two cases it returned to the normal range. The GGT level was elevated in 26 patients before treatment. It decreased to 7 patients after the post-treatment follow-up (OR=0.087; 95% CI=0.03-0.27; $p < 0.001$). AST, total bilirubin, serum creatinine were closer to the normal range after the therapy. Albumin also returned to the normal range in all six cirrhotic patients. The rest of the markers showed no significant improvement (Figure15).

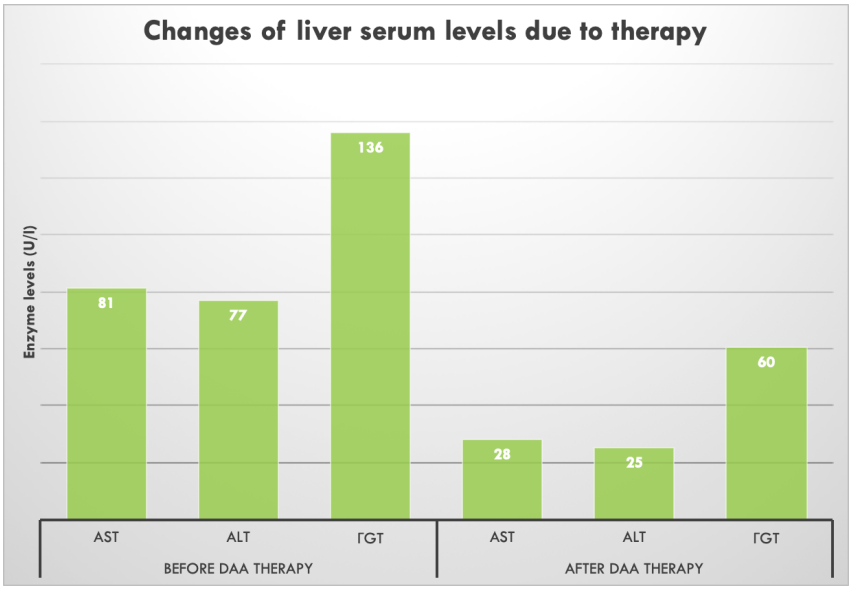

Figure 15. *The liver enzyme values of the patients were in the normal range after the DAA therapy was completed. The change in these parameters clearly shows the moderation of the inflammation taking place in the liver.*

FIB4 score was also calculated, and it also indicated significantly ($p < 0.018$) lower after the treatment compared to the pre-treatment status.

4.2. QUANTITATIVE ULTRASOUND EVALUATION OF HEPATIC STEATOSIS

4.2.1. Diagnosis Of Fatty Liver In The Examined Patient Groups

The final patient population for our research consisted of 101 patients, of whom 49 were men (average age: 56 years, minimum: 36 years, maximum: 78 years) and 52 were women (average age: 57 years, minimum: 24 years, maximum: 76 years). The patients' BMI (standard ± deviation) was 28 kg/m^2 ± 4.37 kg/m^2. Their mean liver stiffness determined by elastography was 9.1 kPa ± 6.0 kPa, while the number of patients with clinically significant (≥F2) liver fibrosis was 34/101 (～34%).

54 of the patients included in the research were diagnosed with steatosis based on MRI-PDFF measurement (≥5% MRI-PDFF), 17 of them showed moderate steatosis (MRI-PDFF 5-10%), and 37 patients showed advanced steatosis (≥10% MRI-PDFF). 62

patients were previously diagnosed with NAFLD during their examination by their internist, of whom we found clinically significant steatosis in 40 patients (≥5% MRI-PDFF), 13 of whom had moderate steatosis (5-10% MRI-PDFF), and 37 of whom were diagnosed with advanced steatosis (≥10% MRI-PDFF).

Among the laboratory parameters, transaminase levels did not show significant differences between the patient groups (Table 5). While <55 MRI-PDFF group AST and ALT were 39.3 U/L ± 23.8 U/L and 41.5 U/L ± 44.6 U/L, in the 5-10% MRI-PDFF group AST was 28.3 U/L ± 8.6 U/L and ALT was 32.9 U/L ± 17.5 U/L, and in the ≥10% MRI-PDFF group AST was 47.9 U/L ± 47.4 U/L, and ALT was 59 U/L ± 53.9 U/L.

Table 5. *Development of clinical parameters according to fatty liver stages. *p-values were corrected according to the Benjamini-Hochberg method; ** standard ± deviation; *** median; interquartile range*

Parameters	**Patients with suspected HS**	**<5% MRI-PDFF**	**5-10% MR-PDFF**	**>10% MRI-PDFF**	**Kruskal-Wallis test p-value**	**Dunn test p-value* <5% vs. 5-10%**	**Dunn test p-value* 5-10% vs. >10%**	**Dunn test p-value* <5% vs. >10%**
PDFF**	9.42% ± 9.15%	2.38% ± 1.30%	7.27% ± 1.66%	19.34 ± 7.49%	-	-	-	-
TAI** (dB/cm/MHz)	0.811 ± 0.167	0.697 ± 0.10	0.789 ± 0.082	0.965 ± 0.141	<0.0001	0.0090	0.0005	<0.0001
TSI**	98.167 ± 11.541	90.7 ± 11.5	101.0 ± 7.04	106.0 ± 5.57	<0.0001	0.0025	0.0155	<0.0001
BMI** (kg/m^2)	28.0 ± 4.37	26.4 ± 4.61	28.9 ± 2.79	29.7 ± 3.97	0.0028	0.0330	0.3168	0.0015
CSD** (cm)	2.06 ± 0.49	1.92 ± 0.50	2.10 ± 0.38	2.22 ± 0.48	0.0092	0.1128	0.1880	0.0036
AST** (U/L)	41.409 ± 34.550	39.3 ± 23.8	28.3 ± 8.59	47.9 ± 47.4	0.3774	0.2266	0.2456	0.2787
ALT** (U/L)	47.457 ± 47.157	41.5 ± 44.6	32.9 ± 17.5	59.0 ± 53.9	0.0521	0.4988	0.1078	0.0297
LS*** (kPa)	7.0; 4.9	7.9; 5.80	6.0; 3.3	6.55; 3.25	0.365	0.2456	0.3231	0.2318
	NAFLD							
PDFF**	10.86% ± 9.71%	2.27% ± 1.22%	7.30% ± 1.83%	19.56% ± 8.43%	-	-	-	-
TAI** (dB/cm/MHz)	0.822 ± 0.158	0.682 ± 0.079	0.792 ± 0.086	0.950 ± 0.126	<0.0001	0.0133	0.0028	<0.0001
TSI**	100.784 ± 9.947	91.6 ± 9.67	102.0 ± 6.21	108.0 ± 4.44	<0.0001	0.0069	0.0167	<0.0001
BMI** (kg/m^2)	28.1 ± 4.37	26.0 ± 4.77	28.8 ± 2.37	29.4 ± 4.33	0.03487	0.0533	0.3913	0.0194
CSD** (cm)	2.05 ± 0.46	1.85 +/- 0.44	2.16 +/- 0.40	2.15 +/- 0.47	0.02171	0.0239	0.4709	0.0172
AST** (U/L)	38.520 ± 31.659	40.1 ± 31.1	29.6 ± 9.07	40.3 ± 36.7	0.8758	0.4944	0.5457	0.9583
ALT** (U/L)	45.960 ± 40.592	44.2 ± 46.2	33.9 ± 18.4	51.0 ± 42.0	0.4111	0.4599	0.2950	0.3224
LS*** (kPa)	6.2 ± 3.4	6.48; 3.6	6.0; 3.3	6.2; 2.27	0.9112	0.4668	1.0000	0.5499

4.2.2. Examination Of TAI In The Detection Of Hepatic Steatosis

Using Spearman's correlation test, we found an excellent, significant correlation between TAI and MRI-PDFF measurement results (p=0.78 ; 95% CI= 0.7012-0.8523; p<0.001). The TAI values showed a steady increase with the increase in fat content determined on the basis of MRI-PDFF, during linear regression analysis we found a significant positive correlation (β=0.39; p<0.001; R^2=0.51) between the two variables. The TAI values also showed a significant difference between the three steatosis groups (Figure 16). The 5-10% MRI-PDFF steatosis group showed significantly higher TAI values compared to the <5% MRI-PDFF group (0.697 dB/cm/MHz ± 0.10 dB/cm/MHz vs. 0.789 dB/cm/MHz ± 0.08 dB/cm/MHz; p=0.009). Also significantly higher TAI values compared to the >10% MRI-PDFF group compared to the 5-10 % MRI-PDFF group (0.789 dB/cm/MHz ± 0.08 dB/cm/MHz vs. 0.965 dB/cm/MHz ± 0.14 dB/cm/MHz; p<0.001) (Table 5).

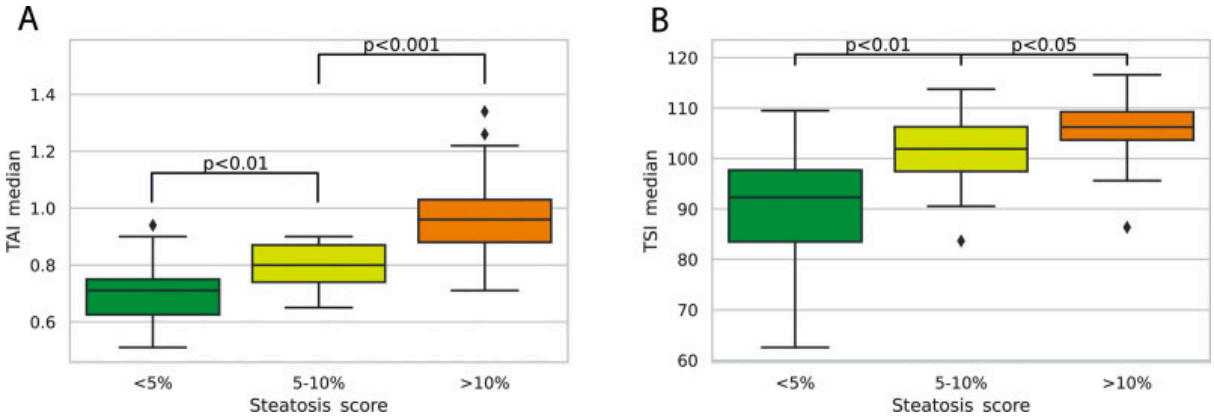

Figure 16. *QUS measurement results according to steatosis stages. Both TAI and TSI showed significant differences in patient groups with <5% MRI-PDFF, 5-10% MRI-PDFF, and >10%-os MRI-PDFF. However, the distribution of TSI values shows a greater overlap between patient groups (13).*

In ROC analysis, TAI showed excellent prediction performance at 25% MRI-PDFF (AUC=0.89, 95%CI=0.83-0.95). The optimal threshold value was 0.765 dB/cm/MHz, at which the accuracy was 82%, the sensitivity 85%, the specificity 79%, the PPV was 82%, and the NPV was 82%. Similarly good results were obtained when examining the detection of ≥10% MRI-PDFF (AUC=0.93 [CI=0.88-0.98]). The optimal threshold here

was 0.845 dB/cm/MHz, in which accuracy was 86%, the sensitivity was 81%, the specificity was 89%, the PPV was 81%, and the NPV was 89%. In cases when only patients diagnosed with primary NAFLD were analyzed, very similar threshold values were obtained. In this case the TAI values showed AUC=0.92 (95% CI= 0.85-0.98) and AUC=0.93 (95% CI= 0.87-0.99). The optional threshold values were 0.760 dB/cm/MHz and 0.845 dB/cm/MHz (Figure 17) (Table 6).

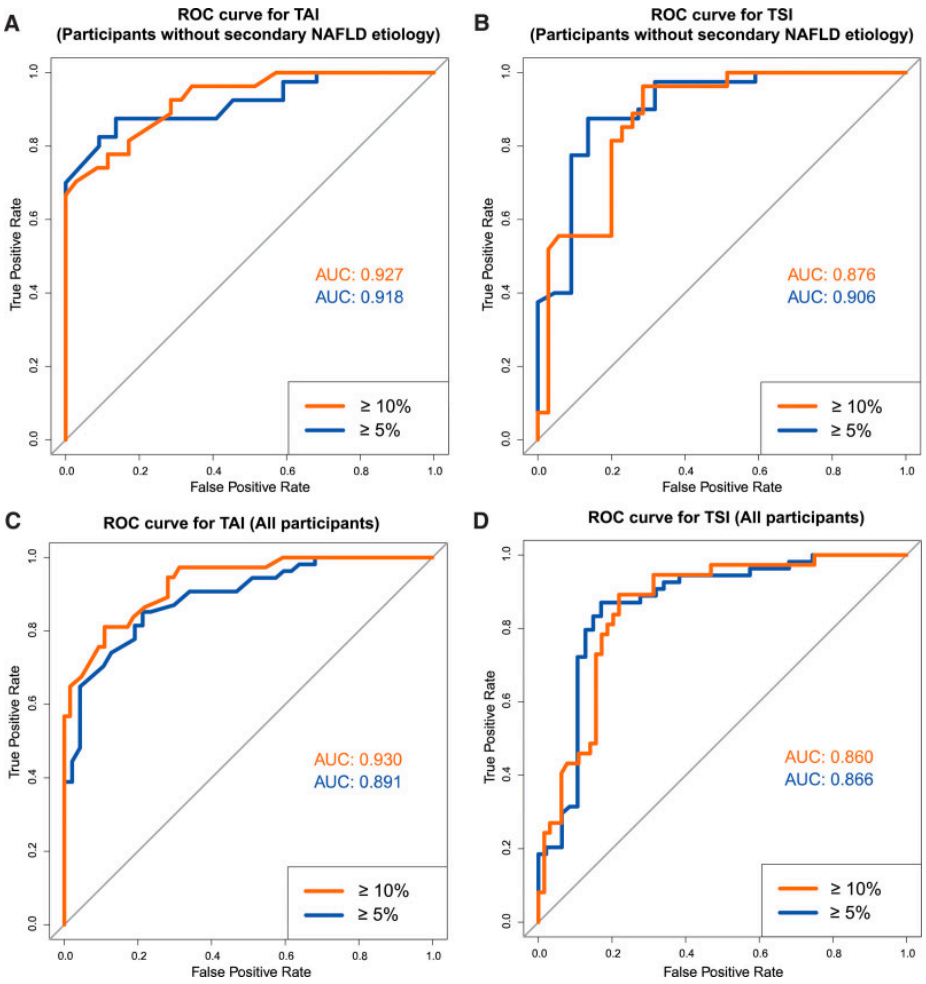

Figure 17. *ROC curve analysis of QUS measurement techniques. Based on ROC curve analysis, both TAI with AUC values 0.927 and 0.918 and TSI with AUC values of 0.876 and 0.906 proved suitable for detecting both ≥5% MRI-PDFF and ≥10% MRI-PDFF values during the analysis of the primary NAFLD group. TAI (AUC= 0.930 and 0.891) and TSI (AUC= 0.860 and 0.866) showed diagnostic accuracy similar to the above shown*

when examining the entire patient population, including NAFLD and secondary NAFLD cases (13).

4.2.3. Examination Of TSI In The Detection Of Hepatic Steatosis

In the case of TSI, we also found significant and strong correlation with MRI-PDFF values p= 0.68 (95% CI= 0.5780-0.7781, p<0.001), although the correlation coefficient was lower than that obtained in the case of TAI. In case of linear regression analysis we obtained a significant positive correlation between TSI and MRI-PDFF values (β=0.004; p<0.001; R^2=0.29). Just as in the case of TAI, TSI values also showed a significant difference between the steatosis groups. [Figure 16] The 5-10% MRI-PDFF steatosis group showed significantly higher TSI values compared to the <5% MRI-PDFF group (90.7 ± 11.5 vs. 101.0 ± 7.0; p<0.003). Significantly higher TSI values characterized also the >10% MRI-PDFF group compared to the 5-10% MRI-PDFF group (101.0 ± 7.0 vs. 106.0 ± 5.6; p<0.016) (Table 6).

During ROC analysis, we obtained an excellent prediction performance in the detection of both ≥5% and ≥10% MRI-PDFF, the optimal threshold value was 99.7, with 85% accuracy, 87% sensitivity, 83% specificity, 85% PPV and 85% NPV. The optimal cut-off for detecting ≥10% MRI-PDFF was 102.0, which gave 82% accuracy, 89% sensitivity, 78% specificity, 70% PPV and 93% NPV. In the case when we performed the analysis only on the primary NAFLD group consisting of 62 cases, we obtained very similar results (Figure 17). In the case of the ≥5% MRI-PDFF group, the AUC was 0.91 (95% CI=0.82-0.99), and the optimal cut-off value was 100.6. In the case of the ≥10% MRI-PDFF group, we obtained an AUC =0.88 (95%CI= 0.79-0.96) and the optimal cut-off value was 103.1 (Table 6).

Table 6. *Diagnostic performance of QUS techniques for the detection of steatosis based on operating characteristic curve analysis.*Area under the ROC curve (AUC) and 95% confidence intervals; **Ideal cutoff in dB/cm/MHz units.*

NAFLD	AUC*	Threshold	Accuracy	Sensitivity	Specificity	PPV	NPV	Ideal cut-off**
TAI								
≥5% MRI-PDFF	0.918; [0.8522-0.9842]	0.586	0.871	0.875	0.864	0.921	0.792	0.760
≥10% MRI-PDFF	0.927; [0.865-0.988]	0.522	0.839	0.778	0.886	0.84	0.838	0.845
TSI								
≥5% MRI-PDFF	0.906; [0.823-0.989]	0.681	0.871	0.875	0.864	0.921	0.792	100.64
≥10% MRI-PDFF	0.876; [0.789-0.962]	0.439	0.81	0.852	0.771	0.742	0.871	103.13
All cases with HS	**AUC***	**Threshold**	**Accuracy**	**Sensitivity**	**Specificity**	**PPV**	**NPV**	**Ideal cut-off****
TAI								
≥5% MRI-PDFF	0.891; [0.830-0.952]	0.437	0.822	0.852	0.787	0.821	0.822	0.765
≥10% MRI-PDFF	0.930; [0.882-0.978]	0.423	0.861	0.8108	0.891	0.811	0.891	0.845
TSI								
≥5% MRI-PDFF	0.866; [0.789-0.942]	0.562	0.851	0.870	0.83	0.855	0.848	99.71
≥10% MRI-PDFF	0.860; [0.786-0.933]	0.392	0.822	0.892	0.781	0.702	0.926	102.045

4.2.4. Examination Of The Reproducibility Of TAI And TSI Measurements

In 52 of the 101 patients, the QUS examination was repeated on the same day by a second examiner independently of the first examiner. The values measured by the two examiners showed excellent, significant correlation in the case of TAI (ρ=0.94; $p<0.001$), while in

the case of TSI we also obtained a significant but only moderately strong correlation (ρ=0.57; p<0.001) (Figure 18). The difference between the values measured by the two examiners was also shown in the Bland-Altmann diagram, where the average difference in the case of TAI was 0.01 cm/dB/MHz, and in the case of TSI it was 1.92, which in both cases represents a minimal difference between examiners. The measurements did not exceed the threshold of acceptability (±1.96 standard deviation) either in the case of TAI or TSI, which indicates good reproducibility of the measurements (Figure 18).

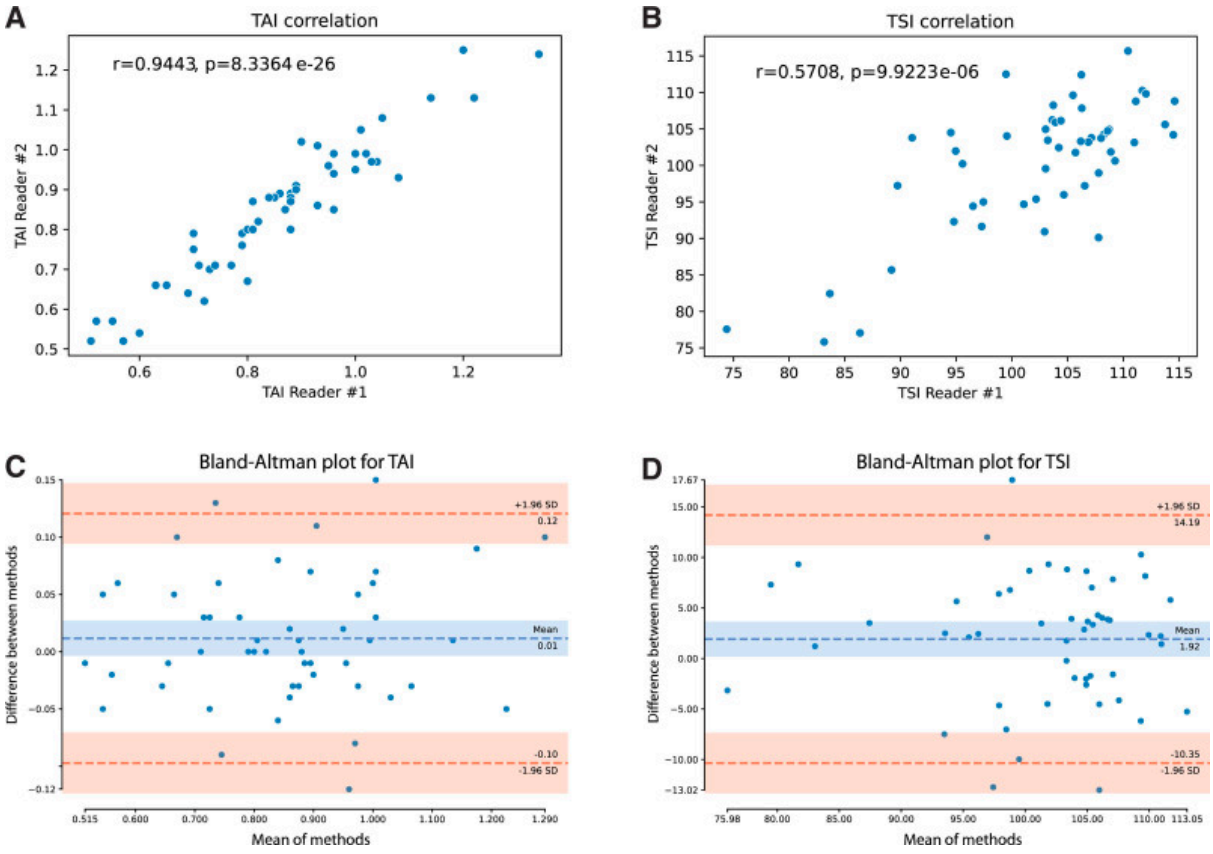

Figure 18. *Analysis of interobserver reproducibility of QUS measurements. Both TAI and TSI showed significant correlation between the two examiners during the interobserver study (rho = 0.94; p<0.01 (A) and rho= 0.57; p<0.01 (B)). The Bland-Altman diagram shows that the average difference between examiners was 0.01 cm/dB/MHz for TAI and 1.92 for TSI (13).*

5. DISCUSSION

The stage of liver fibrosis is a key predictor of complications and mortality in people suffering from chronic HCV infection. Our aim was to observe the effect of sustained antiviral response achieved with DAA therapy on liver fibrosis, which was followed by elastography. We also looked for an answer to how the elastography examination can be integrated into the further care of patients who achieve permanent virus-free status.

In 2012, D'Ambrosio et al. published their article, which summarizes the results of long-term follow-up of chronic HCV infected patients after achieving SVR (110). The patient population of their prospective study consisted of patients who received successful peginterferon and ribavirin therapy and had cirrhotic livers. All individuals who were addicted to drugs or were also infected with HBV or human immunodeficiency virus (HIV), and all those who indicated excessive alcohol consumption were excluded from the research. Their aim was a long-term observation of fibrosis and cirrhosis regression, on pairs of liver biopsy samples before and after the treatment. During their observation, semiquantitative histological staging, morphometric collagen content determination were performed, and the effect of achieving the SVR on necroinflammation and progenitor cell proliferation was also investigated. Their results were the following: In their research, samples were obtained from 38 patients before and after the treatment. According to METAVIR stage classification, all patients were initially stage F4. As a result of the treatment 61% of the patients were reduced to at least 1 METAVIR stage. After the treatment the fibrotic area was significantly reduced in the samples of F4 patients based on the collagen content compared to the samples before the treatment. When examining the serum AST level, it was found that 37 patients initially had elevated values, while 36 patients had normal AST levels at the end of the treatment. We also observed this tendency in our research and we could also discover the regression of fibrosis. They also proved that a significant regression of fibrosis can be observed even in patients who did not fall into a lower METAVIR stage as a result of the treatment (110).

Antonio Facciorusso et al. examined the long-term effects of antiviral therapy on 153 patients by measuring LS with TE (111). Among their patients, 70 received interferon-based therapy, while 83 received DAA therapy. Initially 34.6% of their patients were diagnosed with cirrhosis. 112 of their patients achieved a sustained antiviral response, 41

proved to be non-responders. Using 12.5 kPa as a cut-off value, 32.1% of the patients were classified as METAVIR F4 stage before therapy, while 87.5% were classified as F3. The number of the F4 patients significantly decreased after the end of the treatment, at that time it was only 20.5%. According to their observations, the mean LS value of patients achieving SVR decreased from 12.3 kPa to 6.6 kPa at the 5-year follow-up. The largest reduction was observed in the early period after archiving SVR, which was 2.5 kPa at the end of the treatment and 3.7 kPa after 6 months. The number of cirrhotic patients halved half a year after the end of the therapy, and was less than 5% by the 4th year after treatment. It has been shown that LS decreases significantly with the achievement of an antiviral response (111). Our results are in line with their observations, and point out that in patients with a good antiviral response, we can expect a significant improvement in LS one year after therapy, and the possibility of a further LS reduction even after one year.

According to the American Gastroenterological Association Institute, it is recommended to measure the HCV-RNA level 12 and 48 weeks after the end of therapy, and 24 weeks after the therapy only in selected cases. According to the guidelines, after confirmation of virus-free status by PCR, a routine RNA test is only recommended for patients with a high chance of reinfection. They also recommend endoscopic varix screening for all the patients with cirrhosis, and further tests and follow-up (112).

According to the American Gastroenterological Association Institute, it is recommended that HCV-RNA levels be measured 12 to 48 weeks after EOT, and testing 24 weeks after EOT is recommended only in selected cases (111). According to the directive, routine RNA testing after confirmation of viral freedom by PCR is only recommended for patients with a high risk of re-infection, as other patients have a low probability of late relapse, so if their complaint or symptoms do not make it necessary, further RNA detection-based screening is not required. Endoscopic varicose screening is also recommended for all patients with cirrhosis, the outcome of which (rather than the attainment of SVR) will necessitate further testing and follow-up (113,114). An important objective of the continued follow-ups in SVR is screening for HCC, which is not required in people with stage 0-2 fibrosis. However, in patients who had at least stage 3 fibrosis initially, HCC screening should be continued even after viral clearance using a combination of imaging and AFP measurement twice a year. The screening should be

continued for the rest of the life of the affected patients because the incidence of HCC may remain higher in patients with advanced fibrosis even a long time after viral clearance has been achieved is especially true for those patients who consume alcohol frequently (110,115). Clinically it is significant to continue follow-up and screening for HCC in patients who had at least stage 3 fibrosis initially, even after achieving SVR. The screening should be continued for the rest of the life of the affected patients because the incidence of HCC may remain higher in patients with advanced fibrosis even a long time after viral clearance has been achieved. The passage suggests that a complementary SWE (Shear Wave Elastography) can improve the prognostic value of regular ultrasound screening by identifying patients with resolving fibrosis, who may have a lower risk of HCC and may require less frequent follow-ups (116). Overall, there is a need for continued monitoring and screening in patients with HCV, even after achieving SVR, to detect and manage potential complications such as varices and HCC. However, further research is needed to fully evaluate the long-term effects of SVR on fibrosis and HCC incidence. Our results indicate that a complementary SWE can improve the prognostic value of regular ultrasound screening by identifying patients with resolving fibrosis, who, therefore, may have a lower risk of HCC and may require less frequent follow-ups. Although, multi-center longitudinal studies are still required to determine long-term changes in LS post-SVR as well as their effect on the incidence of HCC.

Clinical studies have also demonstrated that SVR is associated with a lower risk of variceal bleeding (117,118). The Baveno VI Consensus Workshop guideline recommends stratification of patients with a cutoff at LS>20kP and PLT<150,000μ/L to identify the group with a high risk of clinically significant varices (93). However, the utility of the Baveno VI criteria has not yet been evaluated in SVR. We found a reduced risk of esophageal VNT, according to the Baveno VI guidelines, in 73% of the high-risk patients who achieved SVR. Our study is among the first to demonstrate that SWE is able to determine the lower risk of variceal bleeding post-SVR, which may simplify the clinical management of these patients . Recently, the updated Baveno VII criteria has also been formulated, and it recommends that spleen stiffness measurement < 40kPa is safe for ruling out VNT (95). Initial sutdies have also shown that the Baveno VII criteria has outperformed other non-invasive test in selection of compensated ACLD patients for gastroscopy (119).

In conclusion, the risk of serious complications is significantly more favorable for patients who have achieved permanent virus-free status, but the chance of developing HCC is still higher than in the average population, so follow-up with imaging and alpha-fetoprotein (AFP) measurement are recommended. Based on the known research results, in case of non-invasive assessment of fibrosis, it is important to examine the patients before and after the therapy. The procedure helps in risk assessment, such as developing liver cell cancer, or esophageal varicosities. The most significant decrease in LS is expected in the first year after the end of the antiviral treatment. After achieving the virus-free status, non-invasive fibrosis test is not recommended yet, but it can be perfectly integrated into the process of patient follow-up.

Recently several non-invasive methods have become available for the quantitative assessment of hepatic steatosis (55). Among these methods, MRI-PDFF has already been extensively validated. It has been proven that MRI-PDFF is an accurate and reproducible diagnostic method, in addition it can reliably detect microscopic amounts of steatosis and focal inhomogeneities in the liver as well (120). This created a new, non-invasive reference standard for the evaluation of liver steatosis, which is also accepted by the latest professional recommendations (9,121).The main advantage of the QUS based liver steatosis measurement is that it is widely available, the test is less expensive than the MRI examination, and the excellent portability of the instrument enables the screening and follow-up of large patient populations (79). CAP measurement, as the first clinique-based technique available for clinic use, which requires specific instrumentation (101,102). The disadvantage is that its reliability decreases in case of mild steatosis, and that in the absence of a B-mode US image, it does not provide information on the morphology of the liver. In comparative studies, CAP was less accurate for steatosis classification than the MRI-PDFF, and ATI or TAI (122,123).

During our research, we compared two new QUS measurement methods, TAI and TSI with the MRI-PDFF method, which enables the quantitative assessment of liver fat content, as a widely validated and clinically accepted reference. The examined patient group consisted of patients who were either diagnosed with primary NAFLD on the basis of clinical appearance (61%), or were suspected of having secondary NAFLD (39%) due to the presence of other predisposing factors to fatty liver (e.g. they suffered from chronic liver disease).

Both TAI and TSI showed a significant correlation with MRI-PDFF measurement results. In our study TAI showed a strong correlation with MRI-PDFF values (r = 0.78) which was better than the correlation between CAP and MRI-PDFF (r = 0.53-0.61) and our research showed the same results between ATI and MRI-PDFF (r = 0.81) as it was published previously. [66, 68] During the ROC curve analysis, the predictive accuracy of TAI proved to be good in the case of ≥5% MRI-PDFF (AUC = 0.89) and it was excellent in the case of ≥10% MRI-PDFF (AUC = 0.93) fat content. Based on our results, TAI proved to be a more accurate method in the diagnosis of fatty liver compared to CAP measurements (AUC = 0.89 vs. AUC = 0.69-0.80 and AUC = 0.93 vs. AUC = 0.70-0.87) (101,124).

Although the correlation between TSI and MRI-PDFF was weaker than TAI (rho = 0.68), it was also significant. TSI was able to predict cases with ≥5% MRI-PDFF (AUC = 0.87) and ≥10% MRI-PDFF (AUC = 0.86) with very good accuracy, its diagnostic performance was only slightly worse than TAI. Other researches published the diagnostic performance of TSI stronger compared to our study, with the values of AUC = 0.96 in case of ≥5% MRI-PDFF and AUC = 0.94 in case of ≥10% MRI-PDFF, and it exceeded the accuracy of CAP (101,105). We also found that the inter-examiner reproducibility for TSI was weaker compared to TAI (ICC = 0.73 vs. 0.95). At the same time, the excellent reproducibility of the TAI shows that the method is easier to implement.

In case of the patients the optimal threshold values of TAI and TSI were almost the same for all cases, TAI was 0.765 dB/cm/MHz and TSI was 99.7, while in case of only primary NAFLD patients TAI was 0.760 dB/cm/MHz and TSI was 100.6. Furthermore the diagnostic threshold values of both TAI and TSI published in previous studies closely match the threshold values obtained in our own research (TAI = 0.884 db/cm/MHz, TSI = 91.2) (105).

To address the limitations of the presented studies, future research could involve multiple centers with larger sample sizes to increase interobserver reproducibility. Separating NAFLD and secondary NAFLD cases could also provide more accurate diagnosis. due to selection bias, the prevalence of NAFLD (61%) was significantly higher among participants of the study than in the general population. Obtaining tissue samples or exploring non-invasive imaging techniques could provide additional validation of diagnostic thresholds.

6. CONCLUSIONS

In conclusion, quantitative assessment of liver fat and fibrosis content nowadays become severely significant in the evaluation and staging of HCV hepatitis and in the follow-up of NAFLD patients. Liver fat content measured with quantitative ultrasound measurement, applying either TAI or TSI, shows a significant correlation with MRI-PDFF. Therefore TAI and TSI are reliable methods for the detection of clinically significant hepatic steatosis and can be used to diagnose patients with NAFLD with very good accuracy. TSI may also be helpful in the detection of NAFLD associated liver fibrosis. Meanwhile adding SWE to the follow-up imaging protocol can improve patient management by amending initial assessment of fibrosis stage.

7. SUMMARY

We aimed to assess the feasibility of US-based quantitative measurements both in chronic hepatitis and fatty liver disease. Chronic hepatitis is a global problem and HCV infection is a major cause of liver morbidity, but with DAAs it have become the standard therapy for HCV hepatitis therefore it is essential to estimate the severity of liver fibrosis, and non-invasive measurement of LS using elastography is commonly used. According to our research, it has been proven that based on the SWE measurement, liver fibrosis which was classified into four METAVIR stages (F0/1, F2, F3, F4) showed significantly improved fibrosis ($p < 0.001$) and a lower proportion of cirrhotic cases after successful therapy. The number of cirrhotic cases (F4) was also significantly lower (OR = 0.27, 95% CI = 0.09–0.72, $p < 0.016$) at the post-treatment measurement 48 weeks after the completion of antiviral treatment. The average decrease in LS was greater ($p < 0.028$) in cirrhotic cases (F4, Δ-LS =−0.87 ± 0.79 m/s) than in non-cirrhotic cases (F0/1, ΔLS = −0.26 ± 0.37).

NAFLD is the most common chronic liver disease in the world, and its diagnosis can be established when other factors causing liver damage are not present, and the daily alcohol consumption is low. NAFLD in some cases leads to NASH, which may lead to fibrosis, cirrhosis, and HCC. Therefore complex liver ultrasound measurements could be implemented into daily clinical practice in order to give detailed morphological and quantitative information. In the NAFLD patient population we proved a significant correlation (rs = 0.78, 95% confidence interval [CI = 0.701–0.852], $P < .001$) between TAI and reference MRI-PDFF values and also between TSI and MRI-PDFF values (rs = 0.68 (95% CI = 0.578–0.778, $P < .001$)). TAI showed excellent performance for both predicting ≥S1 grade (AUC = 0.89, 95% CI = 0.82–0.97) and ≥S2 grade (AUC = 0.85, 95% CI = 0.75–0.95) of hepatic steatosis.

In summary, using QUS measurement is beneficial to the development of more efficient follow-up protocols. Our studies demonstrated that both in case of chronic HCV infected patients LS showed significant reduction in non-invasive staging of fibrosis a year after SVR is attained, and in the case of NAFLD patient either TAI or TSI, shows a good correlation with MRI-PDFF therefore they are reliable methods for the assessment of clinically significant hepatic steatosis. It is recommended as the initial diagnostic procedure in patients with NAFLD, as it is non-invasive, safe, and cost-effective.

8. REFERENCES

1. Folhoffer A, Rónaszéki AD, Budai BK, Borsos P, Orbán V, Győri G, et al. Follow-Up of Liver Stiffness with Shear Wave Elastography in Chronic Hepatitis C Patients in Sustained Virological Response Augments Clinical Risk Assessment. Processes. 2021 May;9(5):753.
2. European Association for the Study of the Liver. Electronic address: easloffice@easloffice.eu, European Association for the Study of the Liver. EASL Recommendations on Treatment of Hepatitis C 2018. J Hepatol. 2018 Aug;69(2):461–511.
3. European Association for the Study of the Liver. Electronic address: easloffice@easloffice.eu, European Association for the Study of the Liver. EASL Recommendations on Treatment of Hepatitis C 2018. J Hepatol. 2018 Aug;69(2):461–511.
4. Holmes JA, Rutledge SM, Chung RT. Direct-acting antiviral treatment for hepatitis C. Lancet Lond Engl. 2019 Apr 6;393(10179):1392–4.
5. EASL-ALEH Clinical Practice Guidelines: Non-invasive tests for evaluation of liver disease severity and prognosis. J Hepatol. 2015 Jul;63(1):237–64.
6. Simon EG, Callé S, Perrotin F, Remenieras JP. Measurement of shear wave speed dispersion in the placenta by transient elastography: A preliminary ex vivo study. PloS One. 2018;13(4):e0194309.
7. Asrani SK, Devarbhavi H, Eaton J, Kamath PS. Burden of liver diseases in the world. J Hepatol. 2019 Jan;70(1):151–71.
8. Loomba R, Sanyal AJ. The global NAFLD epidemic. Nat Rev Gastroenterol Hepatol. 2013 Nov;10(11):686–90.
9. European Association for the Study of the Liver (EASL), European Association for the Study of Diabetes (EASD), European Association for the Study of Obesity (EASO). EASL-EASD-EASO Clinical Practice Guidelines for the management of non-alcoholic fatty liver disease. J Hepatol. 2016 Jun;64(6):1388–402.
10. NAFLD and liver transplantation: Current burden and expected challenges - PubMed [Internet]. [cited 2023 Feb 21]. Available from: https://pubmed.ncbi.nlm.nih.gov/27486010/

11. Ratziu V, Charlotte F, Heurtier A, Gombert S, Giral P, Bruckert E, et al. Sampling variability of liver biopsy in nonalcoholic fatty liver disease. Gastroenterology. 2005 Jun;128(7):1898–906.
12. Reeder SB, Hu HH, Sirlin CB. Proton density fat-fraction: a standardized MR-based biomarker of tissue fat concentration. J Magn Reson Imaging JMRI. 2012 Nov;36(5):1011–4.
13. Rónaszéki AD, Budai BK, Csongrády B, Stollmayer R, Hagymási K, Werling K, et al. Tissue attenuation imaging and tissue scatter imaging for quantitative ultrasound evaluation of hepatic steatosis. Medicine (Baltimore). 2022 Aug 19;101(33):e29708.
14. Cengiz M, Sentürk S, Cetin B, Bayrak AH, Bilek SU. Sonographic assessment of fatty liver: intraobserver and interobserver variability. Int J Clin Exp Med. 2014;7(12):5453–60.
15. Lin SC, Heba E, Wolfson T, Ang B, Gamst A, Han A, et al. Noninvasive Diagnosis of Nonalcoholic Fatty Liver Disease and Quantification of Liver Fat Using a New Quantitative Ultrasound Technique. Clin Gastroenterol Hepatol Off Clin Pract J Am Gastroenterol Assoc. 2015 Jul;13(7):1337-1345.e6.
16. Kaposi PN, Unger Z, Fejér B, Kucsa A, Tóth A, Folhoffer A, et al. Interobserver agreement and diagnostic accuracy of shearwave elastography for the staging of hepatitis C virus-associated liver fibrosis. J Clin Ultrasound JCU. 2020 Feb;48(2):67–74.
17. Gobran ST, Ancuta P, Shoukry NH. A Tale of Two Viruses: Immunological Insights Into HCV/HIV Coinfection. Front Immunol. 2021;12:726419.
18. Hunyady B, Gerlei Z, Gervain J, Horváth G, Lengyel G, Pár A, et al. [Screening, diagnosis, treatment, and follow up of hepatitis C virus related liver disease. National consensus guideline in Hungary from 22 September 2017]. Orv Hetil. 2018 Feb;159(Suppl 1):3–23.
19. Gervain J. [The diagnosis of hepatitis C virus infection]. Orv Hetil. 2014 Jun 29;155(26):1019–23.
20. Golden-Mason L, Rosen HR. Natural killer cells: multifaceted players with key roles in hepatitis C immunity. Immunol Rev. 2013 Sep;255(1):68–81.
21. Fasbender F, Widera A, Hengstler JG, Watzl C. Natural Killer Cells and Liver

Fibrosis. Front Immunol. 2016;7:19.
22. Guss D, Sherigar J, Rosen P, Mohanty SR. Diagnosis and Management of Hepatitis C Infection in Primary Care Settings. J Gen Intern Med. 2018 Apr;33(4):551–7.
23. European Association for the Study of the Liver. Electronic address: easloffice@easloffice.eu, Clinical Practice Guidelines Panel: Chair:, EASL Governing Board representative:, Panel members: EASL recommendations on treatment of hepatitis C: Final update of the series☆. J Hepatol. 2020 Nov;73(5):1170–218.
24. Lurie Y, Webb M, Cytter-Kuint R, Shteingart S, Lederkremer GZ. Non-invasive diagnosis of liver fibrosis and cirrhosis. World J Gastroenterol. 2015 Nov 7;21(41):11567–83.
25. Söderberg C, Stål P, Askling J, Glaumann H, Lindberg G, Marmur J, et al. Decreased survival of subjects with elevated liver function tests during a 28-year follow-up. Hepatol Baltim Md. 2010 Feb;51(2):595–602.
26. Chalasani N, Younossi Z, Lavine JE, Diehl AM, Brunt EM, Cusi K, et al. The diagnosis and management of non-alcoholic fatty liver disease: practice Guideline by the American Association for the Study of Liver Diseases, American College of Gastroenterology, and the American Gastroenterological Association. Hepatol Baltim Md. 2012 Jun;55(6):2005–23.
27. Sheth SG, Flamm SL, Gordon FD, Chopra S. AST/ALT ratio predicts cirrhosis in patients with chronic hepatitis C virus infection. Am J Gastroenterol. 1998 Jan;93(1):44–8.
28. Joseph J. Serum Marker Panels for Predicting Liver Fibrosis – An Update. Clin Biochem Rev. 2020 May;41(2):67–73.
29. Bedogni G, Miglioli L, Masutti F, Castiglione A, Crocè LS, Tiribelli C, et al. Incidence and natural course of fatty liver in the general population: the Dionysos study. Hepatol Baltim Md. 2007 Nov;46(5):1387–91.
30. Ge X, Zheng L, Wang M, Du Y, Jiang J. Prevalence trends in non-alcoholic fatty liver disease at the global, regional and national levels, 1990-2017: a population-based observational study. BMJ Open. 2020 Aug 3;10(8):e036663.
31. Mitra S, De A, Chowdhury A. Epidemiology of non-alcoholic and alcoholic fatty

liver diseases. Transl Gastroenterol Hepatol. 2020;5:16.

32. Tang S, Zhang J, Mei TT, Guo HQ, Wei XH, Zhang WY, et al. Association of PNPLA3 rs738409 G/C gene polymorphism with nonalcoholic fatty liver disease in children: a meta-analysis. BMC Med Genet. 2020 Aug 18;21(1):163.
33. Liu YL, Reeves HL, Burt AD, Tiniakos D, McPherson S, Leathart JBS, et al. TM6SF2 rs58542926 influences hepatic fibrosis progression in patients with non-alcoholic fatty liver disease. Nat Commun. 2014 Jun 30;5:4309.
34. Egresi A, Lengyel G, Hagymási K. [Non-invasive assessment of fatty liver]. Orv Hetil. 2015 Apr 5;156(14):543–51.
35. Sharp KPH, Schultz M, Coppell KJ. Is non-alcoholic fatty liver disease a reflection of what we eat or simply how much we eat? JGH Open Open Access J Gastroenterol Hepatol. 2018 Apr;2(2):59–74.
36. Tilg H, Moschen AR. Evolution of inflammation in nonalcoholic fatty liver disease: the multiple parallel hits hypothesis. Hepatol Baltim Md. 2010 Nov;52(5):1836–46.
37. Ádám Veronika (szerk.): Orvosi biokémia 4. kiadás. Semmelweis Kiadó és Multimédia Stúdió; 2016, 92–140 p. ISBN: 9789633314005
38. Huang PL. A comprehensive definition for metabolic syndrome. Dis Model Mech. 2009;2(5–6):231–7.
39. Castera L, Friedrich-Rust M, Loomba R. Noninvasive Assessment of Liver Disease in Patients With Nonalcoholic Fatty Liver Disease. Gastroenterology. 2019 Apr;156(5):1264-1281.e4.
40. Petitclerc L, Gilbert G, Nguyen BN, Tang A. Liver Fibrosis Quantification by Magnetic Resonance Imaging. Top Magn Reson Imaging. 2017 Dec;26(6):229–41.
41. Bedossa P, Poynard T. An algorithm for the grading of activity in chronic hepatitis C. The METAVIR Cooperative Study Group. Hepatol Baltim Md. 1996 Aug;24(2):289–93.
42. Intraobserver and interobserver variations in liver biopsy interpretation in patients with chronic hepatitis C. The French METAVIR Cooperative Study Group. Hepatol Baltim Md. 1994 Jul;20(1):15–20.
43. Goodman ZD. Grading and staging systems for inflammation and fibrosis in chronic liver diseases. J Hepatol. 2007 Oct;47(4):598–607.

44. Rockey DC, Caldwell SH, Goodman ZD, Nelson RC, Smith AD, American Association for the Study of Liver Diseases. Liver biopsy. Hepatol Baltim Md. 2009 Mar;49(3):1017–44.
45. Brunt EM, Janney CG, Di Bisceglie AM, Neuschwander-Tetri BA, Bacon BR. Nonalcoholic steatohepatitis: a proposal for grading and staging the histological lesions. Am J Gastroenterol. 1999 Sep;94(9):2467–74.
46. Westin J, Lagging LM, Wejstål R, Norkrans G, Dhillon AP. Interobserver study of liver histopathology using the Ishak score in patients with chronic hepatitis C virus infection. Liver. 1999 Jun;19(3):183–7.
47. Johnson KD, Laoveeravat P, Yee EU, Perisetti A, Thandassery RB, Tharian B. Endoscopic ultrasound guided liver biopsy: Recent evidence. World J Gastrointest Endosc. 2020 Mar 16;12(3):83–97.
48. Bahirwani R, Griffin C. The diagnosis and management of nonalcoholic fatty liver disease: A patient-friendly summary of the 2018 AASLD guidelines. Clin Liver Dis. 2022 Jun;19(6):222–6.
49. Procopet B, Berzigotti A. Diagnosis of cirrhosis and portal hypertension: imaging, non-invasive markers of fibrosis and liver biopsy. Gastroenterol Rep. 2017 May;5(2):79–89.
50. Berzigotti A, Castera L. Update on ultrasound imaging of liver fibrosis. J Hepatol. 2013 Jul;59(1):180–2.
51. Arguedas MR, Heudebert GR, Eloubeidi MA, Abrams GA, Fallon MB. Cost-effectiveness of screening, surveillance, and primary prophylaxis strategies for esophageal varices. Am J Gastroenterol. 2002 Sep;97(9):2441–52.
52. Berzigotti A, Piscaglia F, EFSUMB Education and Professional Standards Committee. Ultrasound in portal hypertension--part 2--and EFSUMB recommendations for the performance and reporting of ultrasound examinations in portal hypertension. Ultraschall Med Stuttg Ger 1980. 2012 Feb;33(1):8–32; quiz 30–1.
53. Staub F, Tournoux-Facon C, Roumy J, Chaigneau C, Morichaut-Beauchant M, Levillain P, et al. Liver fibrosis staging with contrast-enhanced ultrasonography: prospective multicenter study compared with METAVIR scoring. Eur Radiol. 2009 Aug;19(8):1991–7.

54. Maruyama H, Tobari M, Nagamatsu H, Shiina S, Yamaguchi T. Contrast-enhanced ultrasonography for the management of portal hypertension in cirrhosis. Front Med. 2022;9:1057045.
55. Ferraioli G, Soares Monteiro LB. Ultrasound-based techniques for the diagnosis of liver steatosis. World J Gastroenterol. 2019 Oct 28;25(40):6053–62.
56. Zhang YN, Fowler KJ, Hamilton G, Cui JY, Sy EZ, Balanay M, et al. Liver fat imaging—a clinical overview of ultrasound, CT, and MR imaging. Br J Radiol. 2018 Sep;91(1089):20170959.
57. Webb M, Yeshua H, Zelber-Sagi S, Santo E, Brazowski E, Halpern Z, et al. Diagnostic value of a computerized hepatorenal index for sonographic quantification of liver steatosis. AJR Am J Roentgenol. 2009 Apr;192(4):909–14.
58. Marshall RH, Eissa M, Bluth EI, Gulotta PM, Davis NK. Hepatorenal index as an accurate, simple, and effective tool in screening for steatosis. AJR Am J Roentgenol. 2012 Nov;199(5):997–1002.
59. Hamaguchi M, Kojima T, Itoh Y, Harano Y, Fujii K, Nakajima T, et al. The severity of ultrasonographic findings in nonalcoholic fatty liver disease reflects the metabolic syndrome and visceral fat accumulation. Am J Gastroenterol. 2007 Dec;102(12):2708–15.
60. Ballestri S, Lonardo A, Romagnoli D, Carulli L, Losi L, Day CP, et al. Ultrasonographic fatty liver indicator, a novel score which rules out NASH and is correlated with metabolic parameters in NAFLD. Liver Int. 2012;32(8):1242–52.
61. Zhang Y, Zhang XM, Prowda JC, Zhang HL, Sant'Anna Henry C, Shih G, et al. Changes in hepatic venous morphology with cirrhosis on MRI. J Magn Reson Imaging. 2009;29(5):1085–92.
62. Huber A, Ebner L, Heverhagen JT, Christe A. State-of-the-art imaging of liver fibrosis and cirrhosis: A comprehensive review of current applications and future perspectives. Eur J Radiol Open. 2015 Jan 1;2:90–100.
63. Smith AD, Branch CR, Zand K, Subramony C, Zhang H, Thaggard K, et al. Liver Surface Nodularity Quantification from Routine CT Images as a Biomarker for Detection and Evaluation of Cirrhosis. Radiology. 2016 Sep;280(3):771–81.
64. Budai BK, Tóth A, Borsos P, Frank VG, Shariati S, Fejér B, et al. Three-dimensional CT texture analysis of anatomic liver segments can differentiate

between low-grade and high-grade fibrosis. BMC Med Imaging. 2020 Sep 21;20(1):108.

65. Kodama Y, Ng CS, Wu TT, Ayers GD, Curley SA, Abdalla EK, et al. Comparison of CT methods for determining the fat content of the liver. AJR Am J Roentgenol. 2007 May;188(5):1307–12.
66. Lee SS, Park SH. Radiologic evaluation of nonalcoholic fatty liver disease. World J Gastroenterol. 2014 Jun 21;20(23):7392–402.
67. Pokharel SS, Macura KJ, Kamel IR, Zaheer A. Current MR imaging lipid detection techniques for diagnosis of lesions in the abdomen and pelvis. Radiogr Rev Publ Radiol Soc N Am Inc. 2013 May;33(3):681–702.
68. Szczepaniak LS, Babcock EE, Schick F, Dobbins RL, Garg A, Burns DK, et al. Measurement of intracellular triglyceride stores by H spectroscopy: validation in vivo. Am J Physiol. 1999 May;276(5):E977-989.
69. Mehta SR, Thomas EL, Bell JD, Johnston DG, Taylor-Robinson SD. Non-invasive means of measuring hepatic fat content. World J Gastroenterol. 2008 Jun 14;14(22):3476–83.
70. Cassidy FH, Yokoo T, Aganovic L, Hanna RF, Bydder M, Middleton MS, et al. Fatty liver disease: MR imaging techniques for the detection and quantification of liver steatosis. Radiogr Rev Publ Radiol Soc N Am Inc. 2009;29(1):231–60.
71. Hamilton G, Yokoo T, Bydder M, Cruite I, Schroeder ME, Sirlin CB, et al. In vivo characterization of the liver fat ^{1}H MR spectrum. NMR Biomed. 2011 Aug;24(7):784–90.
72. Liu CY, McKenzie CA, Yu H, Brittain JH, Reeder SB. Fat quantification with IDEAL gradient echo imaging: Correction of bias from T1 and noise. Magn Reson Med. 2007;58(2):354–64.
73. Marin D, Dale BM, Bashir MR, Ziemlewicz TJ, Ringe KI, Boll DT, et al. Effectiveness of a three-dimensional dual gradient echo two-point Dixon technique for the characterization of adrenal lesions at 3 Tesla. Eur Radiol. 2012 Jan;22(1):259–68.
74. Reeder SB, Hu HH, Sirlin CB. Proton density fat-fraction: a standardized MR-based biomarker of tissue fat concentration. J Magn Reson Imaging JMRI. 2012 Nov;36(5):1011–4.

75. Hernando D, Kramer JH, Reeder SB. Multipeak fat-corrected complex R2* relaxometry: theory, optimization, and clinical validation. Magn Reson Med. 2013 Nov;70(5):1319–31.
76. Reeder SB, Cruite I, Hamilton G, Sirlin CB. Quantitative Assessment of Liver Fat with Magnetic Resonance Imaging and Spectroscopy. J Magn Reson Imaging JMRI. 2011 Oct;34(4):729–49.
77. Caussy C, Reeder SB, Sirlin CB, Loomba R. Noninvasive, Quantitative Assessment of Liver Fat by MRI-PDFF as an Endpoint in NASH Trials. Hepatol Baltim Md. 2018 Aug;68(2):763–72.
78. Park J, Lee JM, Lee G, Jeon SK, Joo I. Quantitative Evaluation of Hepatic Steatosis Using Advanced Imaging Techniques: Focusing on New Quantitative Ultrasound Techniques. Korean J Radiol. 2022;23(1):13.
79. Ferraioli G, Kumar V, Ozturk A, Nam K, de Korte CL, Barr RG. US Attenuation for Liver Fat Quantification: An AIUM-RSNA QIBA Pulse-Echo Quantitative Ultrasound Initiative. Radiology. 2022 Mar;302(3):495–506.
80. Ferraioli G. Review of Liver Elastography Guidelines. J Ultrasound Med. 2019;38(1):9–14.
81. Bozic D, Podrug K, Mikolasevic I, Grgurevic I. Ultrasound Methods for the Assessment of Liver Steatosis: A Critical Appraisal. Diagnostics. 2022 Oct;12(10):2287.
82. Garcia-Saenz-de-Sicilia M, Al-Obaid L, Hughes DL, Duarte-Rojo A. Mastering Core Recommendations during HEPAtology ROUNDS in Patients with Advanced Chronic Liver Disease. Semin Liver Dis. 2022 Aug;42(3):341–61.
83. Berzigotti A, Piscaglia F, EFSUMB Education and Professional Standards Committee. Ultrasound in portal hypertension--part 2--and EFSUMB recommendations for the performance and reporting of ultrasound examinations in portal hypertension. Ultraschall Med Stuttg Ger 1980. 2012 Feb;33(1):8–32; quiz 30–1.
84. Bamber J, Cosgrove D, Dietrich CF, Fromageau J, Bojunga J, Calliada F, et al. EFSUMB guidelines and recommendations on the clinical use of ultrasound elastography. Part 1: Basic principles and technology. Ultraschall Med Stuttg Ger 1980. 2013 Apr;34(2):169–84.

85. Lee DH, Lee JM, Chang W, Yoon JH, Kim YJ, Lee JH, et al. Prognostic Role of Liver Stiffness Measurements Using Magnetic Resonance Elastography in Patients with Compensated Chronic Liver Disease. Eur Radiol. 2018 Aug;28(8):3513–21.
86. Barr RG, Wilson SR, Rubens D, Garcia-Tsao G, Ferraioli G. Update to the Society of Radiologists in Ultrasound Liver Elastography Consensus Statement. Radiology. 2020 Aug;296(2):263–74.
87. Labyed Y, Milkowski A. Novel Method for Ultrasound-Derived Fat Fraction Using an Integrated Phantom. J Ultrasound Med Off J Am Inst Ultrasound Med. 2020 Dec;39(12):2427–38.
88. Kaposi PN, Unger Z, Fejér B, Kucsa A, Tóth A, Folhoffer A, et al. Interobserver agreement and diagnostic accuracy of shearwave elastography for the staging of hepatitis C virus-associated liver fibrosis. J Clin Ultrasound JCU. 2020 Feb;48(2):67–74.
89. Friedrich-Rust M, Ong MF, Martens S, Sarrazin C, Bojunga J, Zeuzem S, et al. Performance of transient elastography for the staging of liver fibrosis: a meta-analysis. Gastroenterology. 2008 Apr;134(4):960–74.
90. Andersen ES, Christensen PB, Weis N. Transient elastography for liver fibrosis diagnosis. Eur J Intern Med. 2009 Jul;20(4):339–42.
91. Barr RG, Wilson SR, Rubens D, Garcia-Tsao G, Ferraioli G. Update to the Society of Radiologists in Ultrasound Liver Elastography Consensus Statement. Radiology. 2020 Aug;296(2):263–74.
92. Trebicka J, Gu W, de Ledinghen V, Aubé C, Krag A, Praktiknjo M, et al. Two-dimensional shear wave elastography predicts survival in advanced chronic liver disease. Gut. 2022 Feb;71(2):402–14.
93. de Franchis R, Baveno VI Faculty. Expanding consensus in portal hypertension: Report of the Baveno VI Consensus Workshop: Stratifying risk and individualizing care for portal hypertension. J Hepatol. 2015 Sep;63(3):743–52.
94. Kang SH, Baik SK, Kim MY. Application of Baveno Criteria and Modified Baveno Criteria with Shear-wave Elastography in Compensated Advanced Chronic Liver Disease. J Korean Med Sci. 2020 Aug 3;35(30):e249.
95. de Franchis R, Bosch J, Garcia-Tsao G, Reiberger T, Ripoll C, Baveno VII Faculty. Baveno VII - Renewing consensus in portal hypertension. J Hepatol. 2022

Apr;76(4):959–74.
96. Singh S, Muir AJ, Dieterich DT, Falck-Ytter YT. American Gastroenterological Association Institute Technical Review on the Role of Elastography in Chronic Liver Diseases. Gastroenterology. 2017 May;152(6):1544–77.
97. Ferraioli G, Filice C, Castera L, Choi BI, Sporea I, Wilson SR, et al. WFUMB guidelines and recommendations for clinical use of ultrasound elastography: Part 3: liver. Ultrasound Med Biol. 2015 May;41(5):1161–79.
98. European Association for the Study of the Liver. Electronic address: easloffice@easloffice.eu, European Association for the Study of the Liver. EASL Clinical Practice Guidelines: Management of hepatocellular carcinoma. J Hepatol. 2018 Jul;69(1):182–236.
99. Jeon SK, Lee JM, Joo I, Park SJ. Quantitative Ultrasound Radiofrequency Data Analysis for the Assessment of Hepatic Steatosis in Nonalcoholic Fatty Liver Disease Using Magnetic Resonance Imaging Proton Density Fat Fraction as the Reference Standard. Korean J Radiol. 2021 Jul;22(7):1077–86.
100. Kuroda H, Abe T, Fujiwara Y, Nagasawa T, Takikawa Y. Diagnostic accuracy of ultrasound-guided attenuation parameter as a noninvasive test for steatosis in non-alcoholic fatty liver disease. J Med Ultrason 2001. 2021 Oct;48(4):471–80.
101. Caussy C, Alquiraish MH, Nguyen P, Hernandez C, Cepin S, Fortney LE, et al. Optimal threshold of controlled attenuation parameter with MRI-PDFF as the gold standard for the detection of hepatic steatosis. Hepatol Baltim Md. 2018 Apr;67(4):1348–59.
102. Karlas T, Petroff D, Sasso M, Fan JG, Mi YQ, de Lédinghen V, et al. Individual patient data meta-analysis of controlled attenuation parameter (CAP) technology for assessing steatosis. J Hepatol. 2017 May;66(5):1022–30.
103. Ho MC, Lee YH, Jeng YM, Chen CN, Chang KJ, Tsui PH. Relationship between Ultrasound Backscattered Statistics and the Concentration of Fatty Droplets in Livers: An Animal Study. PLOS ONE. 2013 May 21;8(5):e63543.
104. Son JY, Lee JY, Yi NJ, Lee KW, Suh KS, Kim KG, et al. Hepatic Steatosis: Assessment with Acoustic Structure Quantification of US Imaging. Radiology. 2016 Jan;278(1):257–64.
105. Jeon SK, Lee JM, Joo I, Park SJ. Quantitative Ultrasound Radiofrequency Data

Analysis for the Assessment of Hepatic Steatosis in Nonalcoholic Fatty Liver Disease Using Magnetic Resonance Imaging Proton Density Fat Fraction as the Reference Standard. Korean J Radiol. 2021 Jul;22(7):1077–86.

106. Paige JS, Bernstein GS, Heba E, Costa EAC, Fereirra M, Wolfson T, et al. A Pilot Comparative Study of Quantitative Ultrasound, Conventional Ultrasound, and MRI for Predicting Histology-Determined Steatosis Grade in Adult Nonalcoholic Fatty Liver Disease. AJR Am J Roentgenol. 2017 May;208(5):W168–77.
107. Gao J. Ultrasound Derived Fat Fraction (UDFF) and MRI-PDFF of Adult Liver and Spleen: A Preliminary Observation.
108. Jeon SK, Lee JM, Joo I, Yoon JH, Lee G. Two-dimensional Convolutional Neural Network Using Quantitative US for Noninvasive Assessment of Hepatic Steatosis in NAFLD. Radiology. 2023 Jan 3;221510.
109. Jang JK, Lee ES, Seo JW, Kim YR, Kim SY, Cho YY, et al. Two-dimensional Shear-Wave Elastography and US Attenuation Imaging for Nonalcoholic Steatohepatitis Diagnosis: A Cross-sectional, Multicenter Study. Radiology. 2022 Oct;305(1):118–26.
110. D'Ambrosio R, Aghemo A, Rumi MG, Ronchi G, Donato MF, Paradis V, et al. A morphometric and immunohistochemical study to assess the benefit of a sustained virological response in hepatitis C virus patients with cirrhosis. Hepatol Baltim Md. 2012 Aug;56(2):532–43.
111. Facciorusso A, Del Prete V, Turco A, Buccino RV, Nacchiero MC, Muscatiello N. Long-term liver stiffness assessment in hepatitis C virus patients undergoing antiviral therapy: Results from a 5-year cohort study. J Gastroenterol Hepatol. 2018 Apr;33(4):942–9.
112. Jacobson IM, Lim JK, Fried MW. American Gastroenterological Association Institute Clinical Practice Update-Expert Review: Care of Patients Who Have Achieved a Sustained Virologic Response After Antiviral Therapy for Chronic Hepatitis C Infection. Gastroenterology. 2017 May;152(6):1578–87.
113. Ciancio A, Ribaldone DG, Salamone R, Bruno M, Caronna S, Debernardi Venon W, et al. Screening and surveillance of oesophageal varices in patients with HCV-positive liver cirrhosis successfully treated by direct-acting antiviral agents. Liver Int Off J Int Assoc Study Liver. 2022 May;42(5):1121–31.

114. Thabut D, Bureau C, Layese R, Bourcier V, Hammouche M, Cagnot C, et al. Validation of Baveno VI Criteria for Screening and Surveillance of Esophageal Varices in Patients With Compensated Cirrhosis and a Sustained Response to Antiviral Therapy. Gastroenterology. 2019 Mar;156(4):997-1009.e5.
115. Ioannou GN, Beste LA, Green PK, Singal AG, Tapper EB, Waljee AK, et al. Increased Risk for Hepatocellular Carcinoma Persists Up to 10 Years After HCV Eradication in Patients With Baseline Cirrhosis or High FIB-4 Scores. Gastroenterology. 2019 Nov;157(5):1264-1278.e4.
116. Cerrito L, Ainora ME, Nicoletti A, Garcovich M, Riccardi L, Pompili M, et al. Elastography as a predictor of liver cirrhosis complications after hepatitis C virus eradication in the era of direct-acting antivirals. World J Hepatol. 2021 Nov 27;13(11):1663–76.
117. Bruno S, Crosignani A, Facciotto C, Rossi S, Roffi L, Redaelli A, et al. Sustained virologic response prevents the development of esophageal varices in compensated, Child-Pugh class A hepatitis C virus-induced cirrhosis. A 12-year prospective follow-up study. Hepatol Baltim Md. 2010 Jun;51(6):2069–76.
118. Mallet V, Gilgenkrantz H, Serpaggi J, Verkarre V, Vallet-Pichard A, Fontaine H, et al. Brief communication: the relationship of regression of cirrhosis to outcome in chronic hepatitis C. Ann Intern Med. 2008 Sep 16;149(6):399–403.
119. Zhang X, Song J, Zhang Y, Wen B, Dai L, Xi R, et al. Baveno VII algorithm outperformed other models in ruling out high-risk varices in individuals with HBV-related cirrhosis. J Hepatol. 2023 Mar;78(3):574–83.
120. Gu J, Liu S, Du S, Zhang Q, Xiao J, Dong Q, et al. Diagnostic value of MRI-PDFF for hepatic steatosis in patients with non-alcoholic fatty liver disease: a meta-analysis. Eur Radiol. 2019 Jul 1;29(7):3564–73.
121. Cusi K, Isaacs S, Barb D, Basu R, Caprio S, Garvey WT, et al. American Association of Clinical Endocrinology Clinical Practice Guideline for the Diagnosis and Management of Nonalcoholic Fatty Liver Disease in Primary Care and Endocrinology Clinical Settings: Co-Sponsored by the American Association for the Study of Liver Diseases (AASLD). Endocr Pract Off J Am Coll Endocrinol Am Assoc Clin Endocrinol. 2022 May;28(5):528–62.
122. Park CC, Nguyen P, Hernandez C, Bettencourt R, Ramirez K, Fortney L, et al.

Magnetic Resonance Elastography vs Transient Elastography in Detection of Fibrosis and Noninvasive Measurement of Steatosis in Patients With Biopsy-Proven Nonalcoholic Fatty Liver Disease. Gastroenterology. 2017 Feb;152(3):598-607.e2.

123. Ferraioli G, Maiocchi L, Raciti MV, Tinelli C, De Silvestri A, Nichetti M, et al. Detection of Liver Steatosis With a Novel Ultrasound-Based Technique: A Pilot Study Using MRI-Derived Proton Density Fat Fraction as the Gold Standard. Clin Transl Gastroenterol. 2019 Oct;10(10):e00081.
124. Shao CX, Ye J, Dong Z, Li F, Lin Y, Liao B, et al. Steatosis grading consistency between controlled attenuation parameter and MRI-PDFF in monitoring metabolic associated fatty liver disease. Ther Adv Chronic Dis. 2021;12:20406223211033120.

9. BIBLIOGRAPHY OF THE CANDIDATE'S PUBLICATIONS

9.1. PUBLICATIONS RELATED TO THE PRESENT THESIS

Rónaszéki Aladár D, Budai Bettina K, Csongrády Barbara, Stollmayer Róbert, Hagymási
Krisztina, Werling Klára, Fodor Tamás, Folhoffer Anikó, Kalina Ildikó, Győri Gabriella, Maurovich-Horvat Pál, Kaposi Pál N
Tissue attenuation imaging and tissue scatter imaging for quantitative ultrasound evaluation of hepatic steatosis
MEDICINE 101: 33 Paper: e29708, 9 p. (2022)
Original Article | Science
Scopus - Medicine (miscellaneous) SJR: Q3
IF: 1,817

Folhoffer Anikó*, **Rónaszéki Aladár D***, Budai Bettina K, Borsos Petra, Orbán Vince, Győri
Gabriella, Szalay Ferenc, Kaposi Pál N
Follow-Up of Liver Stiffness with Shear Wave Elastography in Chronic Hepatitis C Patients
in Sustained Virological Response Augments Clinical Risk Assessment
PROCESSES 9: 5 Paper: 753, 13 p. (2021)
Original Article | Science
Scopus - Chemical Engineering (miscellaneous) SJR: Q2
Scopus - Bioengineering SJR: Q3
Scopus - Process Chemistry and Technology SJR: Q3
*These authors contributed equally to this work.
IF: 3,352

9.2. PUBLICATIONS NOT RELATED TO THE PRESENT THESIS:

Budai BK, Tánczik Zs, Körmendy B, Zsombor Z, Palotás L, Stollmayer R, **Rónaszéki AD**, Maurovich Horvat P, Kaposi NP.
Radiomikai elemzés - Ami igazán lényeges, az a szemnek sokszor láthatatlan.
Magyar Radiológia Online 2022,13(2):3.
Review Article | Science

Zsombor Z, **Rónaszéki AD**, Csongrády B, Stollmayer R, Budai BK, Folhoffer A, Kalina I, Győri G, Bérczi V, Maurovich-Horvat P, Hagymási K, Kaposi PN.
Evaluation of Artificial Intelligence-Calculated Hepatorenal Index for Diagnosing Mild and Moderate Hepatic Steatosis in Non-Alcoholic Fatty Liver Disease.
Medicina 2023, 59, 469. Doi:59030469
Original Article | Science
IF: 2,948

Rónaszéki Aladár David, Dudás Ibolyka, Zsély Boglarka, Budai Bettina Katalin, Stollmayer
Róbert, Hahn Oszkár, Csongrády Barbara, Park Byung-So, Maurovich-Horvat Pál, Győri Gabriella, Kaposi Novak Pal
Microvascular flow imaging to differentiate focal hepatic lesions: the spoke-wheel pattern as a specific sign of focal nodular hyperplasia
ULTRASONOGRAPHY 42: 1 pp. 172-181. (2023)
Pictorial essay| Science
IF: 4,725

Budai Bettina Katalin, Stollmayer Róbert, **Rónaszéki Aladár Dávid**, Körmendy Borbála, Zsombor Zita, Palotás Lõrinc, Fejér Bence, Szendrõi Attila, Székely Eszter, MaurovichHorvat Pál, Kaposi Novák Pál
Radiomics analysis of contrast-enhanced CT scans can distinguish between clear cell and nonclear cell renal cell carcinoma in different imaging protocols
FRONTIERS IN MEDICINE 9 Paper: 974485, 14 p. (2022)

Original Article | Science

IF: 5,058

Budai BK, Tánczik Zs, Körmendy B, Zsombor Z, Palotás L, Stollmayer R, **Rónaszéki AD**,

Maurovich Horvat P, Kaposi Novák P

Radiomikai elemzés – ami igazán lényeges, az a szemnek sokszor láthatatlan: Metodikai közlemény

MAGYAR RADIOLÓGIA ONLINE 13: 2 Paper: 3, 16 p. (2022)

Review Article | Science

Stollmayer Róbert, Budai Bettina Katalin, **Rónaszéki Aladár**, Zsombor Zita, Kalina Ildikó,

Hartmann Erika, Tóth Gábor, Szoldán Péter, Bérczi Viktor, Maurovich-Horvat Pál, Kaposi

Novák Pál

Focal Liver Lesion MRI Feature Identification Using Efficientnet and MONAI: A Feasibility

Study

CELLS 11: 9 Paper: 1558, 15 p. (2022)

Original Article | Science

IF: 7,666

Zsely Boglarka, **Ronaszeki Aladar David**, Toth Ambrus, Bakos Bence, Szekely Eszter, Gyori

Gabriella, Berczi Viktor, Novak Kaposi Pal

Splenic hamartoma in a patient with peripancreatic arterial arcades: A case report

IMAGING 14: 2 pp. 116-119. (2022)

Short Article | Science

Cumulative impact factor of the candidate's publications related to the thesis: ∑**IF: 5.169**

Total cumulative impact factor of the candidate's publications: ∑**IF: 24,976**

10. ACKNOWLEDGEMENTS

The present work would not have been achievable without the tremendous support of several individuals and I would like to extend my gratitude to all those who made this Ph.D. thesis possible.

First of all, I would like to express my gratitude to my supervisor, Novák Pál Kaposi, whose continuous guidance and support helped me grow as a researcher.

I consider it a privilege that I had the opportunity to spend two fruitful years under his supervision in the Body Imaging Research Group of the Medical Imaging Centre.
I am also grateful to Professor Pál Maurovich-Horvat, whose leadership and constant guidance paved the way for my progress in the scientific field. Without his professional, financial and intellectual support, none of our achievements would have been possible.

During my studies I was fortunate to be surrounded by some of the greatest minds in the field of gastroenterology. I cannot thank Krisztina Hagymási enough for her continued effort to guide me during my Ph.D. studies and for all the patient management and interobserver examinations on every Monday afternoon.

I want to express my appreciation to Bettina Katalin Budai and Róbert Stollmayer for their helpful suggestions and for all the support in statistics, in radiomics and encouragement and support they gave to me during my Ph.D. years.

We would like to thank Ms. Lilla Petovsky, Ms. Éva Juhász, Ms. Ramóna Varga, Mr. Tamás Wenzel, and Mr. Tamás Péntek for performing the MRI examinations. We also thank Ms. Rita Tornai for assistance with ultrasound examinations and Ms. Vilma Kis for assistance with patient scheduling.

I received unending support from my colleagues, and I would like to express my

appreciation to Anikó Folhoffer, Árpád Patai, Professor Viktor Bérczi, Ildikó Kalina, Gabriella Győri. Furthermore, I deeply appreciate the work of devoted assistants and radiographers.

Last but not least, I am thankful to my parents for their tremendous support and I am especially grateful to my significant other, Boglárka Zsély whose continuous support helped me overcome some of this challenging period of my life so far.

processes

MDPI

Article

Follow-Up of Liver Stiffness with Shear Wave Elastography in Chronic Hepatitis C Patients in Sustained Virological Response Augments Clinical Risk Assessment

Anikó Folhoffer [1,†], Aladár D. Rónaszéki [2,*,†], Bettina K. Budai [2], Petra Borsos [2], Vince Orbán [2], Gabriella Győri [2], Ferenc Szalay [1] and Pál N. Kaposi [2]

[1] Department of Internal Medicine and Oncology, Faculty of Medicine, Semmelweis University, Korányi S. u. 2/a, H-1083 Budapest, Hungary; folhoffer.aniko@med.semmelweis-univ.hu (A.F.); szalay.ferenc@med.semmelweis-univ.hu (F.S.)

[2] Department of Radiology, Medical Imaging Centre, Faculty of Medicine, Semmelweis University, Korányi S. u. 2., H-1083 Budapest, Hungary; budai.bettina@med.semmelweis-univ.hu (B.K.B.); petraborsos96@gmail.com (P.B.); orban.vince@med.semmelweis-univ.hu (V.O.); gyori.gabriella@med.semmelweis-univ.hu (G.G.); kaposi.pal@med.semmelweis-univ.hu (P.N.K.)

* Correspondence: ronaszeki.aladar_david@med.semmelweis-univ.hu; Tel./Fax: +36-(1)-459-1500 x.61626

† These authors contributed equally to this work.

Abstract: This study aimed to observe the effect of the direct-acting antiviral (DAA) therapy on liver stiffness (LS) and serum biomarkers. We prospectively observed 35 patients with chronic hepatitis C infection and attained a sustained virological response (SVR) after antiviral therapy. Shear wave elastography (SWE) measurement was performed at the beginning of DAA treatment and at 48 weeks after the end of treatment (EOT48w). The METAVIR score and the score for varices needing treatment (VNT) were determined based on the LS values; the fibrosis-4 (FIB4) score was calculated from laboratory tests. The baseline LS (mean ± standard deviation = 2.59 ± 0.89 m/s) decreased significantly after successful DAA therapy (1.90 ± 0.50 m/s; $p < 0.001$). The METAVIR score showed significant improvement at EOT48w (F0/1 = 9, F2 = 2, F3 = 10, F4 = 14) compared to the initial status (F0/1 = 2, F2 = 1, F3 = 7, F4 = 25; $p < 0.028$). The FIB4 score indicated less fibrosis after therapy (2.04 ± 1.12) than at baseline (3.51 ± 2.24; $p < 0.018$). Meanwhile, the number of patients with a high-risk of VNT was significantly less at EOT48w (4 vs. 15 at baseline; OR = 0.17 95% confidence interval (CI) = 0.05–0.59, $p < 0.007$). SWE indicates a significant resolution of liver fibrosis when chronic hepatitis C patients are in SVR, coinciding with a lower risk of VNT.

Keywords: chronic hepatitis C; HCV virus; direct-acting antivirals; shear wave elastography; liver stiffness

Citation: Folhoffer, A.; Rónaszéki, A.D.; Budai, B.K.; Borsos, P.; Orbán, V.; Győri, G.; Szalay, F.; Kaposi, P.N. Follow-Up of Liver Stiffness with Shear Wave Elastography in Chronic Hepatitis C Patients in Sustained Virological Response Augments Clinical Risk Assessment. *Processes* **2021**, *9*, 753. https://doi.org/10.3390/pr9050753

Academic Editor: Katarzyna Otulak-Kozieł

Received: 30 March 2021
Accepted: 22 April 2021
Published: 24 April 2021

1. Introduction

Hepatitis C infection (HCV) is a major cause of liver morbidity worldwide, with approximately 71 million chronically infected patients. Due to significant progress in the medical therapy of HCV, the World Health Organization (WHO) is aiming for the elimination of HCV infection as a public health threat by 2030, achieving a 90% drop in the incidence compared with 2015 [1]. Interferon (IFN) free direct-acting antivirals (DAAs) have become the standard treatment of HCV hepatitis since 2014 when they were first approved for clinical use by the European Medical Agency [2]. The therapeutic efficiency of DAAs is significantly higher than previous IFN-based regimens, with an eradication rate as high as 90% in non-cirrhotic patients. The DAAs also have accelerated treatment protocols, usually 12 to 24 weeks, cause fewer side effects, and are associated with better patient compliance compared with IFN [3].

Assessment of liver fibrosis is of high importance prior to therapy. The diagnosis of advanced fibrosis (METAVIR stage F3) and cirrhosis (METAVIR stage F4) can alter

the choice of a treatment regimen, the therapeutic response rate, and the post-treatment prognosis in affected patients [2,4]. International guidelines now recommend the treatment of all HCV-infected patients and emphasize that those with significant liver fibrosis or cirrhosis must be considered for treatment without delay. Patients with F3 and F4 stage fibrosis also require continued surveillance for HCC every six months, even after successful completion of therapy. Non-invasive methods are preferred over liver biopsy for initial assessment of liver fibrosis in this setting [5,6]. Shear wave elastography (SWE) is a universally accepted non-invasive technique for the staging of fibrosis in chronic hepatitis C [7,8]. It measures the liver stiffness (LS) and can be completed in accession to routine ultrasound evaluation of liver morphology. SWE was thoroughly validated by multiple studies and was found to have very good accuracy and reproducibility for the diagnosis of clinically significant fibrosis (METAVIR stage $\geq$ F2) and cirrhosis (F4) [9,10]. In addition, SWE does not need specific instrumentation, as this application is commonly available on most newly developed ultrasound scanners, which significantly contributed to the wide-scale acceptance of the technique.

International guidelines universally recommend non-invasive methods for the initial assessment of liver fibrosis in chronic hepatitis C patients. However, we have only limited experience applying elastography for patient follow-up after completing the antiviral treatment [11]. Previous studies mostly used transient elastography (TE) to detect changes in the fibrosis stage in response to INF-based regimens [12,13]. These reports indicated a more substantial decrease in LS of patients with a sustained virological response (SVR) compared to relapsers or non-responders. The short-term improvement in the LS observed at 12 and 24 weeks after the end-of-treatment (EOT) was attributed to the decline in the inflammatory reaction after clearing the HCV infection. Meanwhile, an improved hepatic venous pressure gradient (HVPG) and the resolution of the fibrotic changes on liver biopsy were also reported during long-term follow-up of patients with SVR [14]. Acoustic radiation force impulse (ARFI) elastography, a technique similar to SWE, was used for the follow-up of DAA-treated patients in only a handful of studies, which found significant regression in the fibrosis stage in SVR [15].

There is very little information on the post-treatment follow-up of patients with SWE who have a high-risk of cirrhosis-associated complications. Currently, patients diagnosed pre-treatment with F3 or F4 stage fibrosis need life-long ultrasound surveillance for HCC; however, it is unclear how long the higher risk of HCC persists in SVR and after SWE detects a decrease in fibrosis [16]. Clinically significant HVPG and esophageal varices (EV) are severe complications in compensated advanced chronic liver disease (cACLD) and are also associated with poor disease outcomes [17]. Elastography techniques are able to identify patients with varices needing treatment (VNT) by exposing highly elevated LS values in severe portal hypertension. Consequently, the Baveno VI consensus proposed the assessment of LS and platelet count in its criteria for non-invasive screening for VNTs [18]. Currently, there is limited information available on the risk of VNT after successful antiviral therapy in hepatitis C patients.

The aim of our study was to detect changes in the LS with SWE in chronic hepatitis C patients after treatment with new antiviral protocols. We also aimed to show that SWE can re-evaluate risk factors of cirrhosis-associated complications in SVR.

2. Materials and Methods

2.1. Patient Population

The present study was approved by the institutional ethics committee of our university (SE-TUKEB 163/2017), and written informed consent was obtained from all subjects according to the World Medical Association Declaration of Helsinki, revised in 2000 in Edinburgh. We prospectively enrolled 35 patients who were diagnosed with chronic HCV infection and who attained SVR after treatment with DAA agents (n = 32) or interferon-based treatment (n = 3) between October 2016 and January 2020. The inclusion criteria were the follows: patients had to be older than 18 years, the HCV infection had to be

proved with anti-HCV antibody positivity and HCV RNA positivity by PCR test for at least 6 months prior to the beginning of the antiviral treatment, and the patient had to consent to antiviral therapy and have attained sustained viral response after antiviral therapy. Patients with extrahepatic cholestasis, hepatocellular carcinoma, known congestive heart failure, unsuccessful shear wave elastography measurements, or mixed etiology liver disease were excluded from the study. BMI > 30 kg/m^2, pregnancy, and breastfeeding were also exclusion criteria. The final patient cohort included 19 males and 16 females with a median age of 61 years (interquartile range: 59–65.5 years). All patients underwent a baseline ultrasound scan, which included a liver stiffness measurement with shear wave elastography (SWE) before starting the antiviral treatment. The SWE was repeated in an average of 48 weeks after the end of the antiviral treatment (EOT48w). The patients received the following antiviral combinations: sofosbuvir (SOF)/ledipasvir (n = 5), SOF/ledipasvir/ribavirin (RBV) (n = 10), ombitasvir /paritaprevir /ritonavir/dasabuvir (n = 15), glecaprevir/pibrentasvir (n = 1), SOF/simeprevir (n = 1), peginterferon alpha-2a (PegIFN)/RBV (n = 2), and PegIFN/RBV/boceprevir (n = 1). The treatment duration was 12 weeks in 21 patients, 24 weeks in 11 patients, and 48 weeks in 3 patients.

2.2. Liver Stiffness Measurements with Shear Wave Elastography

A Samsung RS80 Prestige or an RS85A ultrasound scanner (Samsung Medison, Hongcheon, Korea) equipped with the CA1-7A convex probe was used for the liver ultrasound scans. All SWE measurements were performed with the S-Shearwave^{TM} application following the recommended protocol of the manufacturer. The median LS of at least five measurements was reported in m/s units, and it was converted to kilopascal (kPa) to determine the risk of clinically significant hypertension (>20 kPa). Only measurements with a reliable measure index (RMI) $\geq$ 0.4 were considered acceptable. The SWE was technically successful if we were able to collect at least five reliable LS values, and the interquartile range (IQR) of the individual measurements was <30% of the median (Figures 1 and 2). The METAVIR score of liver fibrosis was determined for each patient both before and after the antiviral treatment based on the result of the SWE. The following cutoff values were used: F0/1 < 1.46 m/s, F2 $\geq$ 1.46 m/s, F3 $\geq$ 1.63 m/s, F4 $\geq$ 1.95 m/s, as was described previously [10]. The amount of ascites, if present, was also reported based on the ultrasound scan.

2.3. Collection of Laboratory Tests and Clinical Data

Serum creatinine (CRE), sodium (Na), aspartate transaminase (AST), alanine aminotransferase (ALT), gamma-glutamyl transferase (GGT), total bilirubin (TBILL), albumin (ALB) levels, platelet count (PLT), and international normalization ratio (INR) were collected from electronic medical records of the patients at baseline and at the time of the post-treatment SWE. HCV RNA in the serum was detected with an AmpliPrep/COBAS, TaqMan version 2 assay (Roche, Pleasanton, CA, USA). SVR was defined as undetectable HCV RNA at both 24 and 48 weeks after treatment. The model for end-stage liver disease (MELD) and Child-Turcotte-Pugh (CTP) scores and the Fibrosis-4 score for liver scarring (FIB4) were calculated from laboratory parameters with the MDCalc online tool (www.mdcalc.com, accessed on 12th March 2021). Following the recommendations of the Baveno VI guidelines, the patients were also divided into low-risk and high-risk (PLT < 150 G/L, LS > 20 kPa) groups of esophageal VNT [17] (Figure 3).

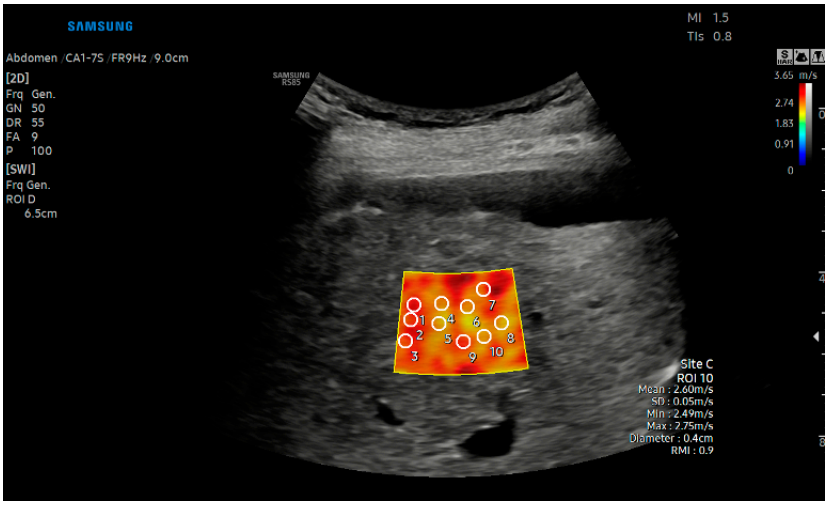

(**a**)

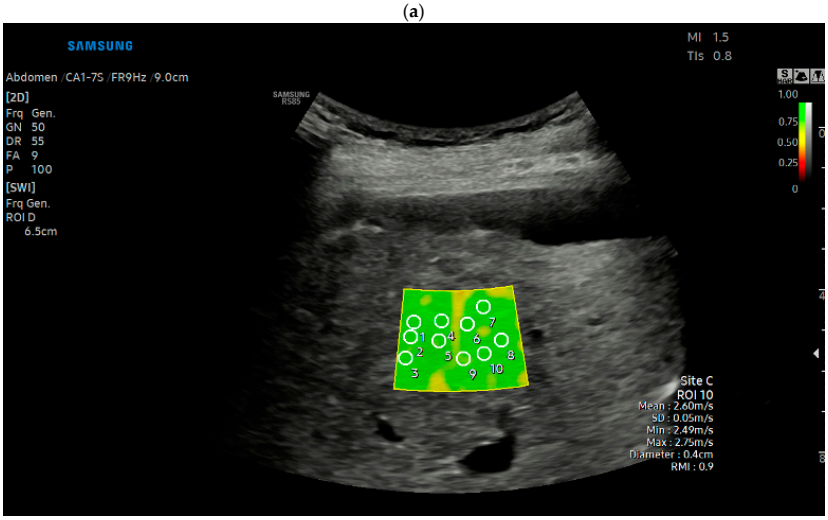

(**b**)

Figure 1. Liver stiffness (LS) measurement with 2D shear wave elastography (SWE). (**a**) LS measurement of a cirrhotic patient. The LS was reported in m/s units. (**b**) Color-coded map of the reliable measure index (RMI) values of SWE measurement was used for ROI selection in the cirrhotic liver parenchyma. Only measurements with an RMI ≥ 0.4 were considered acceptable.

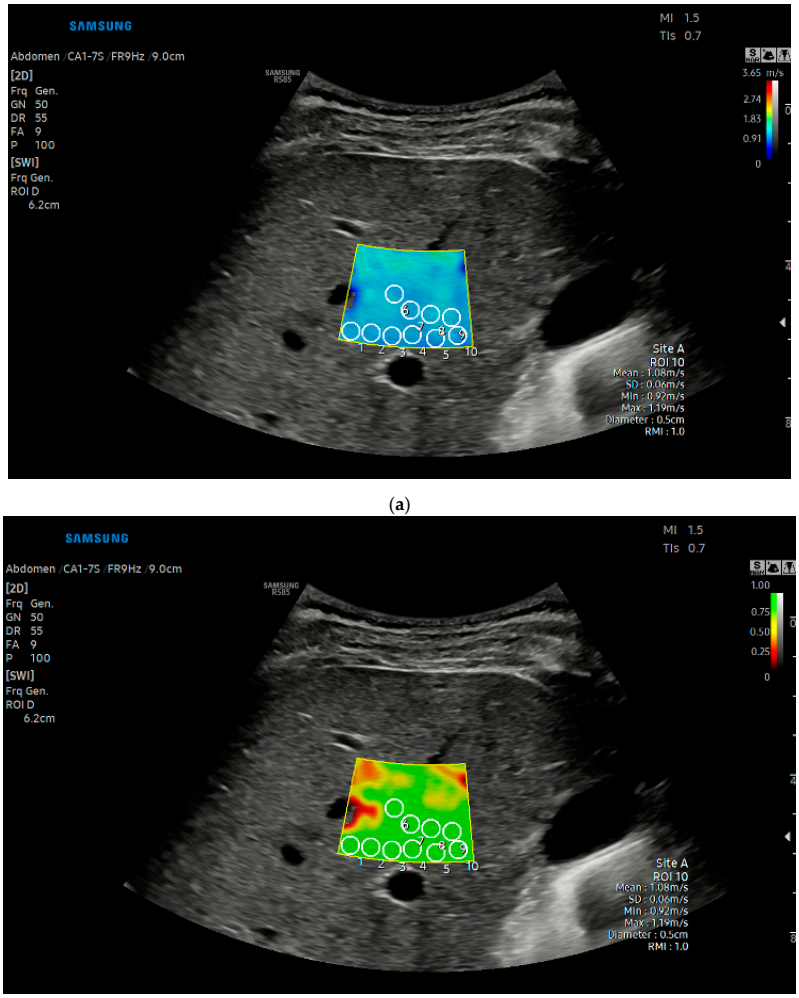

Figure 2. Liver stiffness (LS) measurement with 2D shear wave elastography (SWE). (**a**) SWE measurement of a liver with no significant fibrosis. The LS was reported in m/s units. (**b**) Color-coded map of the RMI was used for the ROI selection during 2D-SWE of a liver with no significant fibrosis.

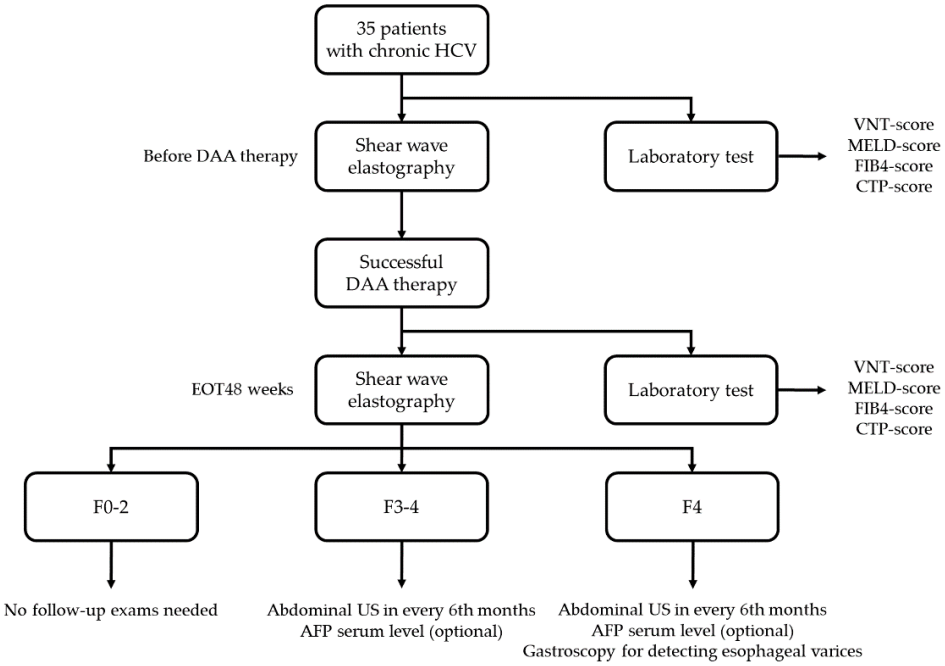

Figure 3. The flowchart shows the design of our prospective study. We prospectively enrolled 35 patients who were diagnosed with chronic hepatitis C virus infection and who attained sustained virological response after treatment with DAA agents or interferon-based treatment. The METAVIR score of liver fibrosis was determined for each patient both before and after the antiviral treatment based on the result of the shear wave elastography measurement. The FIB4 score, the number of patients with varices needing treatment, the Child-Turcotte-Pugh class, and the MELD-score were calculated from laboratory tests as it was described previously [17,19–21]. HCV: hepatitis C virus; DAA: direct-acting antiviral therapy; EOT48w: 48 weeks after successful antiviral treatment; VNT: varices needing treatment; MELD: model for end-stage liver disease; FIB4-score: fibrosis-4 score; CTP: Child-Turcotte-Pugh; AFP: alpha-fetoprotein; US: ultrasound.

2.4. Statistical Analysis

The paired Student's *t*-test was used to compare pre- and post-treatment LS values and laboratory parameters. Fisher's exact test was used to compare the distributions of categorical variables such as cirrhosis stage and VNT risk before and after treatment. The odds ratios (OR) are reported together with the 95% confidence intervals (CI). In the case of continuous variables, we report the mean and the standard deviation (SD); in the case of categorical variables, the frequency and the percentage are reported. We set the limit of statistical significance at $p < 0.05$. The statistical analysis was completed with the R x64 v3.4.1 software package (www.r-project.org accessed on 12th March 2021).

3. Results

3.1. LS Decreases after Successful Antiviral Therapy

The liver stiffness was significantly lower ($p < 0.001$) at 48 weeks after EOT (1.90 ± 0.50 m/s) compared to the matched values before treatment (2.59 ± 0.89 m/s). The METAVIR score was calculated at each time point based on the SWE measurements, and it also showed significant improvement ($p < 0.028$) after treatment (F0/1 = 9, F2 = 2, F3 = 10, F4 = 14)

compared to the baseline (F0/1 = 2, F2 = 1, F3 = 7, F4 = 25) (Figure 4) (Table 1). The number of cirrhotic cases (F4) was also significantly lower (OR = 0.27, 95% CI = 0.09–0.72, $p < 0.016$) at EOT48w. The average decrease in LS was greater ($p < 0.028$) in cirrhotic cases (F4, Δ-LS = -0.87 ± 0.79 m/s) than in non-cirrhotic cases (F0/1, ΔLS = -0.26 ± 0.37). The LS improved in 31 out of 35 patients in SVR, and it slightly increased in only four cases, including two cirrhotic and two F2 grade fibrosis patients (Figure 5).

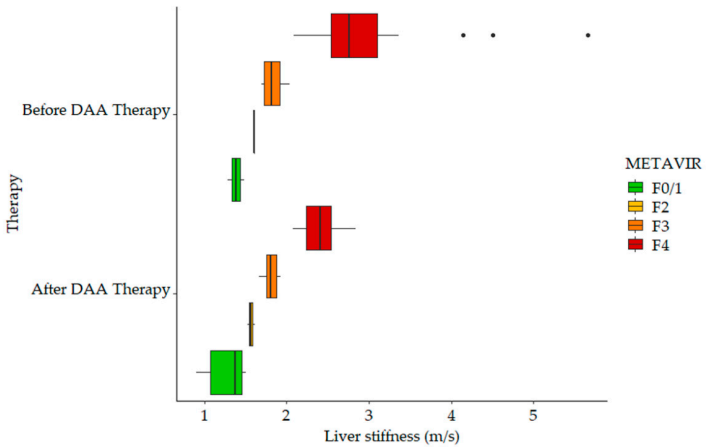

Figure 4. The boxplots demonstrate the improvement of liver fibrosis following antiviral treatment. Liver fibrosis was classified into four METAVIR stages (F0/1, F2, F3, F4) based on the SWE measurement. The post-treatment measurement was performed 48 weeks after the completion of antiviral treatment. We detected significantly improved fibrosis and a lower proportion of cirrhotic cases after successful direct-acting antiviral (DAA) therapy.

Table 1. Comparison between pre- and post-treatment liver stiffness and METAVIR scores.

	Baseline	**EOT48w** [1]	***p*-Value** [2]	**Odds-Ratio**
LS	2.59 ± 0.89 m/s	1.90 ± 0.50 m/s	$p < 0.001$	NA
METAVIR [3]			$p < 0.028$	NA
F0/1	2 (5.7%)	9 (25.7%)	$p < 0.045$	5.71 (1.13–28.74)
F2	1 (2.8%)	2 (5.7%)	$p < 1.00$	2.06 (0.18–23.82)
F3	7 (20%)	10 (28.6%)	$p < 0.578$	1.60 (0.53–4.83)
F4	25 (71.4%)	14 (40%)	$p < 0.015$	0.27 (0.09–0.72)

[1] 48 weeks after the completion of antiviral treatment with sustained virological response. [2] For comparing means between pre- and post-treatment groups, the paired Student's *t*-test was used; for frequencies, the Fisher's exact test was used. [3] The METAVIR score was calculated from liver stiffness by using the previously described cutoff values. LS: liver stiffness; NA: not applicable.

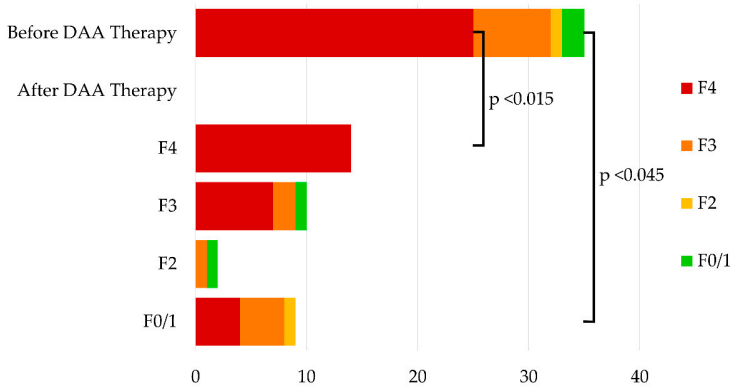

Figure 5. The bar plots demonstrate the improvement of liver fibrosis following antiviral treatment. The liver stiffness was determined during a pre-treatment ultrasound scan with shear wave elastography (SWE). Liver fibrosis was classified into four METAVIR stages (F0/1, F2, F3, F4) based on the SWE measurement. The post-treatment measurement was performed 48 weeks after the completion of antiviral treatment. The number of patients in the different METAVIR stages is represented by the colored bands of the bar plots. Based on the METAVIR score, the number of cirrhotic cases (F4) was significantly lover ($p < 0.015$) at EOT48w, while the number of cases with F0/1 showed significant increasement ($p < 0.045$) after treatment compared to the baseline.

3.2. Laboratory Tests Improve in Parallel with LS

The ALT level significantly improved after treatment, and it returned to the normal range with two exceptions in all patients at EOT48w. In comparison, only 10 patients had normal ALT at the baseline (OR = 0.02, 95% CI = 0.005–0.12, $p < 0.001$). The GGT level was elevated in 26 patients before treatment but only in seven patients at the time of post-treatment follow-up (OR = 0.087, 95% CI = 0.03–0.27, $p < 0.001$). The ALB returned to the normal range in all six cirrhotic patients who had low baseline levels. AST, TBILL, and CRE levels at EOT48w were also closer to the normal range than the pre-treatment levels. The rest of the serum markers, including PLT, INR, and Na, all showed an improvement, but they did not reach statistical significance (Table 2). We calculated the FIB4 score as an alternative non-invasive laboratory marker of liver fibrosis. Similar to the SWE, the FIB4 score also indicated significantly ($p < 0.018$) lower post-treatment fibrosis (2.04 ± 1.12) compared to the pre-treatment status (3.51 ± 2.24).

Table 2. Comparison of laboratory tests before and after treatment.

	Baseline	**EOT48w** [1]	***p*-Value** [2]
AST (IU/L)	75.7	27.7	$p < 0.019$
ALT (IU/L)	92.7	25	$p < 0.001$
GGT (IU/L)	137.1	54.1	$p < 0.001$
TBILL (µmol/L)	20.5	16.9	$p < 0.030$
ALB (g/L)	41.3	43.8	$p < 0.001$
CRE (µmol/L)	70.7	74	$p < 0.023$
Na (mmol/L)	138.1	139.6	$p < 0.104$
INR	1.2	1.3	$p < 0.288$
PLT (10^9/L)	168.5	180	$p < 0.249$

[1] 48 weeks after the completion of antiviral treatment with sustained virological response. [2] For comparing means between pre- and post-treatment groups, the paired Student's *t*-test was used, while for frequencies, the Fisher's exact test was used. ALB: serum albumin, ALT: alanine aminotransferase, AST: aspartate aminotransferase, CRE: serum creatinine, GGT: gamma-glutamyl transpeptidase, INR: international normalized ratio, Na: serum sodium, PLT: platelet, count, TBILL: total bilirubin.

3.3. The Risk of Esophageal VNT Decreases in SVR

We also calculated the CTP and the MELD scores for each patient to assess clinical improvement following antiviral therapy (Table 3). Five CTP class B cirrhotic patients were identified in the original patient cohort, and four of these converted to class A after treatment. A small to moderate amount of ascites was observed in two patients at the baseline and in one patient at EOT48w on the ultrasound scan. The MELD score did not change significantly; out of two patients with high mortality risk (MELD > 20) before treatment, only one had lower risk (MELD $\leq$ 20) at EOT48w (Table 3).

Table 3. Changes in clinical risk factors due to anti-HCV therapy.

	Baseline	**EOT48w** [1]	***p*-Value** [2]	**Odds Ratio**
Ascites	2 (6%)	1 (3%)	$p < 1.00$	0.49 (0.04–5.61)
FIB4 score [3]	3.51 ± 2.24	2.04 ± 1.12	$p < 0.018$	NA
VNT [3]	15 (42%)	4 (11%)	$p < 0.007$	0.17 (0.05–0.59)
CTP class [3]				
A	30 (86%)	34 (97%)	$p < 0.127$	5.67 (0.63–51.27)
B	5 (14%)	1 (3%)		0.18 (0.02–1.60)
C	0	0	NA	NA
MELD score [3]				
<10	25 (71%)	25 (71%)	$p < 1.00$	1.00 (0.35–2.82)
<20	8 (23%)	9 (26%)	$p < 1.00$	0.86 (0.29–2.56)
<25	2 (6%)	1 (3%)	$p < 0.619$	2.06 (0.18–23.82)
≥25	0	0	NA	NA

[1] 48 weeks after the completion of antiviral treatment with sustained virological response. [2] For comparing means between pre- and post-treatment groups, the paired Student's *t*-test was used; for frequencies, the Fisher's exact test was used. [3] The FIB4 score, the number of patients with VNT, the CTP class, and the MELD score were calculated as described previously [17,19–21]. CTP: Child-Turcott-Pugh classification, Fib-4: fibrosis-4 score, MELD: Model for End-Stage Liver Disease, VNT: varices needing treatment.

The risk of VNT was calculated from the PLT and the LS values according to the Baveno VI guidelines. High-risk of esophageal VNT was detected in 15 cirrhotic patients at baseline and in four patients at the follow-up (OR = 0.17, 95% CI = 0.05–0.59, $p < 0.007$).

4. Discussion

Because the stage of liver fibrosis is a key predictor of complications and mortality in patients with chronic HCV infection, we aimed to measure liver fibrosis with SWE before and after SVR in patients treated mainly with DAAs. According to public databases, there is an increasing number of chronic hepatitis C patients with advanced liver fibrosis who became virus-free as a result of modern antiviral therapy [22]. If reversal of fibrosis could be demonstrated with non-invasive techniques, such as SWE, it could result in the reclassification of previously high-risk patients to a lower risk category of liver disease-related complications; eventually, the reassessment with SWE would alter the management and the long-term outcome of these patients.

D'Ambrosio and colleagues published an article in 2012 summarizing the long-term follow-up of 38 chronic hepatitis C patients after reaching SVR [23]. Their prospective study included cirrhotic patients who received successful peg-IFN and ribavirin therapy, attained SVR, and they were followed for at least four years afterward. Semiquantitative histological staging of fibrosis according to the METAVIR system as well as a morphometric determination of collagen content, assessment of necroinflammatory activity, and ductular proliferation were performed on paired pre- and post-treatment liver biopsies. All of the 38 enrolled patients had F4 stage fibrosis pre-treatment according to the METAVIR staging system. As the result of the treatment, the fibrosis in 61% of the patients was categorized as at least one stage lower at an average follow-up of 61 months from SVR. In the samples of post-treatment F4 patients, the fibrotic area was also significantly reduced based on the collagen content compared to the pre-treatment samples. Our result corroborates the above findings as we also observed down-staging of cirrhosis (F4) in 46% and advanced

fibrosis (F3) in an additional 30% of the cases at 48 weeks after EOT based on the SWE. Additionally, we measured lower LS with two exceptions in all patients, including even those who did not change into a lower METAVIR stage. It is important to emphasize that biopsy specimens demonstrated an 89% reduction in collagen content, which could explain the lower LS values in SVR, as LS observed with SWE were clearly shown to be in direct correlation with the amount of fibrosis measured on biopsy [24]. Meanwhile, our follow-up time was much shorter, 12 months vs. 61 months in SVR; thus, the dissolution of the necroinflammatory infiltrates might have contributed to the relatively rapid improvement in LS. Examination of serum AST levels found that 37 patients initially had elevated levels, while 36 patients had AST levels in the normal range at the end of treatment [23]. We also observed a similar trend in our patient population where AST levels returned to the normal range with two exceptions and ALT with one exception in all patients. Similar findings were reported by Tachi et al., who followed 176 INF and DAA-treated patients in SVR with ARFI in a prospective study [25]. The authors also compared the elastography results with another patient cohort of 140 patients who had paired pre- and post-treatment liver biopsies. There was a significant reduction in LS at 24 weeks after EOT compared to the baseline LS in all stages. The highest drop in LS was detected in the F3 stage. The grade of inflammatory activity on the pre-treatment biopsy was also a significant independent predictor of post-treatment LS reduction in a multivariate linear regression analysis. Based on their observations, the authors concluded that, in addition to slow improvement in liver fibrosis, resolution of the inflammation also contributes to short-term improvement in LS after EOT.

Facciorusso et al. examined the long-term effects of antiviral therapy on liver fibrosis in 153 patients using TE [26]. Of their patients, 70 received interferon-based treatment, and 83 received DAA therapy. Initially, 34.6% of their patients were diagnosed with cirrhosis. In total, 112 of their patients attained SVR, and 41 were found to be non-responders. Using 12.5 kPa as the cutoff value, 32.1% of patients were classified as METAVIR stage F4 before therapy, while 87.5% were classified as F3. The number of patients with F4-stage disease decreased significantly at the end of treatment to only 20.5%. The authors observed that the mean LS of patients achieving SVR decreased from 12.3 kPa to 6.6 kPa by the end of the 5 year follow-up. The largest decrease was observed in the early follow-up period, which was 2.5 kPa at EOT and 3.7 kPa at six months after EOT. After the first year, the rate of LS decline slowed down. The number of cirrhotic patients was halved at six months, and it was less than 5% at four years after EOT. Thus, it was demonstrated that LS significantly decreases after SVR is attained, and the rate of decline is the highest during the first year after EOT. Our results are consistent with the above-described observations. However, in our study, we used SWE, our patients were treated mostly with DAAs, and all of them were in SVR at the follow-up at 48 weeks EOT. These differences in the study design may explain why we saw a higher drop in LS, from 2.59 m/s (20.5 kPa) to 1.90 m/s (11.7 kPa), in our patient cohort at one year from EOT.

Attia et al., who used TE and ARFI elastography to follow up with 275 chronic hepatitis C patients after successful DAA treatment, also detected a significant decrease (from 2.04 m/s to 1.75 m/s) in LS at 24 weeks after EOT with both techniques [15]. Both the incidence and the rate of the decline in LS were higher in cirrhotic patients attaining SVR than in patients with lower-grade fibrosis. Meanwhile, the LS of patients with advanced-stage decompensated liver disease at baseline was more likely to progress, even during SVR. In all the patients whose LS progressed during the follow-up, the baseline TE measurement was above 17 kPa, which is associated with clinically significant portal hypertension according to the Baveno VI guidelines. According to the authors, these findings suggest that, in patients with decompensated disease and portal hypertension, the fibrosis reaches a stage where the clearance of HCV cannot reverse the progression. In comparison, our patient cohort included 15 patients with clinically significant hypertension and VNT; however, we found progression in LS in only two of these patients (13%), which indicates improving fibrosis in the majority of the decompensated patients after clearance of HCV.

Therefore, our findings suggest that even patients with advanced-stage fibrosis need efficient antiviral treatment, as it could lower the risk of severe complications.

Clinical studies also demonstrated that SVR is associated with a lower risk of variceal bleeding [27,28]. The Baveno VI Consensus Workshop guideline recommends stratification of patients with a cutoff at LS > 20 kP and PLT < 150,000 μ/L to identify the group with a high risk of clinically significant varices. However, the utility of the Baveno VI criteria is not yet evaluated in SVR. We found a reduced risk of esophageal VNT according to the Baveno VI guidelines in 73% of the high-risk patients who achieved SVR. Our study is among the first to demonstrate that SWE is able to determine the lower risk of variceal bleeding post-SVR, which may simplify the clinical management of these patients. According to the American Gastroenterological Association Institute, it is recommended that HCV-RNA levels be measured 12 to 48 weeks after EOT, and testing 24 weeks after EOT is recommended only in select cases [16]. According to the directive, routine RNA testing after confirmation of viral freedom by PCR is only recommended for patients with a high risk of re-infection, as other patients have a low probability of late relapse, thus, if their complaint or symptoms do not make it necessary, further RNA detection-based screening is not required. Endoscopic varicose screening is also recommended for all patients with cirrhosis, the outcome of which (rather than the attainment of SVR) necessitates further testing and follow-up [16]. An important objective of the continued follow-ups in SVR is screening for HCC, which is not required in people with stage 0–2 fibrosis. However, in patients who had at least stage 3 fibrosis initially, HCC screening should be continued, even after viral clearance, using a combination of imaging and AFP measurement twice a year. The screening should be continued for the rest of the life of the affected patients, because the incidence of HCC may remain higher in patients with advanced fibrosis, even a long time after viral clearance is achieved [25,29]. This is especially true for those patients who consume alcohol frequently. Our results indicate that a complementary SWE can improve the prognostic value of regular ultrasound screening by identifying patients with resolving fibrosis, who, therefore, may have a lower risk of HCC and may require less frequent follow-ups, although multi-center longitudinal studies are still required to determine long-term changes in LS post-SVR as well as their effect on the incidence of HCC.

5. Conclusions

In summary, SVR in chronic hepatitis C is associated with significantly more favorable outcomes and a lower risk of serious complications. Nevertheless, the chance of developing HCC or variceal bleeding still remains higher than in the general population. Therefore, close monitoring with imaging and clinical studies is recommended, especially for patients with advanced-stage pre-treatment fibrosis. Our study demonstrates a significant reduction in LS and consequently in the non-invasive staging of fibrosis a year after SVR is attained. These results may indicate that adding SWE to the follow-up imaging protocol can improve patient management by amending the initial assessment of the fibrosis stage and the identification of patients whose risk of liver disease-related complications is significantly lowered as the result of SVR. Thus, SWE can contribute to the development of more efficient follow-up protocols which are better tailored to the individual needs of chronic hepatitis C patients with liver fibrosis.

Author Contributions: A.F. and P.N.K. were responsible for the conception and design of the study; P.N.K. and G.G. performed the liver ultrasound and elastography measurements; B.K.B., A.D.R., P.B. and V.O. contributed to data collection and analysis; A.F. and F.S. contributed to patient selection and collection of clinical data; B.K.B. and V.O. contributed to editing and reviewing the manuscript. All authors have read and agreed to the published version of the manuscript.

Funding: P.N.K. (Bolyai 386/2017) was supported by the János Bolyai Research Scholarship of the Hungarian Academy of Sciences (https://mta.hu/bolyai-osztondij accessed on 23rd April 2021). B.K.B. and P.N.K. received financial support from the GINOP 2-2-18 grant. The funders had no role in the study design, data collection and analysis, decision to publish, or preparation of the manuscript.

Institutional Review Board Statement: The study was conducted according to the guidelines of the Declaration of Helsinki, and approved by the Ethics Committee of the Semmelweis University (Semmelweis University Regional and Institutional Committee of Science and Research) (SE-TUKEB 163/2017, date of approval: 7 August 2017).

Informed Consent Statement: Informed consent was obtained from all subjects involved in the study.

Data Availability Statement: The data presented in this study are available on request from the corresponding author.

Acknowledgments: The authors would like to express their gratitude to Sonarmed Ltd. and to Samsung Ultrasound Training Center at Semmelweis University for providing an ultrasound scanner for the study. The authors thank László Giay for his enthusiastic support of our research. We are also thankful to Zsuzsa Kizman from the 1st Department of Internal Medicine for her assistance with patient appointments and data collection.

Conflicts of Interest: The authors declare no conflict of interest.

References

1. Lombardi, A.; Mondelli, M.U. ESCMID Study Group for Viral Hepatitis (ESGVH) Hepatitis C: Is eradication possible? *Liver Int.* **2019**, *39*, 416–426. [CrossRef]
2. Pawlotsky, J.-M.; Negro, F.; Aghemo, A.; Berenguer, M.; Dalgard, O.; Dusheiko, G.; Marra, F.; Puoti, M.; Wedemeyer, H. EASL Recommendations on Treatment of Hepatitis C. *J. Hepatol.* **2018**, *69*, 461–511. [CrossRef]
3. Holmes, A.J.; Rutledge, S.M.; Chung, R.T. Direct-Acting Antiviral Treatment for Hepatitis C. *Lancet* **2019**, *393*, 1392–1394. [CrossRef]
4. Ghany, M.G.; Morgan, T.R.; Panel, A.H.C.G.; Marks, K.M.; Wyles, D.L.; Aronsohn, A.I.; Bhattacharya, D.; Broder, T.; Falade-Nwulia, O.O.; Feld, J.J.; et al. Hepatitis C Guidance 2019 Update: American Association for the Study of Liver Diseases–Infectious Diseases Society of America Recommendations for Testing, Managing, and Treating Hepatitis C Virus Infection. *Hepatology* **2019**, *71*, 686–721. [CrossRef] [PubMed]
5. Budai, B.K.; Tóth, A.; Borsos, P.; Frank, V.G.; Shariati, S.; Fejér, B.; Folhoffer, A.; Szalay, F.; Bérczi, V.; Kaposi, P.N. Three-Dimensional CT Texture Analysis of Anatomic Liver Segments can Differentiate between Low-Grade and High-Grade Fibrosis. *BMC Med Imaging* **2020**, *20*, 1–11. [CrossRef] [PubMed]
6. Low, G. General Review of Magnetic Resonance Elastography. *World J. Radiol.* **2016**, *8*, 59–72. [CrossRef]
7. Ferraioli, G.; Tinelli, C.; Bello, B.D.; Zicchetti, M.; Filice, G.; Filice, C.; Liver Fibrosis Study Group. Accuracy of Real-Time Shear Wave Elastography for Assessing Liver Fibrosis in Chronic Hepatitis C: A Pilot Study. *Hepatology* **2012**, *56*, 2125–2133. [CrossRef]
8. Karlas, T.; Pfrepper, C.; Wiegand, J.; Wittekind, C.; Neuschulz, M.; Mössner, J.; Berg, T.; Tröltzsch, M.; Keim, V. Acoustic Radiation Force Impulse Imaging (ARFI) for Non-Invasive Detection of Liver Fibrosis: Examination Standards and Evaluation of Interlobe Differences in Healthy Subjects and Chronic Liver Disease. *Scand. J. Gastroenterol.* **2011**, *46*, 1458–1467. [CrossRef] [PubMed]
9. Bota, S.; Herkner, H.; Sporea, I.; Salzl, P.; Sirli, R.; Neghina, A.M.; Peck-Radosavljevic, M. Meta-Analysis: ARFI Elastography Versus Transient Elastography for the Evaluation of Liver Fibrosis. *Liver Int.* **2013**, *33*, 1138–1147. [CrossRef]
10. Kaposi, P.N.; Unger, Z.; Fejér, B.; Kucsa, A.; Tóth, A.; Folhoffer, A.; Szalay, F.; Bérczi, V. Interobserver Agreement and Diagnostic Accuracy of Shearwave Elastography for the Staging of Hepatitis C Virus-Associated Liver Fibrosis. *J. Clin. Ultrasound* **2019**, *48*, 67–74. [CrossRef] [PubMed]
11. European Association for the Study of the Liver; Asociación Latinoamericana Para el Estudio Del Hígado. EASL-ALEH Clinical Practice Guidelines: Non-Invasive Tests for Evaluation of Liver Disease Severity and Prognosis. *J. Hepatol.* **2015**, *63*, 237–264. [CrossRef] [PubMed]
12. Chekuri, S.; Nickerson, J.; Bichoupan, K.; Sefcik, R.; Doobay, K.; Chang, S.; DelBello, D.; Harty, A.; Dieterich, U.T.; Perumalswami, P.V.; et al. Liver Stiffness Decreases Rapidly in Response to Successful Hepatitis C Treatment and Then Plateaus. *PLoS ONE* **2016**, *11*, e0159413. [CrossRef]
13. Hézode, C.; Castéra, L.; Roudot-Thoraval, F.; Bouvier-Alias, M.; Rosa, I.; Roulot, D.; Leroy, V.; Mallat, A.; Pawlotsky, J.-M. Liver Stiffness Diminishes with Antiviral Response in Chronic Hepatitis C. *Aliment. Pharmacol. Ther.* **2011**, *34*, 656–663. [CrossRef] [PubMed]
14. Libânio, D.; Marinho, R.T. Impact of Hepatitis C Oral Therapy in Portal Hypertension. *World J. Gastroenterol.* **2017**, *23*, 4669–4674. [CrossRef] [PubMed]
15. Attia, D.; Deterding, K.; Cornberg, J.; Gebel, M.J.; Cornberg, M.; Manns, M.P.; Wedemeyer, H.; Potthoff, A. Different Kinetics of Liver Stiffness using Shear Wave Elastography in Patients with Chronic Hepatitis C Infection Treated with Interferon-Free Regimens. *Eur. J. Gastroenterol. Hepatol.* **2019**, *31*, 67–74. [CrossRef] [PubMed]
16. Jacobson, I.M.; Lim, J.K.; Fried, M.W. American Gastroenterological Association Institute Clinical Practice Update—Expert Review: Care of Patients Who Have Achieved a Sustained Virologic Response After Antiviral Therapy for Chronic Hepatitis C Infection. *Gastroenterology* **2017**, *152*, 1578–1587. [CrossRef]
17. De Franchis, R. Expanding Consensus in Portal Hypertension. *J. Hepatol.* **2015**, *63*, 743–752. [CrossRef]

18. Paternostro, R.; Reiberger, T.; Bucsics, T. Elastography-Based Screening for Esophageal Varices in Patients with Advanced Chronic Liver Disease. *World J. Gastroenterol.* **2019**, *25*, 308–329. [CrossRef] [PubMed]
19. Kamath, P.S.; Kim, W.R. The Model for End-Stage Liver Disease (MELD) & Dagger. *Hepatology* **2007**, *45*, 797–805. [CrossRef]
20. Sterling, R.K.; Lissen, E.; Clumeck, N.; Sola, R.; Correa, M.C.; Montaner, J.; Sulkowski, M.S.; Torriani, F.J.; Dieterich, D.T.; Thomas, D.L.; et al. Development of a Simple Noninvasive Index to Predict Significant Fibrosis in Patients with HIV/HCV Coinfection. *Hepatology* **2006**, *43*, 1317–1325. [CrossRef] [PubMed]
21. Pugh, R.N.H.; Murray-Lyon, I.M.; Dawson, J.L.; Pietroni, M.C.; Williams, R. Transection of the Oesophagus for Bleeding Oesophageal Varices. *BJS* **2005**, *60*, 646–649. [CrossRef]
22. Marshall, A.D.; Pawlotsky, J.-M.; Lazarus, J.V.; Aghemo, A.; Dore, G.J.; Grebely, J. The Removal of DAA Restrictions in Europe—One Step Closer to Eliminating HCV as a Major Public Health Threat. *J. Hepatol.* **2018**, *69*, 1188–1196. [CrossRef] [PubMed]
23. D'Ambrosio, R.; Aghemo, A.; Rumi, M.G.; Ronchi, G.; Donato, M.F.; Paradis, V.; Colombo, M.; Bedossa, P. A Morphometric and Immunohistochemical Study to Assess the Benefit of a Sustained Virological Response in Hepatitis C Virus Patients with Cirrhosis. *Hepatology* **2012**, *56*, 532–543. [CrossRef] [PubMed]
24. Ferraioli, G.; Tinelli, C.; Lissandrin, R.; Zicchetti, M.; Bello, B.D.; Filice, G.; Filice, C. Point Shear Wave Elastography Method for Assessing Liver Stiffness. *World J. Gastroenterol.* **2014**, *20*, 4787–4796. [CrossRef] [PubMed]
25. Tachi, Y.; Hirai, T.; Kojima, Y.; Ishizu, Y.; Honda, T.; Kuzuya, T.; Hayashi, K.; Ishigami, M.; Goto, H. Liver Stiffness Reduction Correlates with Histological Characteristics of Hepatitis C Patients with Sustained Virological Response. *Liver Int.* **2017**, *38*, 59–67. [CrossRef]
26. Facciorusso, A.; Del Prete, V.; Turco, A.; Buccino, R.V.; Nacchiero, M.C.; Muscatiello, N. Long-Term Liver Stiffness Assessment in Hepatitis C Virus Patients Undergoing Antiviral Therapy: Results From a 5-year Cohort Study. *J. Gastroenterol. Hepatol.* **2018**, *33*, 942–949. [CrossRef]
27. Bruno, S.; Crosignani, A.; Facciotto, C.; Rossi, S.; Roffi, L.; Redaelli, A.; De Franchis, R.; Almasio, P.L.; Maisonneuve, P. Sustained Virologic Response Prevents the Development of Esophageal Varices in Compensated, Child-Pugh Class A Hepatitis C Virus-Induced Cirrhosis. A 12-Year Prospective Follow-Up Study. *Hepatology* **2010**, *51*, 2069–2076. [CrossRef]
28. Mallet, V.; Gilgenkrantz, H.; Serpaggi, J.; Verkarre, V.; Vallet-Pichard, A.; Fontaine, H.; Pol, S. Brief Communication: The Relationship of Regression of Cirrhosis to Outcome in Chronic Hepatitis C. *Ann. Intern. Med.* **2008**, *149*, 399–403. [CrossRef]
29. Nagaoki, Y.; Aikata, H.; Nakano, N.; Shinohara, F.; Nakamura, Y.; Hatooka, M.; Morio, K.; Kan, H.; Fujino, H.; Kobayashi, T.; et al. Development of Hepatocellular Carcinoma in Patients with Hepatitis C Virus Infection Who Achieved Sustained Virological Response Following Interferon Therapy: A Large-Scale, Long-Term Cohort Study. *J. Gastroenterol. Hepatol.* **2015**, *31*, 1009–1015. [CrossRef] [PubMed]

Observational Study

Medicine

OPEN

Tissue attenuation imaging and tissue scatter imaging for quantitative ultrasound evaluation of hepatic steatosis

Aladár D. Rónaszéki, MD[a,*], Bettina K. Budai, MD[a], Barbara Csongrády, MD[a], Róbert Stollmayer, MD[a], Krisztina Hagymási, MD, PhD[b], Klára Werling, MD, PhD[b], Tamás Fodor, MD[c], Anikó Folhoffer, MD, PhD[c], Ildikó Kalina, MD, PhD[a], Gabriella Győri, MD[a], Pál Maurovich-Horvat, MD, PhD, DSc[a], Pál N. Kaposi, MD, PhD[a]

Abstract

We aimed to assess the feasibility of ultrasound-based tissue attenuation imaging (TAI) and tissue scatter distribution imaging (TSI) for quantification of liver steatosis in patients with nonalcoholic fatty liver disease (NAFLD). We prospectively enrolled 101 participants with suspected NAFLD. The TAI and TSI measurements of the liver were performed with a Samsung RS85 Prestige ultrasound system. Based on the magnetic resonance imaging proton density fat fraction (MRI-PDFF), patients were divided into ≤5%, 5–10%, and ≥10% of MRI-PDFF groups. We determined the correlation between TAI, TSI, and MRI-PDFF and used multiple linear regression analysis to identify any association with clinical variables. The diagnostic performance of TAI, TSI was determined based on the area under the receiver operating characteristic curve (AUC). The intraclass correlation coefficient (ICC) was calculated to assess interobserver reliability.

Both TAI (r_s = 0.78, P < .001) and TSI (r_s = 0.68, P < .001) showed significant correlation with MRI-PDFF. TAI overperformed TSI in the detection of both ≥5% MRI-PDFF (AUC = 0.89 vs 0.87) and ≥10% (AUC = 0.93 vs 0.86). MRI-PDFF proved to be an independent predictor of TAI (β = 1.03; P < .001), while both MRI-PDFF (β = 50.9; P < .001) and liver stiffness (β = −0.86; P < .001) were independent predictors of TSI. Interobserver analysis showed excellent reproducibility of TAI (ICC = 0.95) and moderate reproducibility of TSI (ICC = 0.73).

TAI and TSI could be used successfully to diagnose and estimate the severity of hepatic steatosis in routine clinical practice.

Abbreviations: ALT = alanine transaminase, AST = aspartate aminotransferase, ATI = attenuation imaging, AUC = area under the receiver operating characteristic curve, BMI = body mass index, CAP = controlled attenuation parameter, CI = confidence interval, CSD = liver capsule distance from the skin surface, ICC = intraclass correlation coefficient, LS = liver stiffness, MRI-PDFF = magnetic resonance imaging-based proton density fat fraction measurement, NAFLD = nonalcoholic fatty liver disease, NPV = negative predictive value, PDFF = proton density fat fraction measurement, PPV = positive predictive value, QUS = quantitative ultrasound, ROC = receiver operating characteristic curve, SD = standard deviation, SWE = Shear wave elastography, TAI = tissue attenuation imaging, TE = Echo time, TR = Repetition time, TSI = tissue scatter distribution imaging.

Keywords: liver imaging, nonalcoholic fatty liver disease, quantitative ultrasound imaging, ultrasonography

1. Introduction

Nowadays, the prevalence of nonalcoholic fatty liver disease (NAFLD) is increasing worldwide.[1] Recent studies suggest around 25% prevalence globally.[2,3] If obesity and/or type 2 diabetes are present, the incidental finding of raised liver enzymes in patients with metabolic risk factors should prompt noninvasive screening to predict steatosis, nonalcoholic steatohepatitis (NASH), and fibrosis.[4] NAFLD in some cases leads to NASH, which may lead to fibrosis, cirrhosis, and hepatocellular carcinoma and is a preeminent cause of liver transplantation.[5] Consequently, accurate evaluation of liver fat content is essential in the diagnosis, treatment and follow-up of NAFLD patients.

B.K.B. was supported by the ÚNKP-21-3 New National Excellence Program of the Ministry for Innovation and Technology from the source of the National Research, Development and Innovation fund.

P.N.K. has served as a speaker for Samsung Medison Ltd. All other authors declare no conflict of interest.

The datasets generated during and/or analyzed during the current study are available from the corresponding author on reasonable request.

Supplemental Digital Content is available for this article.

[a] Department of Radiology, Medical Imaging Centre, Faculty of Medicine, Semmelweis University, Budapest, Hungary, [b] Department of Surgery, Transplantation and Gastroenterology, Faculty of Medicine, Semmelweis University, Budapest, Hungary, and [c] Department of Internal Medicine and Oncology, Faculty of Medicine, Semmelweis University, Budapest, Hungary.

**Correspondence: Aladár D. Rónaszéki, MD, Department of Radiology, Medical Imaging Centre, Faculty of Medicine, Semmelweis University, Korányi Sándor str. 2., H-1082 Budapest, Hungary (e-mail: ronaszeki.aladar_david@med.semmelweis-univ.hu).*

How to cite this article: Rónaszéki AD, Budai BK, Csongrády B, Stollmayer R, Hagymási K, Werling K, Fodor T, Folhoffer A, Kalina I, Győri G, Maurovich-Horvat P, Kaposi PN. Tissue attenuation imaging and tissue scatter imaging for quantitative ultrasound evaluation of hepatic steatosis. Medicine 2022;101:33(e29708).

Received: 30 November 2021 / Received in final form: 28 April 2022 / Accepted: 16 May 2022

http://dx.doi.org/10.1097/MD.0000000000029708

For diagnosing and staging liver steatosis, till recently liver biopsy used to be the gold standard method, even though diffuse liver diseases have high spatial heterogeneity leading to sampling error, high inter-reader variability, and invasive side-effects.[6] Therefore, imaging-based, noninvasive methods for fat quantification are highly demanded.[7] Magnetic resonance imaging-based proton density fat fraction (MRI-PDFF) is a robust imaging biomarker; however, it is not routinely performed for clinical screening due to its high cost and limited availability.[8] Recent guidelines suggest ultrasound as the initial diagnostic procedure in patients with NAFLD, as it is a safe, noninvasive, and cost-effective method.[4,9] However, ultrasound-based assessments of liver steatosis are subject to interobserver variability.[10,11] Classical sonographic signs of fatty liver are increased echogenicity relative to the renal cortex, blur of liver parenchyma, poorly visualized portal venous wall and diaphragm.[12] Semiquantitative classifications such as the Hamaguchi index and US-FLI score have poor sensitivity for mild steatosis.[13] Meanwhile, quantitative ultrasound (QUS) techniques determine tissue composition based on acoustic signal analysis, including tissue attenuation imaging (TAI) and tissue scatter distribution imaging (TSI). A significant correlation has already been shown between tissue scattering imaging and MRI-PDFF.[14]

The purpose of our study was to investigate the diagnostic performance of the QUS biomarkers such as TAI and TSI with multiparametric analysis that can be used reliably and reproducibly to determine steatosis in patients with NAFLD using MRI-PDFF as the reference standard.

2. Methods

2.1. Study population and selection criteria

This single-center prospective cohort study was approved by the regional and institutional committee of science and research ethics of our university, and written informed consent was obtained from all participants according to the World Medical Association Declaration of Helsinki, revised in Edinburgh in 2000. We enrolled 110 participants examined for suspected liver steatosis between July 2020 and September 2021. The eligibility criteria to participate in the study included the following: 18 years or older, referral to an imaging study and either ultrasound or MRI for clinically suspected liver steatosis. The participants' demographic data, including the history of alcohol consumption, were collected from a personal survey, the medical history and laboratory tests were collected from electronic medical reports. Participants who reported daily alcohol consumption of ≥20 g (2 drinks) for females or ≥30 g (3 drinks) for males in the last 2 years, as well as patients whose liver iron content was above the normal range (≥2 mg/g) or had a positive genetic test for hereditary hemochromatosis, were excluded from the study (Fig. 1).

The final cohort included 101 subjects (52 females and 49 males), who fulfilled the eligibility criteria, did not meet any of the exclusion criteria and had valid ultrasonography and MRI measurements of hepatic steatosis. The mean age of the participants was 56 years (range 24–78 years). Among the participants, 62 were clinically suspected for NAFLD based on the diagnostic criteria of the European Clinical Practice guidelines.[4] A secondary NAFLD was clinically suspected in 39 patients, as listed in Table 1.

2.2. Quantitative ultrasound-based measurement of hepatic steatosis

All 101 participants were scanned with a Samsung RS85 Prestige ultrasound system (Samsung Medison Co. Ltd., Hongcheon, Korea) using the CA 1-7S convex probe by an expert radiologist with more than 10 years of experience in abdominal ultrasonography. The participants fasted at least 4 hours before the ultrasound scan and were examined in a supine position with the right arm elevated above the head. We performed all QUS measurements in the right liver lobe near the hilum through an intercostal window.[15] To obtain TAI and TSI values, the operator placed a fan-shaped region of interest (ROI) onto the liver parenchyma at least 3 cm below the capsule avoiding large vessels (Fig. 2). The TAI and TSI measurements were repeated 5 times, and the median of the 5 measurements was used for fat quantification. Only TAI values with $R^2 \geq 0.6$ were considered reliable. The TAI was reported in units of dB/cm/MHz, while the TSI was reported in arbitrary units. The distance of the liver capsule from the skin surface (CSD) in mm was also recorded.

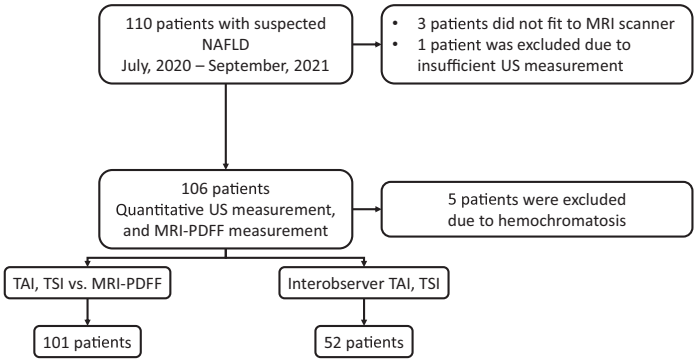

Figure 1. Patient selection and study design. We enrolled 110 participants with suspected NAFLD into this prospective study. One hundred six patients with suspected liver steatosis who fulfilled the inclusion criteria underwent both quantitative ultrasound and MRI-PDFF measurements to determine the liver's fat content. Three morbidly obese patients had been excluded because they did not fit into the MRI scanner, an additional patient was excluded due to failure of the ultrasound measurement, and further 5 patients were excluded due to hemochromatosis, which can interfere with MRI-PDFF. The final patient cohort included 101 NAFLD patients. In 52 cases, 2 examiners independent from each other performed quantitative ultrasound measurements to assess the interobserver reproducibility of TAI and TSI values. MRI-PDFF = magnetic resonance imaging-based proton density fat fraction measurement, NAFLD = nonalcoholic fatty liver disease, TAI = tissue attenuation imaging, TSI = tissue scatter distribution imaging.

Table 1

Demographics of the patient population stratified according to hepatic steatosis.

	All participants and participants without secondary NAFLD etiology			
	All patients	**Control (<5% MRI-PDFF)**	**NAFLD (>5% MRI-PDFF)**	***P***
Total (n)	101	47	54	–
Male (n)	49/101 (48.51%)	27/47 (57.45%)	22/54 (40.74%)	0.094
Age* (yrs)	56.4 ± 12.4	58.1 ± 10.9	54.2 ± 14.0	0.313
Female (n)	52/101 (51.49%)	20/47 (42.55%)	32/54 (59.26%)	–
Age* (yrs)	56.9 ± 12.0	53.7 ± 13.1	59.0 ± 10.9	0.151
P value for age between sex	.693	.33	.223	–
Secondary NAFLD etiology				
Chemotherapy	22/101 (21.78%)	14/47 (29.79%)	8/54 (14.81%)	
Chronic HBV/HCV infection	9/101 (8.91%)	8/47 (17.02%)	1/54 (1.85%)	
AIH	4/101 (3.96%)	2/47 (4.26%)	2/54 (3.70%)	
Wilson disease	4/101 (3.96%)	1/47 (2.13%)	3/54 (5.56%)	
NAFLD				
Total (n)	62	22	40	-
Male (n)	28/62 (45.16%)	10/22 (45.45%)	18/40 (45.00%)	0.973
Age* (yrs)	55.3 ± 14.0	55.1 ± 13.9	55.4 ± 14.5	0.867
Female (n)	34/62 (54.83%)	12/22 (54.55%)	22/40 (55.00%)	–
Age* (yrs)	56.5 ± 12.6	48.3 ± 12.8	60.9 ± 1.2	0.004
P value for age between sex	.552	.487	.276	–

*Reported as mean ± standard deviation.

AIH = autoimmune hepatitis, ALT = alanine aminotransferase, AST = aspartate aminotransferase, BMI = body mass index, HBV = hepatitis B virus, HCV = hepatitis C virus, MRI-PDFF = magnetic resonance imaging-based proton density fat fraction, NAFLD = nonalcoholic fatty liver disease, SD = standard deviation.

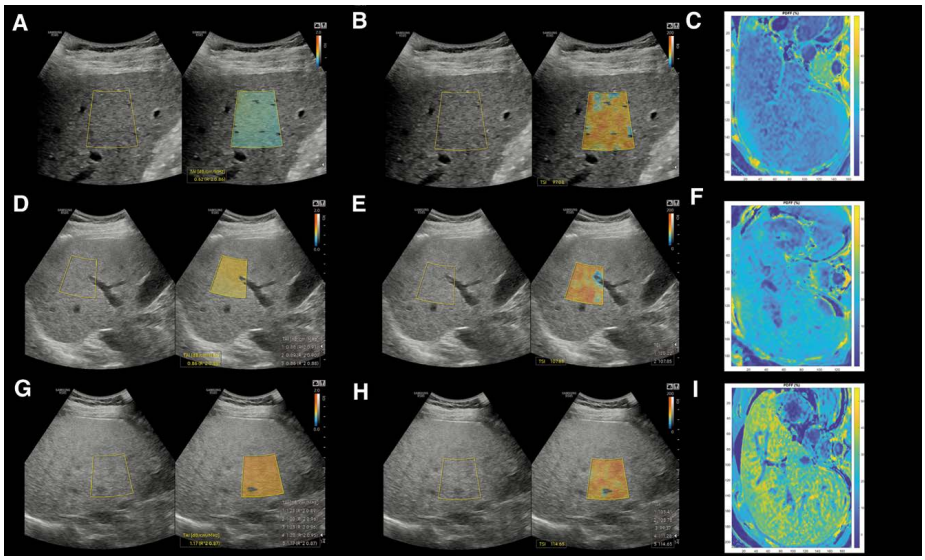

Figure 2. Quantitative ultrasound measurement of the liver fat. Tissue attenuation imaging (A) and tissue scatter distribution imaging (B) of participants with a liver fat content of <5%. For visual reference, colormaps from magnitude-based estimation of MRI-PDFF values were also reconstructed on axial slices where livers with < 5% MRI-PDFF showed blue color indicating no significant steatosis (C). Patients with 5–10% of MRI-PDFF had higher TAI (D) and TSI (E) values compared to patients with no significant hepatic steatosis, while the MRI-PDFF colormap of the liver turned green (F). Finally, patients with ≥ 10% of MRI-PDFF had the highest TAI (G) and TSI values (G), and they had a yellowish color on the MRI-PDFF colormap (I). MRI-PDFF = magnetic resonance imaging-based proton density fat fraction measurement, TAI = tissue attenuation imaging, TSI = tissue scatter distribution imaging.

A second examiner, a trainee with 4 years of experience in abdominal ultrasonography, repeated the QUS measurements in 52 participants on the same day. The examiners were blinded from each other's measurements and the result of MRI-PDFF. In 98 subjects, liver stiffness (LS) was also measured in kPa units using the S-Shearwave Imaging application. For a detailed protocol of shear wave electrography (2D-SWE), we refer to a previous publication.[9]

2.3. Magnetic resonance imaging and measurement of MRI-PDFF

We used the MRQuantif examination protocol and software (https://imagemed.univ-rennes1.fr/en/mrquantif) to measure the magnetic resonance imaging proton density fat fraction (MRI-PDFF) of the livers.[16] In brief, axial images of the liver at the level of the porta hepatis were acquired with a multiecho gradient echo sequence during a single breath-hold of 18 seconds or less. Twelve echos were collected from each slab by changing the echo time (TE) with equally spaced 1.2 ms increments starting from 1.2 ms. Imaging parameters included a flip angle of 20°, a slice thickness of 7 mm, a repetition time (TR) of 120 ms, a field-of-view of 400 × 350 mm, a reconstruction matrix of 128 × 116 pixels, and an interslice gap of 10 mm. A Philips Ingenia 1.5 T MRI scanner (Philips Healthcare, Amsterdam, the Netherlands) and the Q-Body coil were used for all scans. The software calculated the R2* and the MRI-PDFF using an exponential decay model integrating the variation of the signal linked to the 3 main fat peaks determined by Hamilton et al.[17] For visual reference, we used color-coded maps of magnitude-based estimation of MRI-PDFF corrected for multiple fat peaks, field inhomogeneity, and R2* using the MATLAB (The Mathworks, Natick, MA) code (https://github.com/marcsous/pdff) of Bydder et al.[18]

The MRI scan was completed within 1 week of the QUS. A threshold of ≥5% MRI-PDFF was selected to diagnose patients with hepatic steatosis, as recommended by current clinical guidelines.[4] A second threshold at ≥10% MRI-PDFF was used to diagnose fatty liver disease in a more advanced stage.[19,20] We also classified the hepatic steatosis into 4 grades (S0-S3) using the MRI-PDFF cutoff points reported by Park et al.[21]

2.4. Statistical analysis

The normality of the continuous variables was checked by the Shapiro-Wilk test. We used the chi-squared test for estimating the differences between categorical variables, while continuous variables were compared using the Mann-Whitney *U* test. The differences in clinical parameters between steatosis stages were compared with the Kruskal-Wallis test. During the post hoc Dunn test, the Benjamini-Hochberg method was used for multiple testing corrections. Spearman correlation analysis was performed to assess the correlation between QUS and MRI-PDFF. A receiver operating characteristic (ROC) curve analysis was performed with TAI and TSI to predict the severity of steatosis. The best threshold values were determined based on the closest top-left cutoff point of the ROC curve. We performed a ROC curve power analysis based on the formula described by Obuchowski et al to estimate the smallest sample size that allows for accurate discrimination between categories with a type I error rate of <0.05 and a type II error rate of ≤0.2.[22] Simple and multiple linear regression models were built to identify significant confounding factors of TAI and TSI measurements. We calculated the intraclass correlation coefficient (ICC) using 2-way random effects, absolute agreement, single rater/measurement model to evaluate the inter-rater reproducibility of TAI and TSI.

The statistical analysis was performed with "stats," "dplyr," "regclass," "pROC," "spearmanCI," "dunn.test," and "irr" packages in R v.3.5.3 (www.r-project.org). The threshold of $P < .05$ was used to determine significance in all comparisons.

3. Results

3.1. Detection of liver steatosis in the study population

We prospectively enrolled 101 participants with the suspected fatty liver disease into our study, including 49 (48.5%) males with a mean age of 56 years (range: 36–78 years), as well as 52 (51.5%) females with a mean age of 57 years (range: 24–76 years) (Table 1). The mean body mass index (BMI) (±standard deviation, SD) and the mean LS were 28 kg/m² (±4.37 kg/m²) and 9.1 kPa (±6.0 kPa) in the study population, respectively. The prevalence of significant liver fibrosis (≥F2) among study participants was 34% (34/101).

Among the study participants, 54 (53.5%) had hepatic steatosis (≥5% MRI-PDFF), including 17 (31.5%) patients with ≥5% and <10%, and 37 (68.5%) patients with ≥10% MRI-PDFF. In the cohort, 62 (61.4%) participants were clinically suspected to have NAFLD without secondary etiology, of which 13 (21%) had ≥5% and <10%, and 27 (43.5%) had ≥10% MRI-PDFF (Table 1, Supplemental Digital Content, http://links.lww.com/MD/G977).

We also assigned a steatosis grade (S0-S3) to each participant based on MRI-PDFF. Thus, the study cohort included 38 (37.6%), 35 (34.7%), 6 (5.9%), and 22 (21.8%) participants with S0, S1, S2, and S3 grades hepatic steatosis, respectively.

3.2. Evaluation of the diagnostic performance of TAI for the detection of hepatic steatosis

We found a significant, strong correlation ($r_s = 0.78$, 95% confidence interval [CI = 0.701–0.852], $P < .001$) between TAI and MRI-PDFF values. We also detected a significant positive association ($F[1,99] = 101$, $P < .001$, $R^2 = 0.51$, $\beta = 0.39$) between TAI and MRI-PDFF during simple linear regression analysis.

The mean TAI value (0.789 ± 0.08 dB/cm/MHz) of all patients with ≥5% and <10% MRI-PDFF was significantly higher compared with controls without steatosis (0.697 ± 0.10 dB/cm/MHz, Dunn test $P = .009$); also, a significantly higher TAI (0.965 ± 0.14 dB/cm/MHz, $P < .001$) was detected in patients with ≥10% MRI-PDFF compared with other subjects in the hepatic steatosis group (Fig. 3). The mean TAI in the NAFLD cohort also showed significant difference among the groups without steatosis (0.682 ± 0.08 dB/cm/MHz), with ≥5% and <10% MRI-PDFF (0.792 ± 0.09 dB/cm/MHz, $P < .014$) and ≥10% MRI-PDFF (0.95 ± 0.13 dB/cm/MHz, $P < .003$) (Table 1, Supplemental Digital Content, http://links.lww.com/MD/G977).

Including all the 101 participants to the analysis the area under the receiver operating characteristic curve (AUC) of TAI for the detection of ≥5% MRI-PDFF was 0.89 [CI = 0.83–0.95] with power of 1.00 at significance level of $P < .05$ (Fig. 4). The optimal cutoff value at 0.765 dB/cm/MHz had a sensitivity, specificity, negative predictive value (NPV), positive predictive value (PPV) and accuracy of 85%, 79%, 82%, 82%, and 82%, respectively. For the detection of ≥10% MRI-PDFF, the AUC was 0.93 (CI = 0.88–0.98) with power of 1.00 at significance level of $P < .05$; and with a cutoff at 0.845 dB/cm/MHz, the sensitivity, specificity, NPV, PPV, and accuracy were 81%, 89%, 89%, 81%, and 86%, respectively. In the NAFLD cohort, the AUC of TAI for the prediction of ≥5% and ≥10% MRI-PDFF were 0.92 (CI = 0.85–0.98) and 0.93 (CI = 0.87–0.99) both with power of 1.00 at significance level of $P < .05$, respectively. The threshold for diagnosing ≥5% MRI-PDFF in NAFLD was at 0.76 dB/cm/MHz, and for the detection of ≥10% MRI-PDFF at 0.85 dB/cm/MHz, which had a sensitivity, specificity, NPV, PPV, and accuracy of 88%, 86%, 79%, 92%, and 87%, and 78%, 89%, 84%, 84%, and 84%, respectively (Table 2).

A ROC analysis was also performed to determine if TAI measurements can differentiate between steatosis grades. TAI showed excellent performance for both predicting ≥S1 grade (AUC = 0.89, 95% CI = 0.82–0.97) and ≥S2 grade (AUC = 0.85, 95% CI = 0.75–0.95) of hepatic steatosis. The results of this analysis are provided in Table 2 (Supplemental Digital Content, http://links.lww.com/MD/G978), Figure 3 (Supplemental Digital Content, http://links.lww.com/MD/G979), and Figure 4 (Supplemental Digital Content, http://links.lww.com/MD/G980).

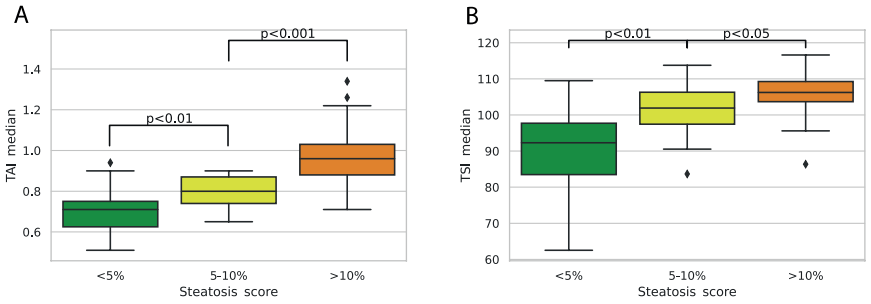

Figure 3. Comparison of quantitative ultrasound metrics between different amounts of hepatic steatosis. Both TAI and TSI showed significant differences between hepatic steatosis of < 5% vs 5–10% vs ≥10% MRI-PDFF. The TSI values showed a greater overlap between the different categories compared to TAI measurements. MRI-PDFF = magnetic resonance imaging-based proton density fat fraction measurement, TAI = tissue attenuation imaging, TSI = tissue scatter distribution imaging.

3.3. Evaluation of the diagnostic performance of TSI for the detection of hepatic steatosis

The correlation between TSI and MRI-PDFF values was strong and significant (r_s = 0.68 (95% CI = 0.578–0.778, P < .001)). We also found a significant positive association between TSI and MRI-PDFF (F[1,99] = 40.4, P < .001, R^2 = 0.29, β = 0.004) in a simple regression analysis. Consequently, the mean TSI (106.0 ± 5.6) of the group with ≥10% MRI-PDFF was significantly higher than the mean TSI (101.0 ± 7.0, P < .016) in hepatic steatosis with ≥5% and <10% MRI-PDFF and the mean TSI (90.7 ± 11.5, P < .003) of controls without steatosis (Fig. 3). In NAFLD, the mean TSI was also significantly different among groups without steatosis (91.6 ± 9.7) with ≥5% and <10% MRI-PDFF (102.0 ± 6.2, P < .007) and with ≥10% MRI-PDFF (108.0 ± 4.4, P < .017) (Table 1, Supplemental Digital Content, http://links.lww.com/MD/G977).

The AUCs of TSI for ≥5% and ≥10% MRI-PDFF were 0.87 (CI = 0.79–0.94) and 0.86 (CI = 0.79–0.93) both with power of 1.00 at significance level of P < .05, respectively (Fig. 4). The optimal thresholds to predict ≥5%, and ≥10% MRI-PDFF were at 99.7 and 102.0, which had a sensitivity, specificity, NPV, PPV, and accuracy of 87%, 83%, 85%, 85%, and 85% and 89%, 78%, 93%, 70%, and 82%, respectively. When the ROC analysis was performed on the NAFLD cohort, the AUC of TSI for ≥5% MRI-PDFF was 0.91 (CI = 0.82–0.99), and the AUC for ≥10% MRI-PDFF was 0.88 (CI = 0.79–0.96) both with power of 1.00 at significance level of P < .05. The cutoff points were highly similar to those calculated for all participants, including a TSI of 100.6 for ≥5% and a TSI of 103.1 for ≥10% MRI-PDFF resulting in a sensitivity, specificity, NPV, PPV, and accuracy of 88%, 86%, 79%, 92%, and 87% and of 85%, 77%, 87%, 74%, and 81%, respectively (Table 2).

We also performed a ROC analysis for TSI to determine whether it is able to identify patients with at least mild (≥S1 grade) or moderate (≥S2 grade) hepatic steatosis determined by MRI-PDFF. TSI showed comparable results with TAI with AUC of 0.93 (95% CI = 0.86–1.0) for predicting ≥ S1 grade and AUC of 0.813 (95% CI = 0.70–0.92) for predicting ≥ S2 grade in the NAFLD patient cohort. Both TAI and TSI showed very similar classification accuracy in the full cohort including all NAFLD and secondary NAFLD cases, where TAI showed superior performance compared to TSI. The results of this analysis are provided in Table 1 (Supplemental Digital Content, http://links.lww.com/MD/G977), Figure 3 (Supplemental Digital Content, http://links.lww.com/MD/G979), and Figure 4 (Supplemental Digital Content, http://links.lww.com/MD/G980).

3.4. Interobserver reproducibility and reliability of TAI and TSI measurements

In 52 participants, the QUS was repeated by a second examiner on the same day. The correlation between the 2 observers' measurements was excellent for TAI (r_s = 0.94, P < .001) and moderate for TSI (r_s = 0.57, P < .001). According to the Bland-Altmann plots, the mean of differences between the examiners was 0.01 dB/cm/MHz with TAI and 1.92 with TSI. In the case of both TAI and TSI, most differences (49/52, 94%) fell between the limits of agreement (±1.96 SD), which suggested good reproducibility (Fig. 5). We found excellent interobserver agreement with TAI (ICC = 0.95, 95% CI = 0.91–0.97) and moderate agreement with TSI (ICC = 0.73, 95% CI = 0.56–0.84).

3.5. Analysis of confounding factors of TAI and TSI measurements

Among MRI-PDFF, BMI, CSD, LS, aspartate aminotransferase (AST), and alanine transaminase (ALT), MRI-PDFF was the only independent predictor of TAI in a multivariable regression analysis (F[3,69] = 28.4, P < .001, R^2 = 0.53, β = 1.03). Meanwhile, TSI was significantly influenced by both MRI-PDFF (β = 50.9, P < .001), and LS (β = –0.86, P < .001) in a multivariable model (F[4,68] = 14.4, P < .001, R^2 = 0.43) (Table 5, Supplemental Digital Content, http://links.lww.com/MD/G981). We also found significant collinearity between BMI (r_s = 0.49, P < .001), CSD (r_s = 0.45, P < .001), and MRI-PDFF.

4. Discussion

Recently, multiple noninvasive methods have become available for the quantitative assessment of hepatic steatosis.[23] The main 2 advantages of ultrasound-based hepatic steatosis quantification are the lower cost and the excellent portability of the instrument, which allow for the screening and follow-up of large patient populations. The controlled attenuation parameter (CAP) measurement was the first ultrasound-based technique available for clinical use; however, it requires special instrumentation and has been less accurate for grading steatosis than MRI-PDFF or other ultrasound-based techniques such as attenuation imaging (ATI) and TAI in comparative studies.[21,24] In addition, TAI and TSI can be performed with standard ultrasound scanners; thus, any alterations in liver morphology can be concomitantly evaluated.

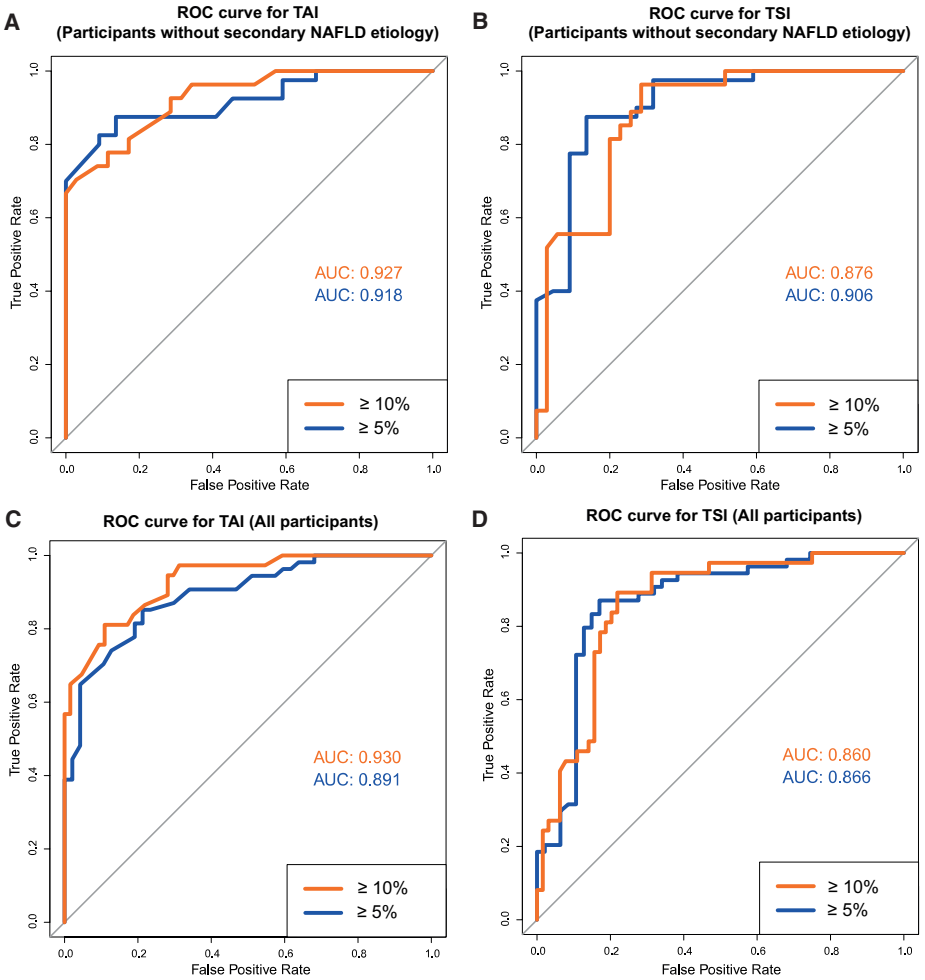

Figure 4. Receiver operating characteristic curve analysis for quantitative ultrasound metrics. According to the receiver operating characteristic curve analysis of NAFLD cases without secondary etiology TAI had excellent AUCs of 0.927 and 0.918 (A), while TSI had very good and excellent AUCs of 0.876 and 0.906 (B), to detect ≥ 5% and ≥ 10% MRI-PDFF, respectively. The TAI (AUC = 0.930 and 0.891) (C) and TSI (AUC = 0.860 and 0.866) (D) had similarly good classification accuracy for ≥ 5% and ≥ 10% MRI-PDFF in all participants. AUC = area under the receiver operating characteristic curve, MRI-PDFF = magnetic resonance imaging-based proton density fat fraction measurement, NAFLD = nonalcoholic fatty liver disease, ROC = receiver operating characteristic curve, TAI = tissue attenuation imaging, TSI = tissue scatter distribution imaging.

Recently, the diagnostic accuracy of TAI was assessed in NAFLD patients in a single-center study by Jeon et al, who reported a moderate correlation between TAI and MRI-PDFF (R = 0.659).[20] In our study, TAI showed a strong correlation with MRI-PDFF (r_s = 0.78), which was better than the correlation between CAP and MRI-PDFF (R = 0.53–0.61) and comparable to the correlation between ATI and MRI-PDFF (R = 0.81) reported previously.[24–26] The classification accuracy of TAI was very good for ≥5% (AUC = 0.89) and excellent for ≥10% (AUC = 0.93) MRI-PDFF fat content, and TAI proved to be superior to CAP to diagnose hepatic steatosis (AUC = 0.69–0.80 and 0.70–0.87, respectively) when our results were compared to prior studies.[19,27]

The correlation between TSI and MRI-PDFF was strong (r_s = 0.68), but the coefficient was weaker compared with TAI. Meanwhile, TSI was able to detect ≥5% MRI-PDFF (AUC = 0.87) and ≥10% MRI-PDFF (AUC = 0.86) with very good accuracy, and its ability to diagnose hepatic steatosis was only slightly inferior to TAI. The diagnostic performance of TSI in our study was weaker than the AUC reported for ≥5% and ≥10% MRI-PDFF in a prior study (0.96 and 0.94, respectively),

Table 2

Diagnostic accuracy of quantitative ultrasound metrics for the detection of hepatic steatosis.

NAFLD	AUC*	Threshold	Accuracy	Sensitivity	Specificity	PPV	NPV	Ideal cutoff
TAI								
≥5% MRI-PDFF	0.918 (0.852–0.984)	0.586	0.871	0.875	0.864	0.921	0.792	0.760 dB/cm/MHz
≥10% MRI-PDFF	0.927 (0.86 5–0.989)	0.522	0.839	0.778	0.886	0.84	0.838	0.845 dB/cm/MHz
TSI								
≥5% MRI-PDFF	0.906 (0.824–0.989)	0.681	0.871	0.875	0.864	0.921	0.792	100.64
≥10% MRI-PDFF	0.876 (0.789–0.962)	0.439	0.807	0.852	0.772	0.742	0.871	103.13
NAFLD and secondary NAFLD								
TAI								
≥5% MRI-PDFF	0.891 (0.830–0.952)	0.438	0.822	0.852	0.787	0.821	0.822	0.765 dB/cm/MHz
≥10% MRI-PDFF	0.930 (0.882–0.979)	0.424	0.861	0.811	0.891	0.811	0.891	0.845 dB/cm/MHz
TSI								
≥5% MRI-PDFF	0.866 (0.790–0.943)	0.562	0.852	0.870	0.830	0.854	0.848	99.71
≥10% MRI-PDFF	0.860 (0.787–0.933)	0.393	0.822	0.892	0.781	0.702	0.926	102.045

*Reported as mean and 95% confidence interval.

AUC = area under the receiver operating characteristic curve, MRI = magnetic resonance imaging, NAFLD = nonalcoholic fatty liver disease, NPV = negative predictive value, PDFF = proton density fat fraction, PPV = positive predictive value, SD = standard deviation, TAI = tissue attenuation imaging, TSI = tissue scatter distribution imaging.

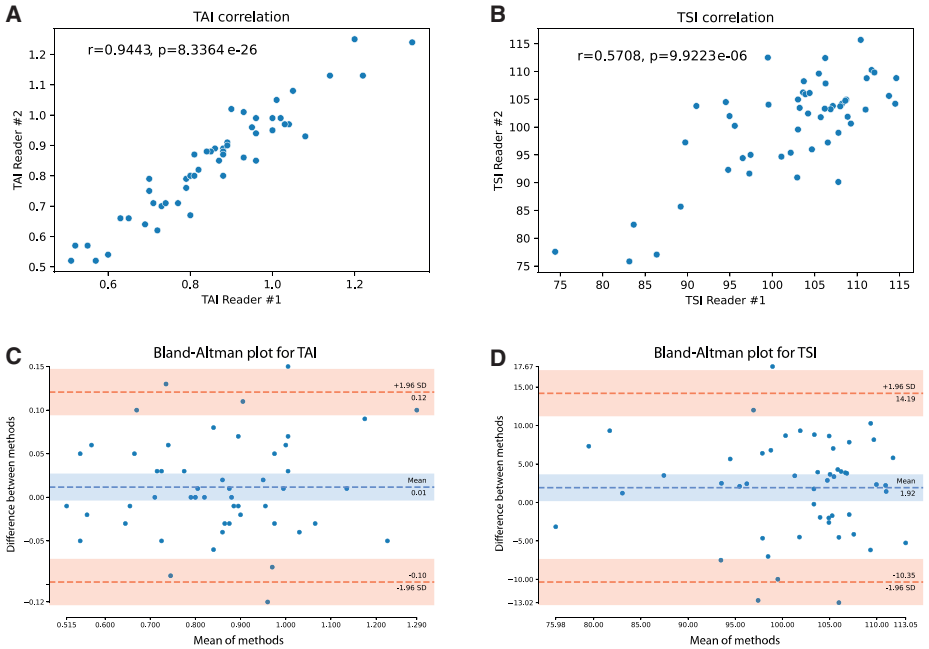

Figure 5. Analysis of interobserver agreement with quantitative ultrasound. The TAI and TSI values measured by the 2 examiners both showed a strong correlation with a Spearman rho of 0.94, $P < .001$ (A) and 0.57, $P < 001$ (B), respectively. The average interobserver difference (dashed blue line) was 0.01 cm/dB/MHz with TAI (C) and 1.92 with TSI (D). Both TAI and TSI showed good reproducibility according to the Bland-Altman plot, where 94% (49/52) of the interobserver differences fell within the 95% confidence interval with limits (dashed red lines) at 1.96 standard deviations. SD = standard deviation, TAI = tissue attenuation imaging, TSI = tissue scatter distribution imaging.

but still exceeded the accuracy of CAP in a similar classification.[19,20] We also found that the interobserver agreement was weaker with TSI than with TAI (ICC = 0.73 vs 0.95) or than the interobserver reliability of TSI in previous studies (ICC = 0.96–0.98), which can be in part attributed to the different levels of experience of the expert and trainee examiners.[20,28]

Our patient cohort consisted of patients who were either diagnosed with NAFLD (61%) on the basis of clinical presentation

or were investigated for secondary NAFLD (39%). The accuracy and the cutoff values of TAI and TSI for the detection of hepatic steatosis were almost identical when the analysis included all participants (TAI = 0.765 dB/cm/MHz, TSI = 99.7) or just NAFLD cases without secondary etiology (TAI = 0.760 dB/cm/MHz, TSI = 100.6). Moreover, the diagnostic thresholds of both TAI and TSI closely matched cutoff values (TAI = 0.884 dB/cm/MHz, TSI = 91.2) reported in a previous study, which investigated solely NAFLD patients.[20] Therefore, we do not consider a significant drawback of our study that it includes NAFLD and secondary NAFLD cases.

We also analyzed the influence of confounding variables on TAI and TSI values. Interestingly, we found a significant negative association between LS measured with 2D-SWE and TSI values. Previously, a similar negative relationship was found between TSI, which represents the Nakagami parameter, and the severity of liver fibrosis detected with transient elastography.[15] Conversely, the Nakagami parameter is derived from the distribution of ultrasound scatter, which follows a Rayleigh distribution in healthy livers and deviates toward a pre-Rayleigh distribution in fibrotic livers.[29]

Our study has several limitations. First, this is a single-center study, which contains a relatively small number of participants. Second, the study cohort was a mix of NAFLD and secondary NAFLD cases, which may hinder the classification of participants, and may cause inaccuracy of the diagnostic thresholds for TAI and TSI. Third, due to selection bias, the prevalence of NAFLD (61%) was significantly higher among participants of the study than in the general population. Fourth, tissue samples were not available for correlation with histopathology.

In conclusion, the liver fat content measured with QUS, using either TAI or TSI, shows a good correlation with MRI-PDFF. Both TAI and TSI are reliable methods for the assessment of hepatic steatosis and can be used to diagnose patients with NAFLD with very good accuracy. TSI may also be helpful in the detection of NAFLD associated liver fibrosis.

Acknowledgments

We would like to thank Prof Zoltán Harkányi for reviewing the article and for his expert comments. We would like to express their gratitude to László Szakács for giving advice on the statistical analysis and the expert discussion of the article. We would like to thank Ms. Lilla Petovsky, Ms. Éva Juhász, Ms. Ramóna Varga, Mr. Tamás Wenzel, and Mr. Tamás Péntek for performing the MRI examinations. We also thank Ms. Rita Tornai for assistance with ultrasound examinations and Ms. Vilma Kis for assistance with patient scheduling.

Author contributions

Aladár D. Rónaszéki - Conceptualization, Data curation, Investigation, Writing – original draft
Bettina K. Budai - Conceptualization, Data curation, Formal analysis, Visualization, Writing – original draft
Barbara Csongrády - Data curation
Róbert Stollmayer - Data curation, Software
Krisztina Hagymási - Conceptualization, Investigation, Validation
Klára Werling - Investigation, Validation
Tamás Fodor - Investigation, Validation
Anikó Folhoffer - Conceptualization, Investigation, Validation
Ildikó Kalina - Resources, Supervision
Gabriella Győri - Investigation, Resources, Supervision
Pál Maurovich-Horvat - Resources, Supervision
Pál N. Kaposi- Project administration, Conceptualization, Methodology, Supervision, Writing – review & editing.

References

[1] Asrani SK, Devarbhavi H, Eaton J, et al. Burden of liver diseases in the world. J Hepatol. 2019;70:151–71.
[2] Mitra S, De A, Chowdhury A. Epidemiology of non-alcoholic and alcoholic fatty liver diseases. Transl Gastroenterol Hepatol. 2020;5:16–16.
[3] Younossi ZM, Koenig AB, Abdelatif D, et al. Global epidemiology of nonalcoholic fatty liver disease-meta-analytic assessment of prevalence, incidence, and outcomes. Hepatology. 2016;64:73–84.
[4] European Association for the Study of the Liver (EASL); European Association for the Study of Diabetes (EASD); European Association for the Study of Obesity (EASO). EASL-EASD-EASO Clinical Practice Guidelines for the management of non-alcoholic fatty liver disease. J Hepatol. 2016;64:1388–402.
[5] Pais R, Barritt AS, Calmus Y, et al. NAFLD and liver transplantation: current burden and expected challenges. J Hepatol. 2016;65:1245–57.
[6] Ratziu V, Charlotte F, Heurtier A, et al. Sampling variability of liver biopsy in nonalcoholic fatty liver disease. Gastroenterology. 2005;128:1898–906.
[7] Ma X, Holalkere NS, Kambadakone RA, et al. Imaging-based quantification of hepatic fat: methods and clinical applications. Radiographics. 2009;29:1253–77.
[8] Reeder SB, Hu HH, Sirlin CB. Proton density fat-fraction: a standardized MR-based biomarker of tissue fat concentration. J Magn Reson Imaging. 2012;36:1011–4.
[9] Folhoffer A, Rónaszéki AD, Budai BK, et al. Follow-up of liver stiffness with shear wave elastography in chronic hepatitis c patients in sustained virological response augments clinical risk assessment. Processes. 2021;9:753.
[10] Kaposi PN, Unger Z, Fejér B, et al. Interobserver agreement and diagnostic accuracy of shearwave elastography for the staging of hepatitis C virus-associated liver fibrosis. J clin ultrasound. 2020;48:67–74.
[11] Strauss S, Gavish E, Gottlieb P, et al. Interobserver and intraobserver variability in the sonographic assessment of fatty liver. AJR Am J Roentgenol. 2007;189:W320–3.
[12] Cengiz M, Sentürk S, Cetin B, et al. Sonographic assessment of fatty liver: intraobserver and interobserver variability. Int J Clin Exp Med. 2014;7:5453–60.
[13] Ibacahe C, Correa-Burrows P, Burrows R, et al. Accuracy of a semi-quantitative ultrasound method to determine liver fat infiltration in early adulthood. Diagnostics (Basel). 2020;10:431.
[14] Lin SC, Heba E, Wolfson T, et al. Noninvasive diagnosis of nonalcoholic fatty liver disease and quantification of liver fat using a new quantitative ultrasound technique. Clin Gastroenterol Hepatol. 2015;13:1337–1345.e1336.
[15] Jeon SK, Joo I, Kim SY, et al. Quantitative ultrasound radiofrequency data analysis for the assessment of hepatic steatosis using the controlled attenuation parameter as a reference standard. Ultrasonography. 2021;40:136–46.
[16] Henninger B, Alustiza J, Garbowski M, et al. Practical guide to quantification of hepatic iron with MRI. Eur Radiol. 2020;30:383–93.
[17] Hamilton G, Yokoo T, Bydder M, et al. In vivo characterization of the liver fat ^{1}H MR spectrum. NMR Biomed. 2011;24:784–90.
[18] Bydder M, Ghodrati V, Gao Y, et al. Constraints in estimating the proton density fat fraction. Magn Reson Imaging. 2020;66:1–8.
[19] Caussy C, Alquiraish MH, Nguyen P, et al. Optimal threshold of controlled attenuation parameter with MRI-PDFF as the gold standard for the detection of hepatic steatosis. Hepatology. 2018;67:1348–59.
[20] Jeon SK, Lee JM, Joo I, et al. Quantitative ultrasound radiofrequency data analysis for the assessment of hepatic steatosis in nonalcoholic fatty liver disease using magnetic resonance imaging proton density fat fraction as the reference standard. Korean J Radiol. 2021;22:1077–86.
[21] Park CC, Nguyen P, Hernandez C, et al. Magnetic resonance elastography vs transient elastography in detection of fibrosis and noninvasive measurement of steatosis in patients with biopsy-proven nonalcoholic fatty liver disease. Gastroenterology. 2017;152:598–607.e2.
[22] Obuchowski NA, Lieber ML, Wians FH Jr. ROC curves in clinical chemistry: uses, misuses, and possible solutions. Clin Chem. 2004;50:1118–25.
[23] Ferraioli G, Berzigotti A, Barr RG, et al. Quantification of liver fat content with ultrasound: a WFUMB position paper. Ultrasound Med Biol. 2021;47:2803–20.
[24] Ferraioli G, Maiocchi L, Raciti MV, et al. Detection of liver steatosis with a novel ultrasound-based technique: a pilot study using MRI-derived proton density fat fraction as the gold standard. Clin Transl Gastroenterol. 2019;10:e00081e00081.
[25] Beyer C, Hutton C, Andersson A, et al. Comparison between magnetic resonance and ultrasound-derived indicators of hepatic steatosis in a pooled NAFLD cohort. PLoS One. 2021;16:e0249491.

[26] Ferraioli G, Maiocchi L, Savietto G, et al. Performance of the attenuation imaging technology in the detection of liver steatosis. J Ultrasound Med. 2021;40:1325–32.
[27] Shao C, Ye J, Dong Z, et al. Steatosis grading consistency between controlled attenuation parameter and MRI-PDFF in monitoring metabolic associated fatty liver disease. Ther Adv Chronic Dis. 2021;12:20406223211033119.
[28] Jeon SK, Lee JM, Joo I. Clinical feasibility of quantitative ultrasound imaging for suspected hepatic steatosis: intra- and inter-examiner reliability and correlation with controlled attenuation parameter. Ultrasound Med Biol. 2021;47:438–45.
[29] Tsui PH, Ho MC, Tai DI, et al. Acoustic structure quantification by using ultrasound nakagami imaging for assessing liver fibrosis. Sci Rep. 2016;6:33075.